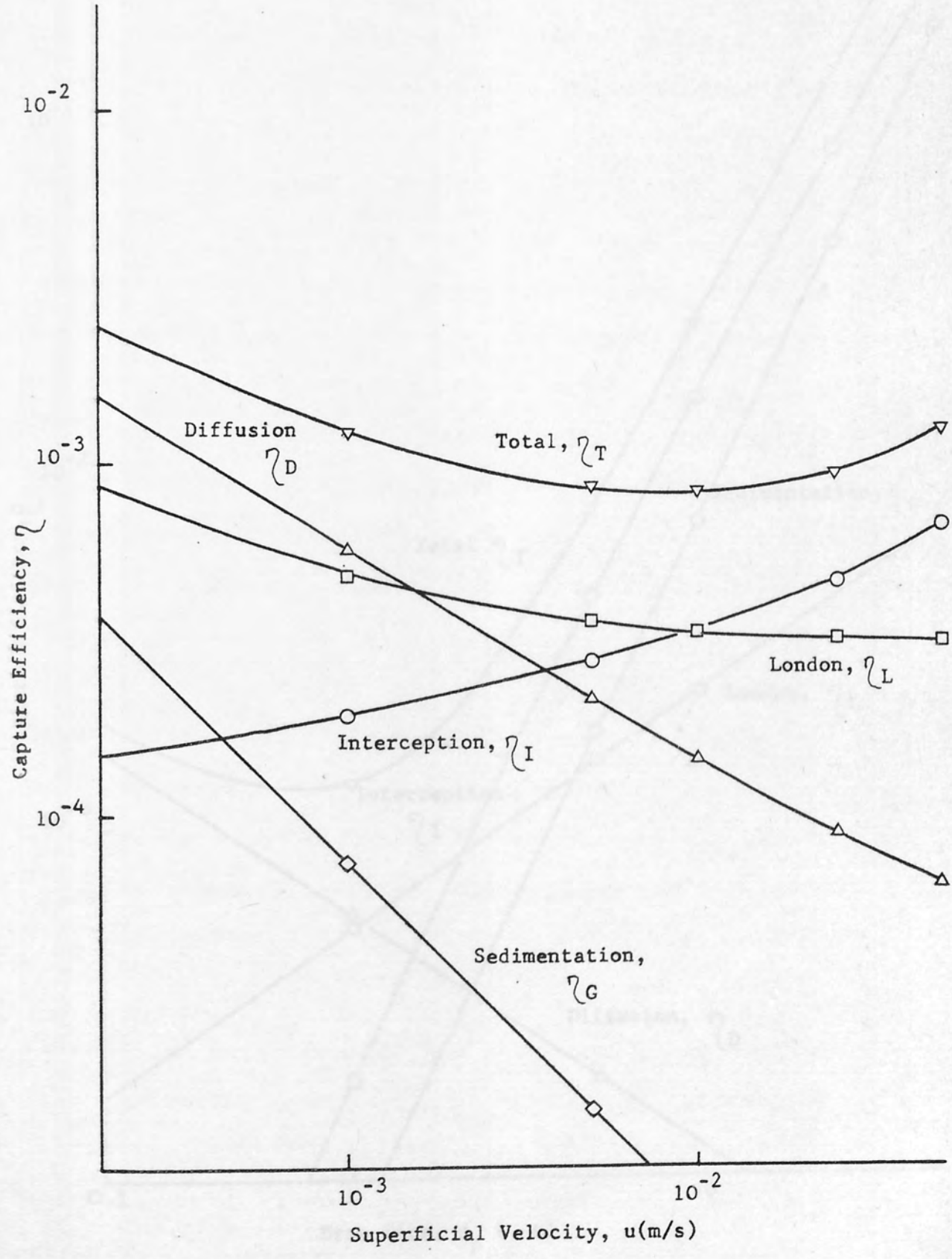

Fig 10.2. Variation of Capture Efficiences with Velocity at .1 μm

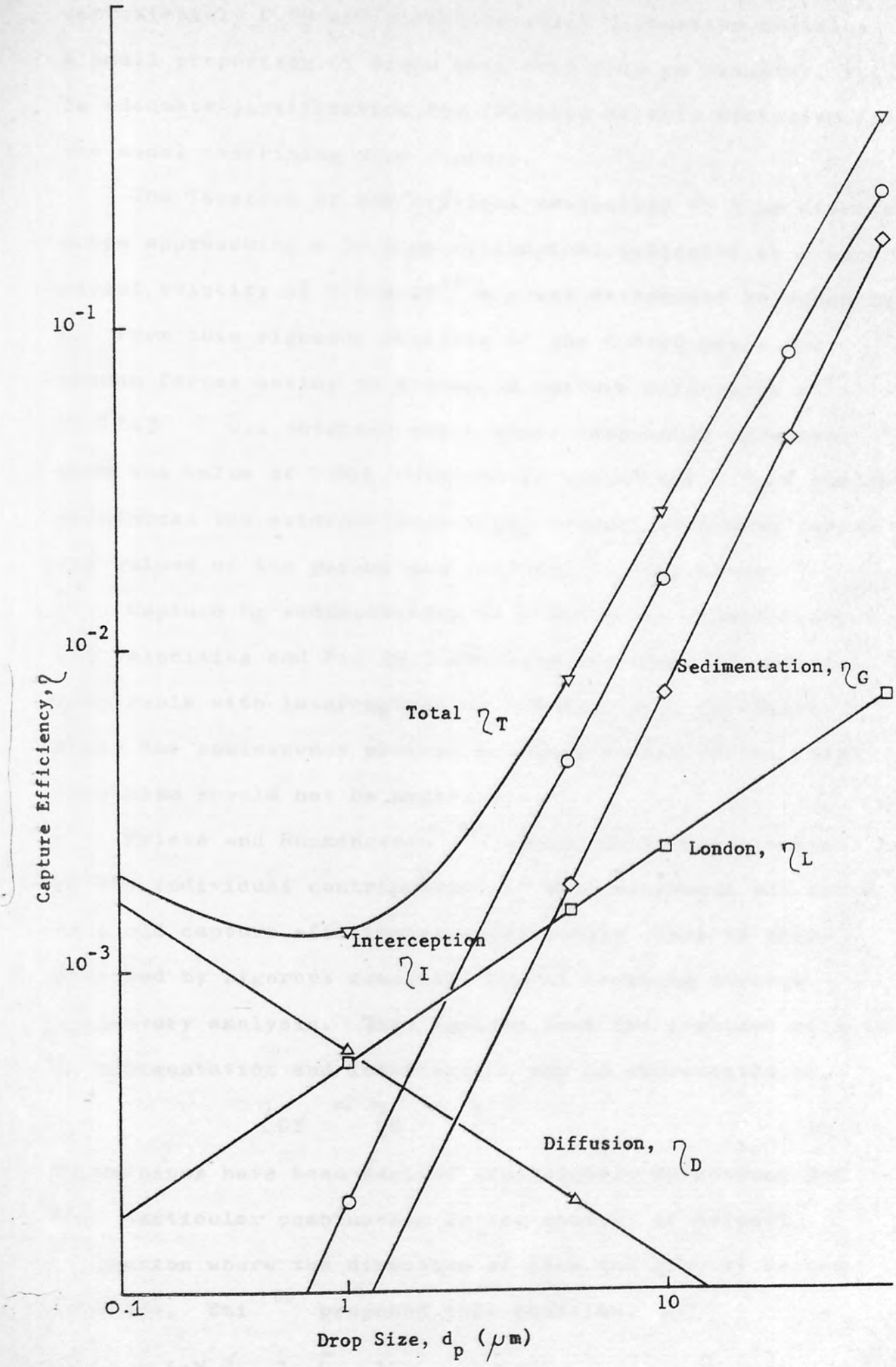

Fig 10.3. Variation of Capture Efficiences with Drop Size at 0.1×10^{-2} m/s.

approximately 0.03 and since the inlet dispersion contains a small proportion of drops less than 5-10 μm diameter, this is adequate justification for omission of this mechanism from the model describing drop capture.

The location of the critical trajectory of 5 μm diameter drops approaching a 30.5 μm cylindrical collector at a superficial velocity of 0.5×10^{-2} m/s was determined in Appendix M. From this rigorous analysis of the hydrodynamic and London forces acting on a drop, a capture efficiency of 0.0263 was obtained which shows reasonable agreement with the value of 0.008 obtained in Appendix L. This further reinforces the evidence supporting neglect of London forces for values of the parameters relevant to this study.

Capture by sedimentation is shown to be significant at low velocities and Fig 10.3 demonstrates that its effect is comparable with interception as the drop size increases. Since the coalescence process produces larger drops, this mechanism should not be neglected.

Prieve and Ruckenstein [78] showed that superposition of the individual contributions of each mechanism was found to yield capture efficiences sufficiently close to those obtained by rigorous consideration of coupling through trajectory analysis. This implies that the combined effects of sedimentation and interception may be represented by,

$$\eta_{GI} = \eta_G + \eta_I \qquad 10.6$$

Expressions have been derived analytically to account for this particular combination in the context of aerosol filtration where the direction of flow and gravity forces coincide. Emi [80] proposed this equation,

$$\eta_{GI} = \frac{1+N_R}{1+N_G}\left\{ \frac{1}{2A}\left[\frac{1}{(1+N_R)^2} - 1 + \log_e(1+N_R)^2\right] + N_G \right\} \qquad 10.7$$

Pich [125], who investigated the variation of capture by gravity forces with the angular position of a particle relative to a collector, suggested an alternative form,

$$\eta_{GI} = \eta_I + \eta_G + N_R N_G \qquad 10.8$$

Within the range of variables relevant to this experimental study, sedimentation is predicted to be most significant when the velocity is 0.5×10^{-2} m/s and the drop diameter is 50 μm.

Then from Table 10.2 $N_R = 1.639, N_{Re} = 0.1525, N_G = 0.0362$

from equation 5.1 $\eta_I = 0.3687$

from equation 5.5 $\eta_G = 0.0362$

For the combined effects of interception and sedimentation,

from the Additivity rule, equation 10.6, $\eta_{GI} = 0.4049$

from equation 10.7, $\eta_{GI} = 0.3677$

from equation 10.8, $\eta_{GI} = 0.4182$

From these results, the validity of the expression proposed by Emi must be jeopardised since it predicts a negative effect by coupling of the mechanisms which cannot be physically justified. As Pich's equation gives an efficiency which differs by only 3% from the result obtained using the additivity rule, the latter was selected as the equation for calculation of the drop capture efficiency.

10.3. RATE OF DROP CAPTURE.

Having established an equation to describe the drop capture efficiency of a single cylindrical collector, it is now possible to estimate the capture rate for a coalescer consisting of a series of meshes, each of which comprises an array of cylindrical fibres.

From Section 10.2, for a single cylindrical collector,

$$\eta_{GI} = \frac{1}{2A}\left[2(1+N_R)\log_e(1+N_R) + \frac{1}{(1+N_R)} - (1+N_R)\right] + N_G \qquad 10.9$$

It was demonstrated in Chapter 9 that use of the hydrodynamic function derived by Keller predicted a Kozeny constant which showed excellent agreement with experimental values. Thus, it may be concluded that the Keller[73] equation adequately characterises flow through a bed of meshes that is initially free from the dispersed phase,

$$A = 1.257\,(1-r)^{2.5} \qquad 10.10$$

$$\text{where} \quad r = \frac{d_c}{d_c + d_a}$$

The efficiency given by equation 10.9 is based upon the projected area of the collector and therefore the efficiency per layer, η_i is related to the fractional open area of the mesh,

$$\eta_i = \eta_{GL}\left[1 - \left\{\frac{d_a}{d_a + d_c}\right\}^2\right] \qquad 10.11$$

The inlet drop size distribution curve (see Fig 7.3) was fitted to a distribution function by polynomi al regression and the resulting expression employed to calculate the number of drops in each drop diameter interval (2 μm). The total capture rate for a mesh layer was then calculated by application of equations 10.9 and 10.11 to each size interval. Assuming no drop redispersion, the input of suspended drops to the second layer was determined as the difference between the drops entering the bed inlet and those captured in the first layer.

This calculation procedure was repeated, for a bed consisting of 120 mesh layers, using a computer program given in Appendix N. A graph, presented in Fig 10.4., was plotted from the program output, which shows the removal rate of suspended drops as a function of bed depth. Changing the value of velocity has a negligible effect on this curve because only the Gravity number in equation 10.9

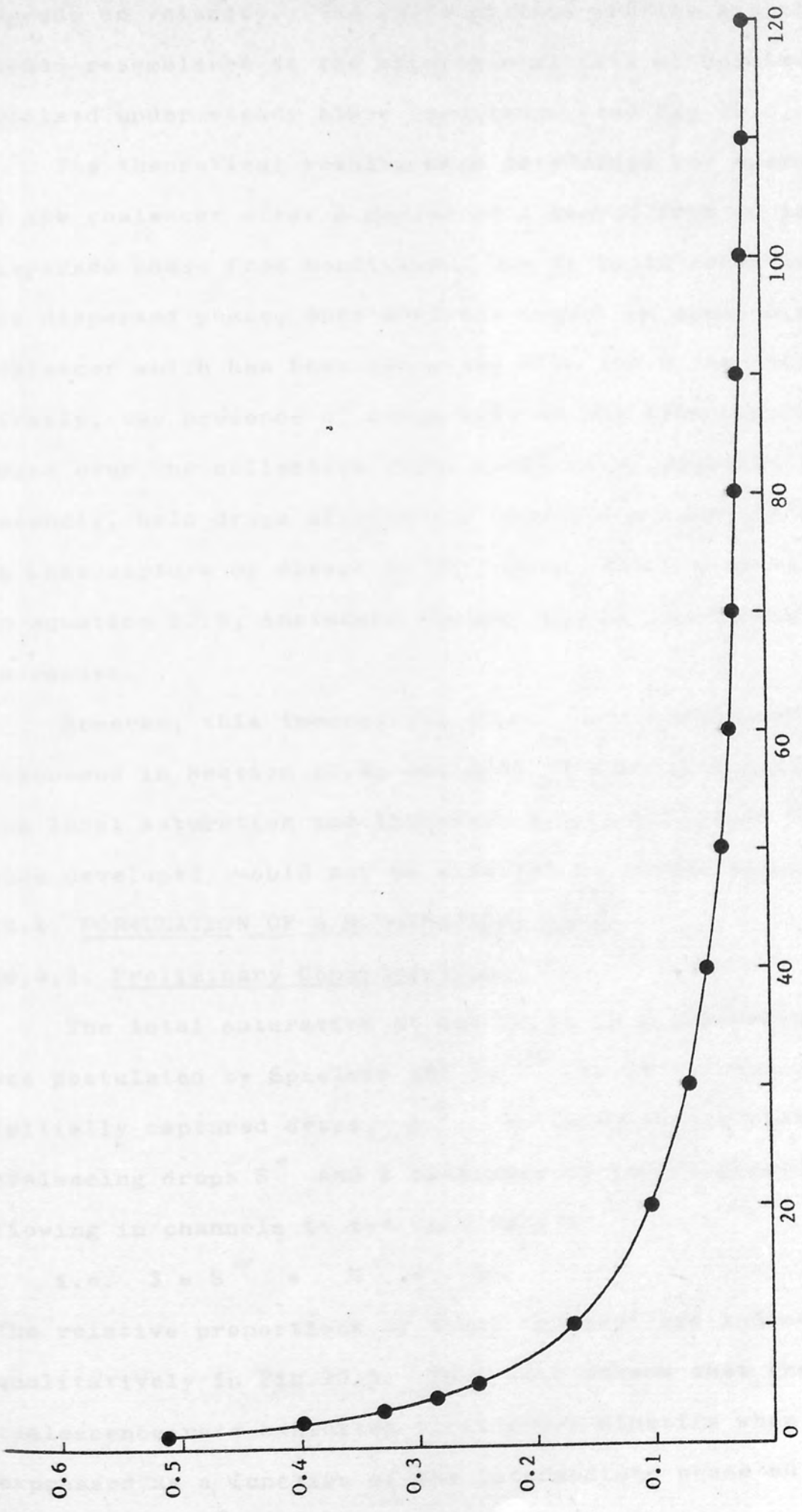

Fig.10.4 Variation of Volume Fraction of Dispersed Phase Uncaptured with Bed Depth.

depends on velocity. The shape of this profile exhibits a marked resemblance to the experimental data of Spielman [67] obtained under steady state conditions (see Fig 10.6).

The theoretical results were determined for operation of the coalescer after a period of 1 second from an initially dispersed phase free condition. Due to rapid accumulation of the dispersed phase, this analysis cannot be applied to a coalescer which has been operating even for a few seconds. Firstly, the presence of drops affects the flow of continuous phase over the collectors which invalidates equation 10.10. Secondly, held drops effectively reduce the aperture diameter so that capture by direct interception, which does not feature in equation 10.9, increases rapidly as the local saturation increases.

However, this theoretical approach is useful because, as discussed in Section 10.4, the drop capture rate depends on the local saturation and therefore the drop capture profile, once developed, would not be expected to change significantly.

10.4. FORMULATION OF A MATHEMATICAL MODEL.

10.4.1. Preliminary Considerations.

The total saturation at any point in a coalescing bed was postulated by Spielman and Su [67] to be the sum of the initially captured drops, S''' an intermediate phase of coalescing drops S'' and a continuum of the dispersed phase flowing in channels to the exit face S'

$$\text{i.e. } S = S''' + S'' + S' \qquad 10.12$$

The relative proportions of these 'phases' are indicated qualitatively in Fig.10.5. They also showed that the coalescence rate exhibited first order kinetics when expressed as a function of the intermediate phase saturation, S'' but that the permeability to the continuous phase depended on the total saturation, S. It was further assumed

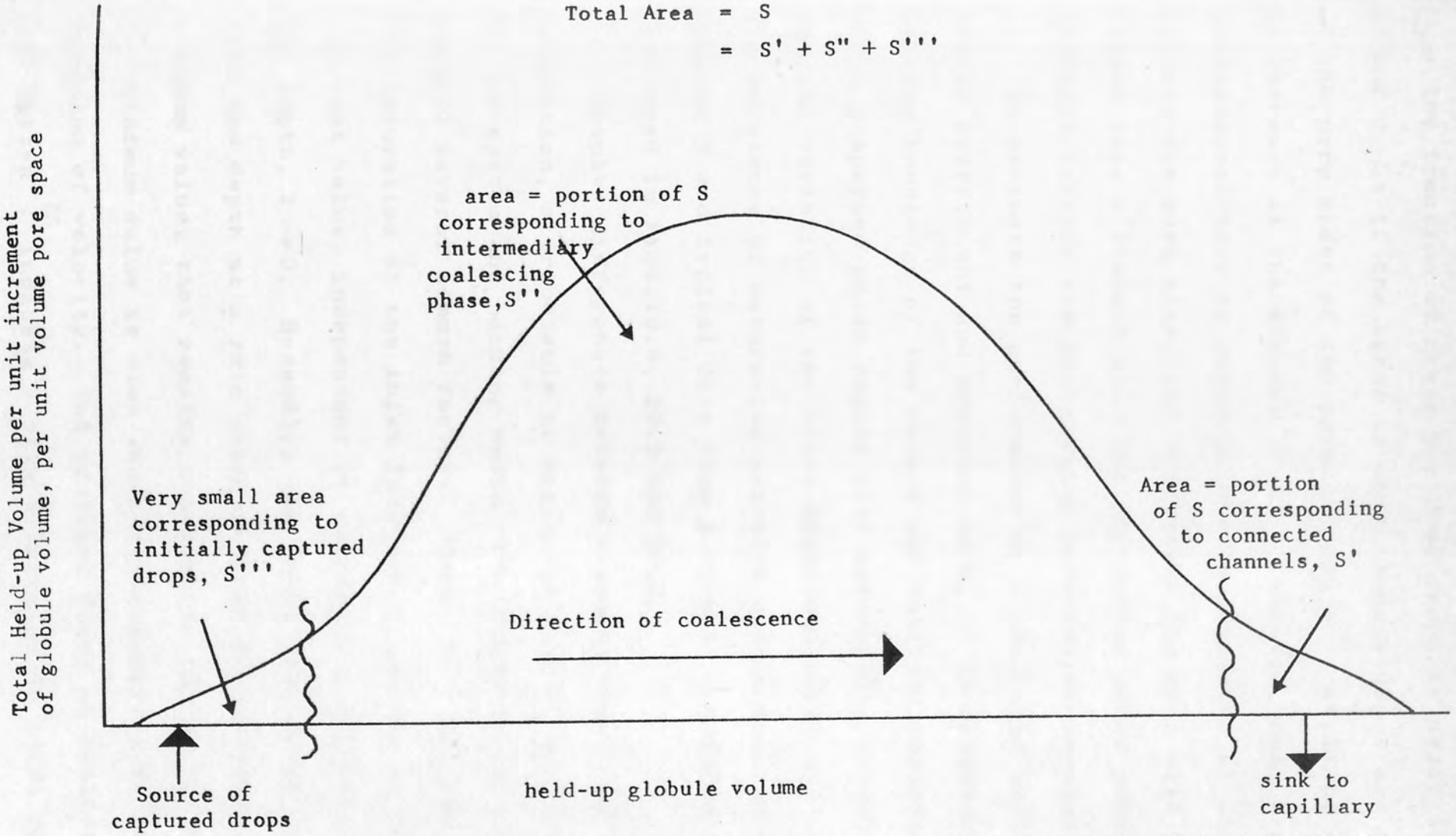

Fig.10.5 Qualitative distribution of the total volume of held-up oil over individual held-up globule volumes. Drops are captured at the left hand end of the spectrum. Dispersed phase is transferred to successively larger drops by coalescence eventually leaving by capillary condunction at the right.

that the fraction of newly captured drops is negligible i.e. $S'' \longrightarrow 0$ but if the sizes of these source drops are comparable to the pore sizes of the packing then S''' would be expected to increase at the expense of S'' . that is, only a few coalescences have to occur before the diameter of the drop exceeds the pore size, and eventually the drop will be forced into a channel when the continuous phase pressure gradient exceeds the restraining interfacial tension forces

To evaluate the performance of a coalescer in terms of filter coefficient and pressure drop, it is necessary to combine knowledge of the nature and relative amounts of the local dispersed phase regime with information concerning the spatial variation of the total dispersed phase saturation. The existence of saturation profiles has been discussed in Chapter 5 and typical data from a number of studies is presented in Figs.10.6, 10.7 and 10.8.

Despite differences between absolute values of local saturation, attributable to different operating parameters of the system and packing media, the shapes of the profiles exhibit several common factors. There is a maximum value of the saturation at the inlet face which appears to have a constant value, independent of superficial velocity, as the bed depth, $l \rightarrow 0$. Secondly, the local saturation decays with bed depth at a rate which depends on velocity, to a minimum value, that remains constant as far as the exit face. The minimum value is also shown experimentally to be a function of velocity. The profiles found by Shalhoub[70] and Bitten[85] indicate a slight increase in local saturation just upstream of the exit face for which no satisfactory explanation is available at present.

In this experimental study, it was not possible to measure the saturation profile without interfering with the

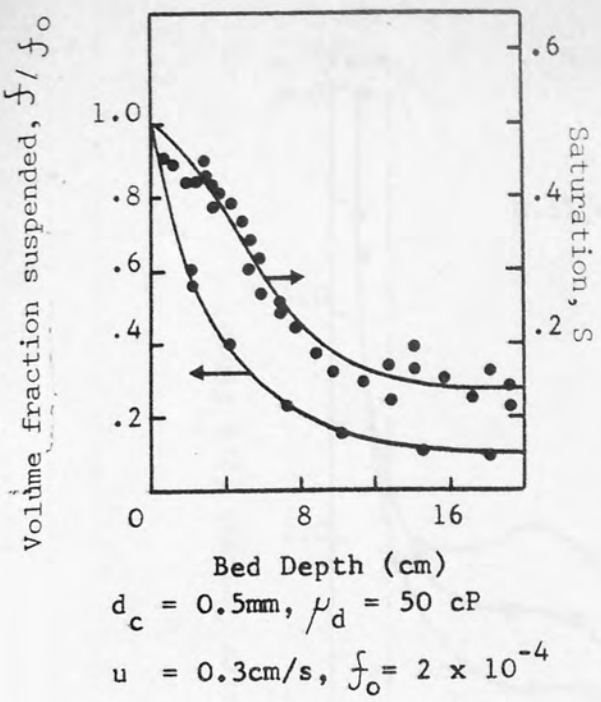

d_c = 0.5mm, μ_d = 50 cP

u = 0.3cm/s, $f_o = 2 \times 10^{-4}$

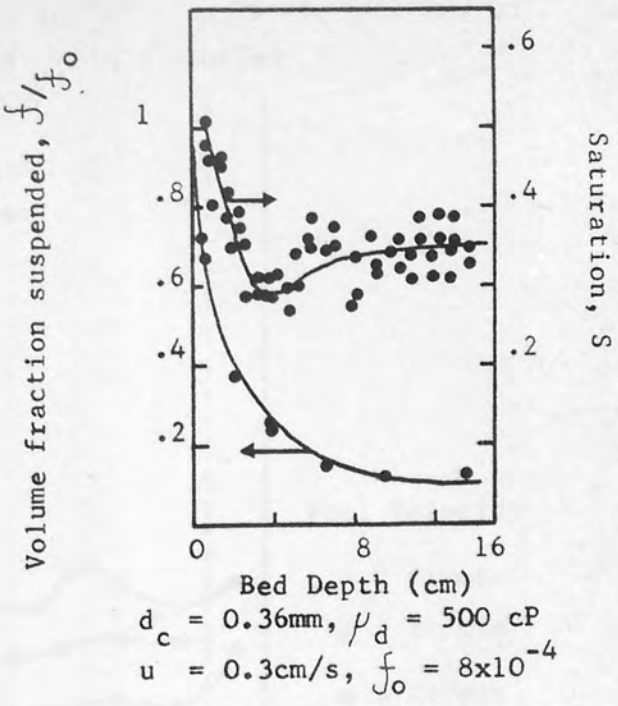

d_c = 0.36mm, μ_d = 500 cP

u = 0.3cm/s, $f_o = 8 \times 10^{-4}$

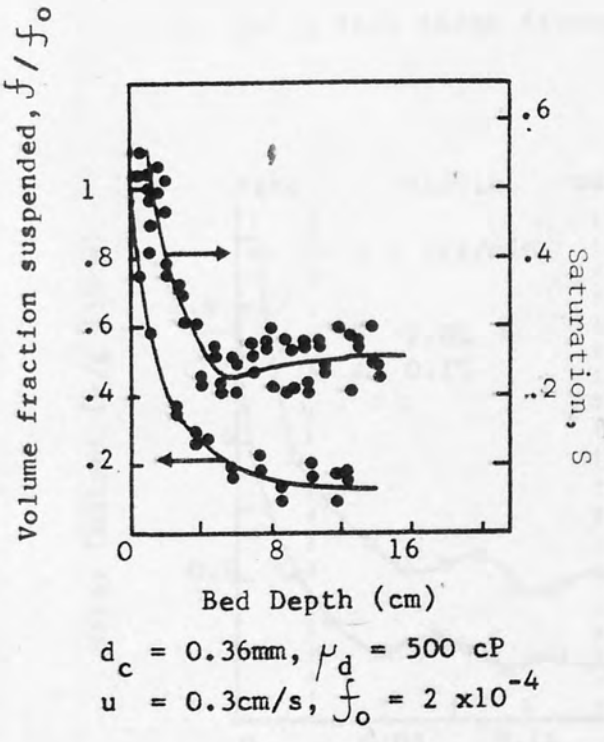

d_c = 0.36mm, μ_d = 500 cP

u = 0.3cm/s, $f_o = 2 \times 10^{-4}$

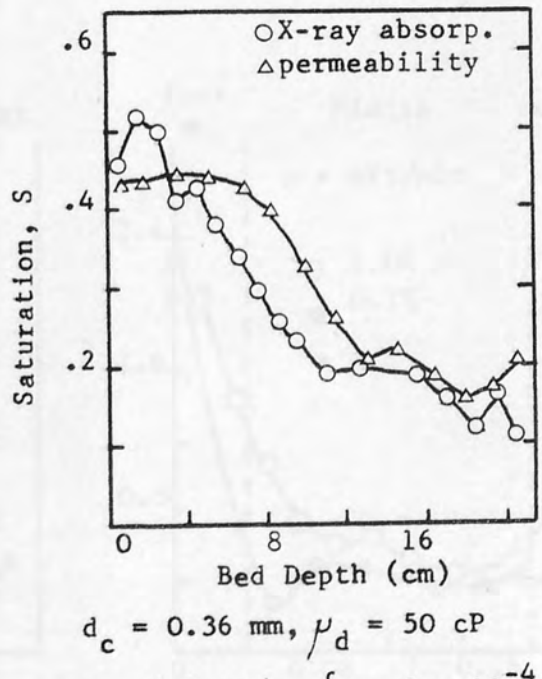

d_c = 0.36 mm, μ_d = 50 cP

u = 0.6 cm/s, $f_o = 2 \times 10^{-4}$

Fig 10.6 Variation of Volume Fraction of Suspended Drops and Dispersed Phase Saturation with Bed Depth.

(Data of Spielman and Su)

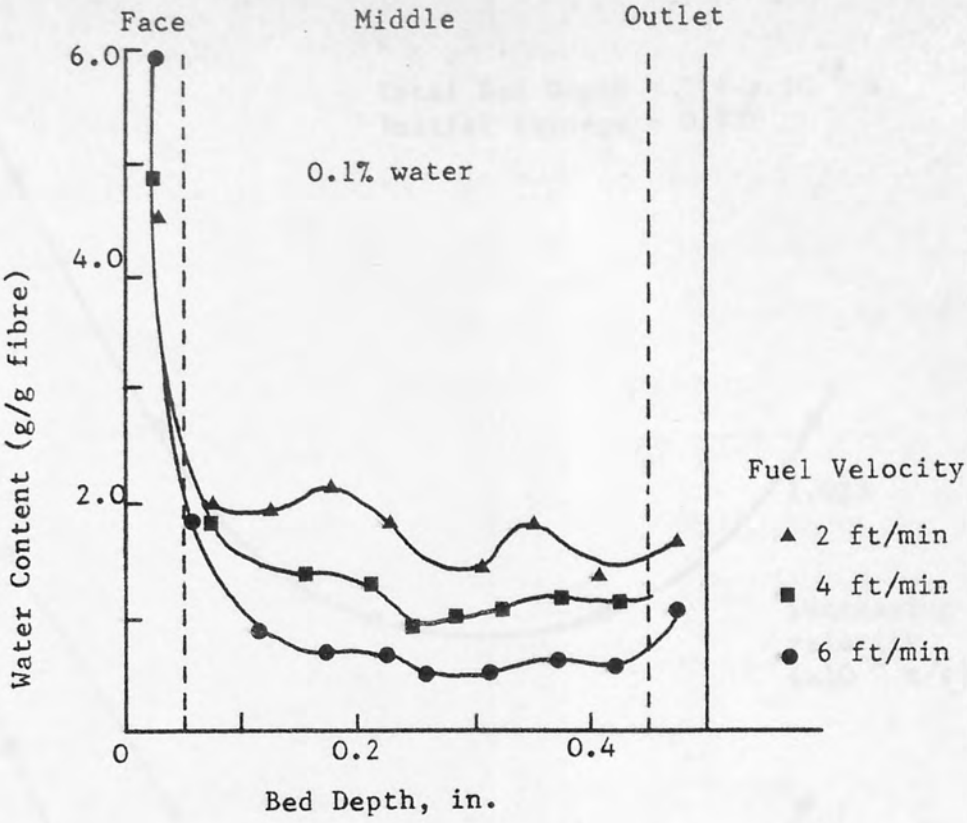

(a) ½ inch thick fibreglass coalescer (6 lb/ft^3).

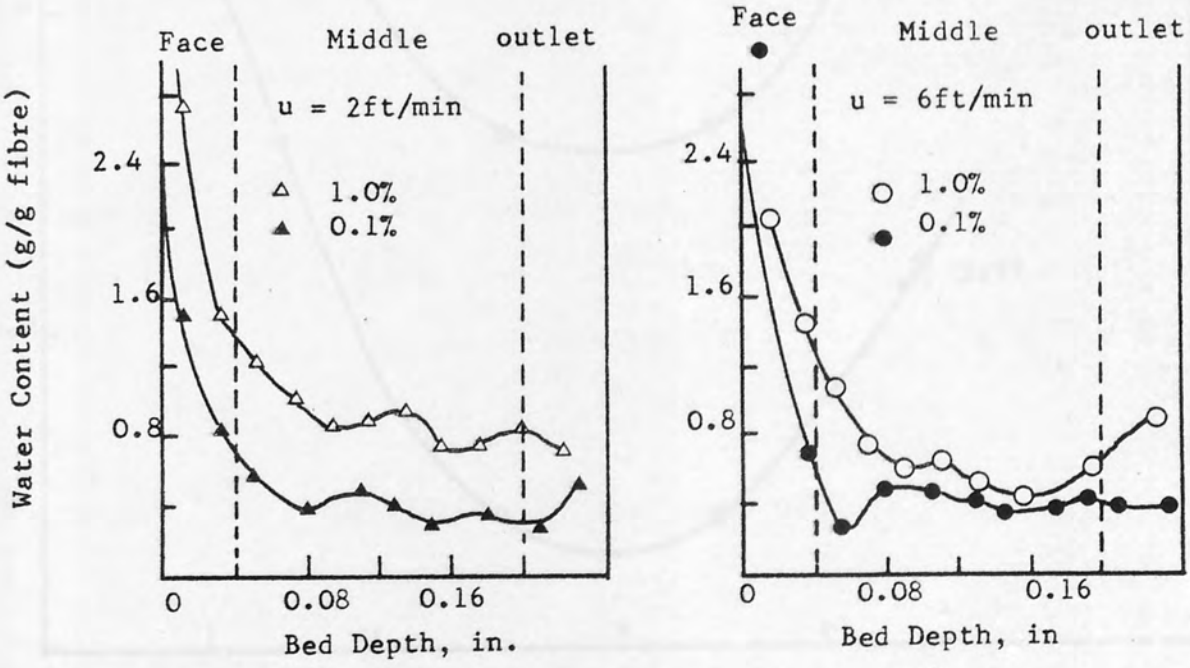

(b) ½ inch thick fibreglass coalescer (14 lb/ft^3)

Fig 10.7 Variation of Hold-up with Bed Depth.
(Data of Bitten and Fochtman).

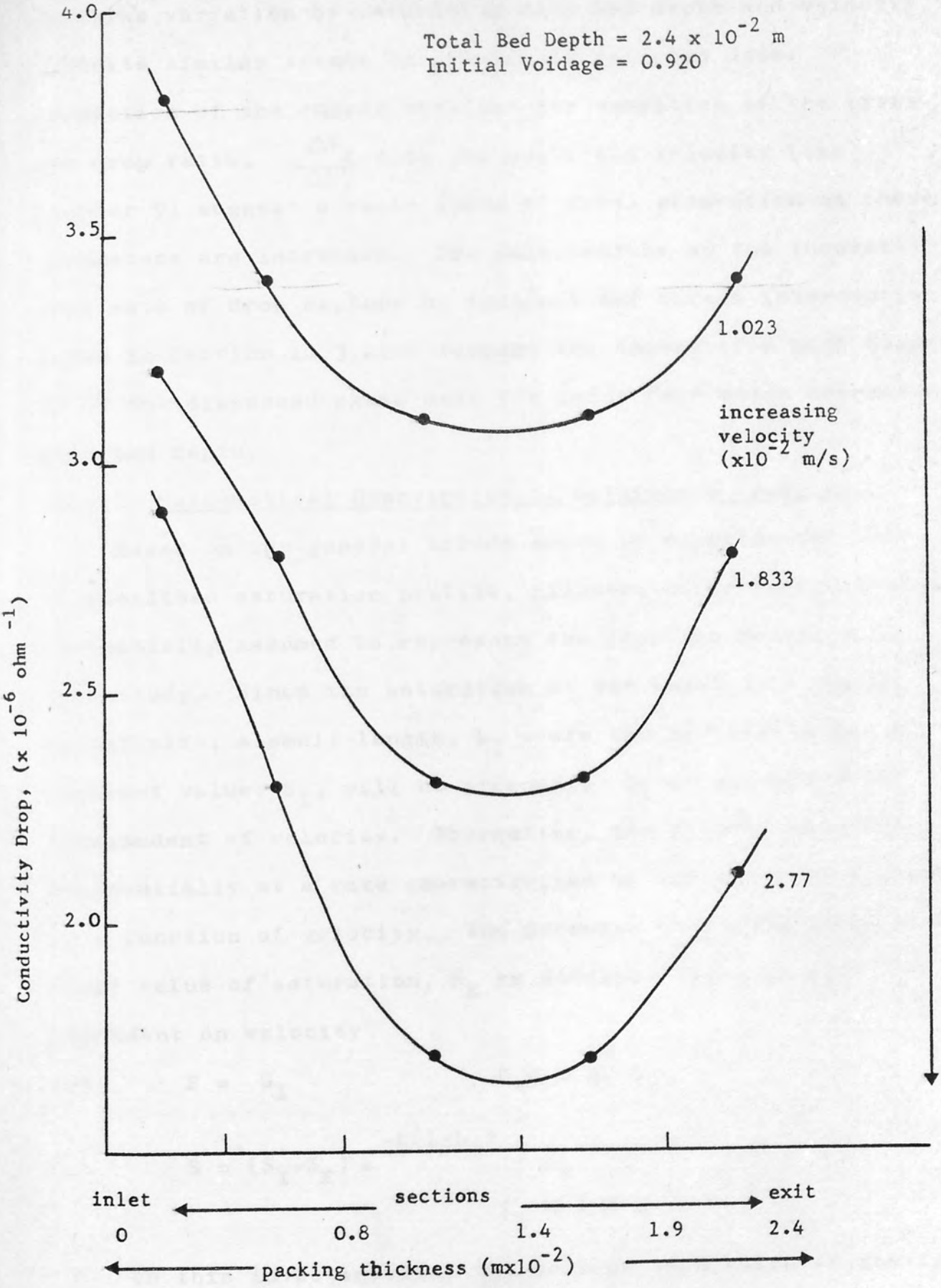

Fig 10.8 Variation of Hold-up with Superficial Velocity (Data of Shalhoub).

coalescence process and therefore it was necessary to assume that the variation of saturation with bed depth and velocity exhibits similar trends to previously reported data. Inspection of the curves obtained for variation of the pressure drop ratio, $\frac{\Delta P_2}{\Delta P_1}$ with bed depth and velocity (see Chapter 9) suggest a rapid decay of local saturation as these parameters are increased. The calculations of the theoretical rate of drop capture by indirect and direct interception given in Section 10.3 also support the theory of a high hold-up of the dispersed phase near the inlet face which decreases with bed depth.

10.4.2. Mathematical Description of Saturation Profiles.

Based on the general trends shown by experimental data, an idealised saturation profile, illustrated in Fig.10.9 will be initially assumed to represent the profiles existing in this study. Since the saturation at the inlet face cannot be infinite, a small length, L_I where the saturation has a constant value, S_I, will be proposed. S_I is assumed to be independent of velocity. Thereafter, the saturation decays exponentially at a rate characterised by the value of k which is a function of velocity. The decrease continues until a final value of saturation, S_E is attained which is also dependent on velocity.

i.e. $S = S_I \qquad 0 < 1 \leqslant L_I$

$$S = (S_I - S_E)\, e^{-k(1-L_I)} + S_E \qquad L_I \leqslant 1 \leqslant L \qquad 10.13$$

In this investigation, the average saturation at steady state, $\bar{S}$ was determined on completion of an experiment and may be expressed mathematically by integration of the profile between 0 and L,

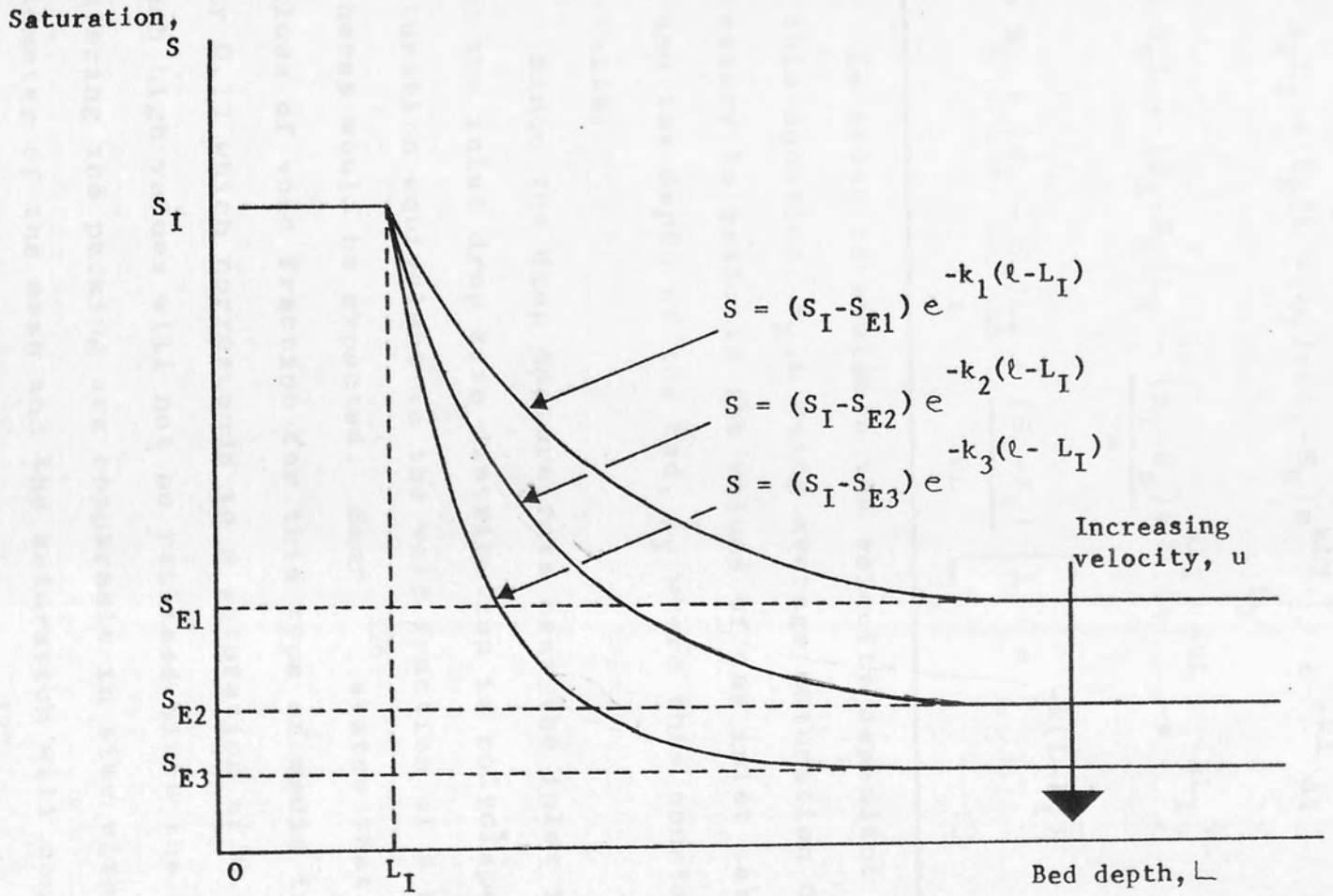

Fig. 10.9. Idealised Saturation Profiles.

$$\bar{S} = \frac{\int_o^L S\,dl}{\int_o^L dl}$$

$$\bar{S}L = \int_o^{L_I} S_I\,dl + \int_{L_I}^{L} (S_I - S_E)e^{-k(l-L_I)} + S_E\,dl$$

$$= S_I L_I + S_E(L - L_I) + (S_I - S_E)e^{kL_I}\int_{L_I}^{L} e^{-kl}\,dl$$

$$= S_E L + (S_I - S_E)L_I - \frac{(S_I - S_E)}{k}e^{kL_I}(e^{-kL} - e^{-kL_I})$$

$$\bar{S} = S_E + (S_I - S_E)\frac{L_I}{L} + \frac{(S_I - S_E)}{kL}\left[1 - e^{-k(L-L_I)}\right] \qquad 10.14$$

In order to evaluate the velocity dependent parameters of this equation, S_E, k using average saturation data, it is necessary to estimate the values of the inlet saturation, S_I and the depth of the bed, L_I where this constant value prevails.

Since the drop capture rate near the inlet face is high and the inlet drop size distribution is polydisperse, a saturation equivalent to the void fraction of a bed of mixed spheres would be expected. Bear [126] states that typical values of void fraction for this type of media is approximately 0.17 which corresponds to a saturation of 0.83. However, such high values will not be realised since the drops entering the packing are comparable in size with the aperture diameter of the mesh and the saturation will consequently be reduced by this 'wall effect'. Brown [127] gives a correlation between void fraction and the diameter ratio, $\frac{d_p}{d_a}$ which for a mean drop size of 25 μm and a aperture diameter of 53 μm, $\frac{d_p}{d_a} = 0.472$ gives $e_p = 0.45$ corresponding to a

saturation of 0.55. This value is in close agreement with the data of Spielman and will be used as an initial estimate of S_I.

The experimentally determined profiles all indicate that the decay of saturation with bed depth occurs very close to the inlet face implying that L_I is very small. However, since the saturation must be zero at the inlet face, in the absence of flooding, a small finite value will be assigned to L_I. Again, as an initial estimate, L_I will be assumed to be equal to the length of a single layer of mesh i.e. $2d_c$. Although the saturation will increase from 0 to S_I within a very small distance from the inlet face ie $\ll L_I$, omission of this section of the saturation profile from the integration of equation 10.13 will not incur any significant error.

Inspection of equation 10.14 shows that if the parameter, k is large, then the decay will approximate to a step change in saturation at L_I from S_I to S_E, and equation 10.14 becomes

$$\bar{S} \simeq S_E + (S_I - S_E) \frac{L_I}{L} \quad \text{for large k} \qquad 10.15$$

Figs.10.6, 10.7 and 10.8 indicate that this condition may be satisfied, especially for high velocities and bed depths.

10.5. TWO PHASE PRESSURE DROP PREDICTION.

10.5.1. Previous Models.

The prediction of pressure drop across a coalescing bed has been attempted only by those workers who advocated the travelling drop model which implies a constant saturation throughout the length of the bed. The equation proposed by Sherony [64] was based on the Blake-Kozeny equation which on rearrangement, may be expressed as,

$$\frac{\Delta P_2}{\Delta P_1} = \frac{\left[1 - e_1 (1-\bar{S})\right]^2}{(1-e_1)^2(1-\bar{S})^3} \qquad 10.16$$

where the saturation, $\bar{S}$ is determined from a curve giving the variation of $\frac{e_1 \bar{S}}{(1-e_1)}$ with Reynolds Number, $N_{Re} = \frac{u d_c \rho_c}{\mu_c}$

Rosenfeld and Wasan suggest a similar, simplified equation,

$$\frac{\Delta P_2}{\Delta P_1} = \left[1 + \frac{e_1 \bar{S}}{1-e_1}\right]^{2/3} \qquad 10.17$$

where $\bar{S}$ may be correlated with superficial velocity using

$$\bar{S} = C \frac{(1-e_1)u}{e_1}^{-n}$$

Rosenfeld determined the values of the parameters, C and n to be 0.8 and 0.2 respectively when u is measured in ft/min. These models are inadequate representations of experimental data since they predict that the pressure drop ratio is independent of bed depth which is contrary to the variation shown in Figs.9.6, 9.7, 9.8, 9.9, 9.10, 9.11. An entirely empirical approach was adopted by Euzen [124] who fitted their data to the following type equation,

$$\frac{\Delta P_2}{\Delta P_1} = k^1 (uL)^{-0.14} \qquad 10.18$$

where the constant k^1 depends on the liquid system studied. Correlation of the data in the above form was attempted in Chapter 9 but the value of the exponent was found to vary considerably for different mesh types and a better fit was obtained by considering the exponent of u and L separately.

10.5.2. Derivation of Proposed Equation.

Therefore, generally, the ability of existing equations to predict two phase pressure drop for the operating conditions applied in this study was not acceptable. As the

Blake-Kozeny equation proved to be successful for correlating single phase pressure drop, it was used as the basis for this model. However, the Blake Kozeny equation must be modified since during two phase flow, the bed consists of a mixture of 'cylinders' and 'spheres' which possess different values of specific surface, a.

For single phase flow through an element of bed depth; δl,

$$\frac{\delta P_1}{\delta l} = \frac{K \mu_c u (1-e_1)^2 a_1^2}{e_1^3} \qquad 10.19$$

by writing equation 10.19 by analogy for two phase flow

$$\frac{\delta P_2}{\delta l} = \frac{K \mu_c u (1-e_2)^2 a_2^2}{e_2^3} \qquad 10.20$$

where $e_2 = e_1 (1 - S)$

$$a_2 = \frac{\left[\frac{6e_1S}{d_p} + \frac{4(1-e_1(1-S))}{d_c}\right]}{1 - e_1(1-S)}$$ for a

mixture of spheres and cylinders (see Appendix O)

substituting for e_2 and a_2 into 10.20 and taking the limit as $\delta l \longrightarrow 0$

$$\frac{dP_2}{dl} = \frac{K\mu_c u}{e_1^3} \frac{\left[\frac{6e_1S_1(1-e_1(1-S))}{d_p} + \frac{4(1-e_1(1-S))}{d_c}\right]^2}{(1 - S)^3} \qquad 10.21$$

The total two phase pressure drop may now be determined by integration of equation 10.21 between the limits of 0 and L

$$\therefore \Delta P_2 = \frac{K\mu_c u}{e_1^3} \int_0^L \frac{\left[\frac{6e_1S\left[1-e_1(1-S)\right]}{d_p} + \frac{4\left[1-e_1(1-S)\right]}{d_c}\right]^2}{(1-S)^3} dl \qquad 10.22$$

Similarly from equation 10.19,

$$\Delta P_1 = \frac{16K \mu_c u (1-e_1)^2 L}{d_c^2 e_1^3} \qquad 10.23$$

$$\text{then } \frac{\Delta P_2}{\Delta P_1} = \frac{d_c^2}{16(1-e_1)^2 L} \int_0^L f(S)\, dl \qquad 10.24$$

$$\text{where } f(S) = \frac{\left\{ \frac{6}{d_p}\left[e_1 S \left(1-e_1(1-S) \right) \right] + \frac{4}{d_c}\left[1-e_1(1-S) \right] \right\}^2}{(1-S)^3} \qquad 10.25$$

by letting $a' = \frac{6}{d_p}$ and $b' = \frac{4}{d_c}$, the numerator of the right hand side of equation 10.25 becomes,

$$\left\{ a' e_1 S \left[1-e_1 + e_1 S \right] + b' \left[1-e_1 + e_1 S \right] \right\}^2$$

further rearrangement gives,

$$\left\{ a' e_1^2 S^2 + e_1 \left[b' + a'(1-e_1) \right] S + b'(1-e_1) \right\}^2$$

introducing the following constants to simplify the coefficients,

let $c' = a' e_1^2$; $d' = e_1 \left[b' + a'(1-e_1) \right]$

$$e' = b'(1-e_1)$$

equation 10.25 is given by,

$$f(S) = \frac{(c'S^2 + d'S + e')^2}{(1-S)^3}$$

$$\text{or } f(S) = \frac{aS^4 + bS^3 + cS^2 + dS + f}{(1-S)^3}$$

where $a = c'^2$; $b = 2b'c'$; $c = 2c'e' + d'^2$

$$d = 2d'e' \; ; \; f = e'^2$$

considering equation 10.24, the integration of $f(S)$ cannot be performed in one stage since a discontinuity appears in the mathematical description of the saturation profile. From equation 10.13, when $0 < l \leqslant L_I$, $S = S_I$ and is independent

of l, therefore,

$$\int_0^{L_I} f(S)dl = \left[\frac{a\,S_I^4+bS_I^3+bS_I^3+cS_I^2+dS_I+f}{(1-S_I)^3}\right] L_I \qquad 10.26$$

When $L_I \leqslant l \leqslant L$, $S = (S_I-S_E)e^{-k(l-L_I)} + S_E$

Letting $g = (S_I - S_E)$; $h = S_E$

and substituting $v = ge^{-k(l-L_I)} + h$

$$\frac{dv}{dl} = -kge^{-k(l-L_I)}$$

$$= -k\,(v-h)$$

$$\text{or} \quad dl = -\frac{dv}{k(v-h)}$$

also when $l = L_I$, $v = g + h$

$l = L$, $v = ge^{-k(L-L_I)} + h$

$$\therefore \int_{L_I}^{L} f(S)\,dl = \int_{g+h}^{ge^{-k(L-L_I)}+h} f(v)\ \frac{-dv}{k(v-h)}$$

$$= \frac{1}{k}\int_{ge^{-k(L-L_I)}+h}^{g+h} \frac{(av^4+bv^3+cv^2+dv+f)}{(v-h)(1-v)^3}\,dv \qquad 10.27$$

Evaluation of the integral given by equation 10.27 is fairly straightforward but tedious and so has been completed in Appendix P. The final result (equation P.9) is lengthy and expansion of the presented form would be complex and unnecessary but quite feasible since this is an analytical solution.

The total pressure drop across the bed will therefore be predicted using,

$$\frac{\Delta P_2}{\Delta P_1} = \frac{d_c^2}{16(1-e_1)L}\left[\int_0^{L_I} f(S)dl + \int_{L_I}^{L} f(S)dl\right] \qquad 10.28$$

where $\int_0^{L_I} f(S)\,dl$ is determined using equation 10.26

and $\int_{L_I}^{L} f(S)\,dl$ is determined using equation P.9.

10.6. TESTING THE MODEL.

10.6.1. Evaluation of Parameters from Saturation Data.

As discussed in Section 10.4.2., using assumed values of S_I and L_I, it is possible to estimate the exit saturation, S_E and the decay factor, k. From equation 10.14,

$$\bar{S} = S_E + (S_I - S_E)\ \frac{L_I}{L} + \frac{(S_I - S_E)}{kL}\left[1 - e^{-k(L-L_I)}\right] \qquad 10.14$$

When the rate of decay is large and L_I is small compared with L, then $e^{-k(L-L_I)} \longrightarrow 0$ and equation 10.14 becomes,

$$S = S_E + (S_I - S_E)\ (L_I + \frac{1}{k}).\ \frac{1}{L} \qquad 10.29$$

The average saturation results for the stainless steel meshes were plotted against the reciprocal of bed depth as shown in Fig 10.10. The linear relationship produced for all velocities confirms that the model is qualitatively valid.

The intercept, S_E and the slope, $(S_I - S_E)(L_I + \frac{1}{k})$ were determined by linear regression analysis of the data in Fig 10.10. Then the four parameters characterising the proposed saturation profiles, S_I, S_E, L_I and k were used to predict the two phase pressure drop ratio from equation 10.28.

10.6.2. Comparison with Experimental Data.

A computer program was employed to calculate $\frac{\Delta P_2}{\Delta P_1}$ (see Appendix Q.1) from the parameters extracted from saturation data and the output, which expresses the ratio, $\frac{\Delta P_2}{\Delta P_1}$ in terms of total bed depth for each velocity, is given in Appendix Q.2. The predicted ratios were then plotted against experimental values from Appendix H Although some

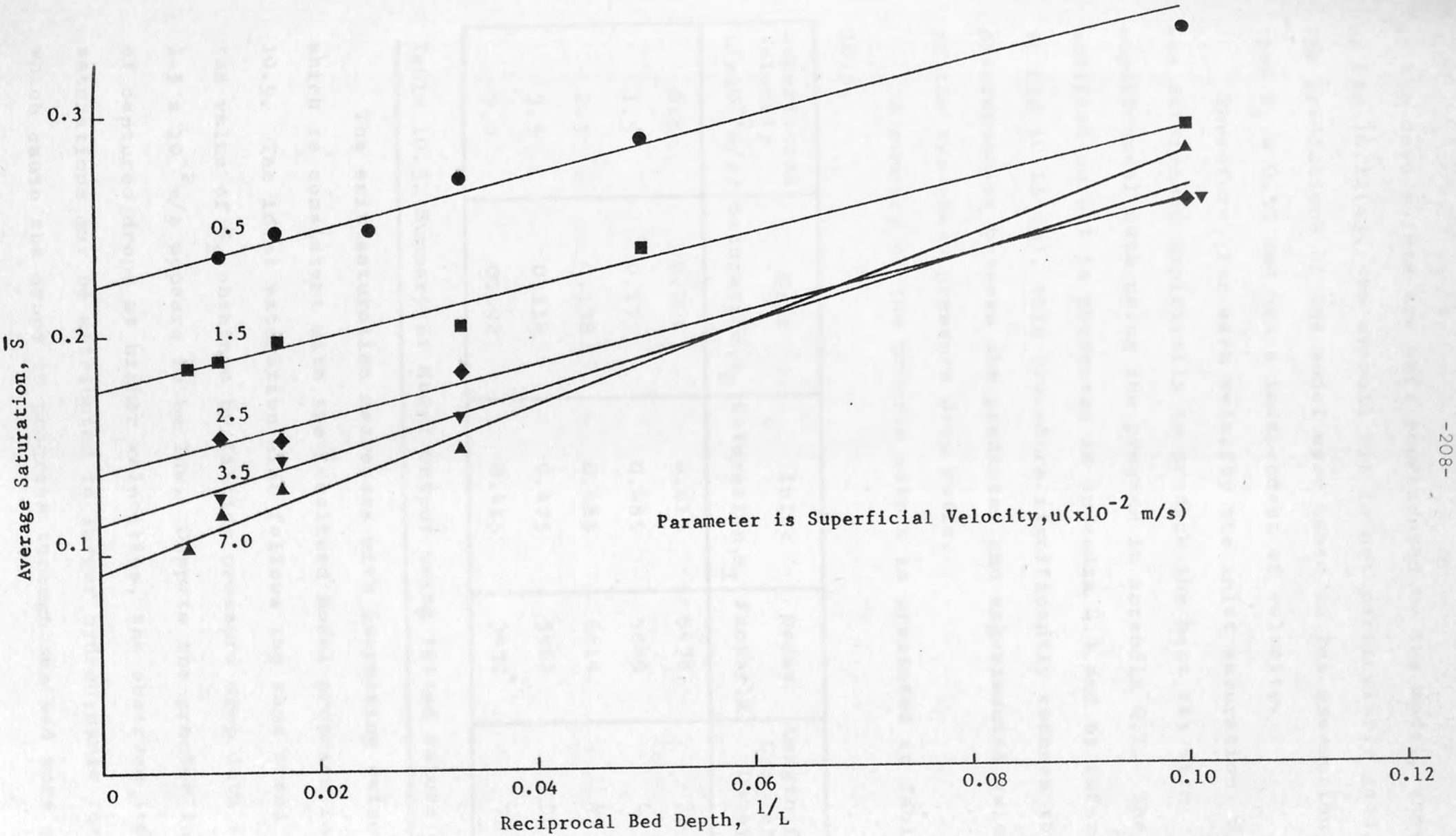

Fig. 10.10. Plot of average Saturation VS. Reciprocal Bed Depth for S300 Mesh at different velocities.

of the data points are well represented by the model, shown by Fig 10.11(a), the overall fit is not particularly good. The predictions of the model were based on the assumption that S_I = 0.55 and hence independent of velocity.

Therefore, for each velocity the inlet saturation, S_I was determined empirically to produce the best fit with experimental data using the program in Appendix Q.1. The modified output is presented in Appendix Q.3 and by reference to Fig 10.11 (b), this procedure significantly reduces the discrepancies between the predicted and experimental values of the two phase pressure drop ratio.

A summary of the program output is presented in Table 10.5.

Superficial Velocity $u(x10^{-2}m/s)$	Exit Saturation, S_E	Inlet Saturation, S_I	Decay Factor, k	Length for Complete Decay
0.5	0.226	0.615	8478	33
1.5	0.175	0.485	5849	47
2.5	0.138	0.485	6614	41
3.5	0.114	0.475	5462	50
7.0	0.092	0.415	3432	78

Table 10.5. Summary of Model Output using fitted values of S_I

The exit saturation decreases with increasing velocity which is consistent with the idealised model proposed in Fig 10.9. The inlet saturation also follows the same trend but the value of S_I obtained by fitting pressure drop data for 1.5 x 10^{-2}m/s appears to be low. Despite the greater influx of captured drops at higher velocities, the observed lower saturations may be attributed to larger hydrodynamic forces which cause the drops to progress through the bed more quickly.

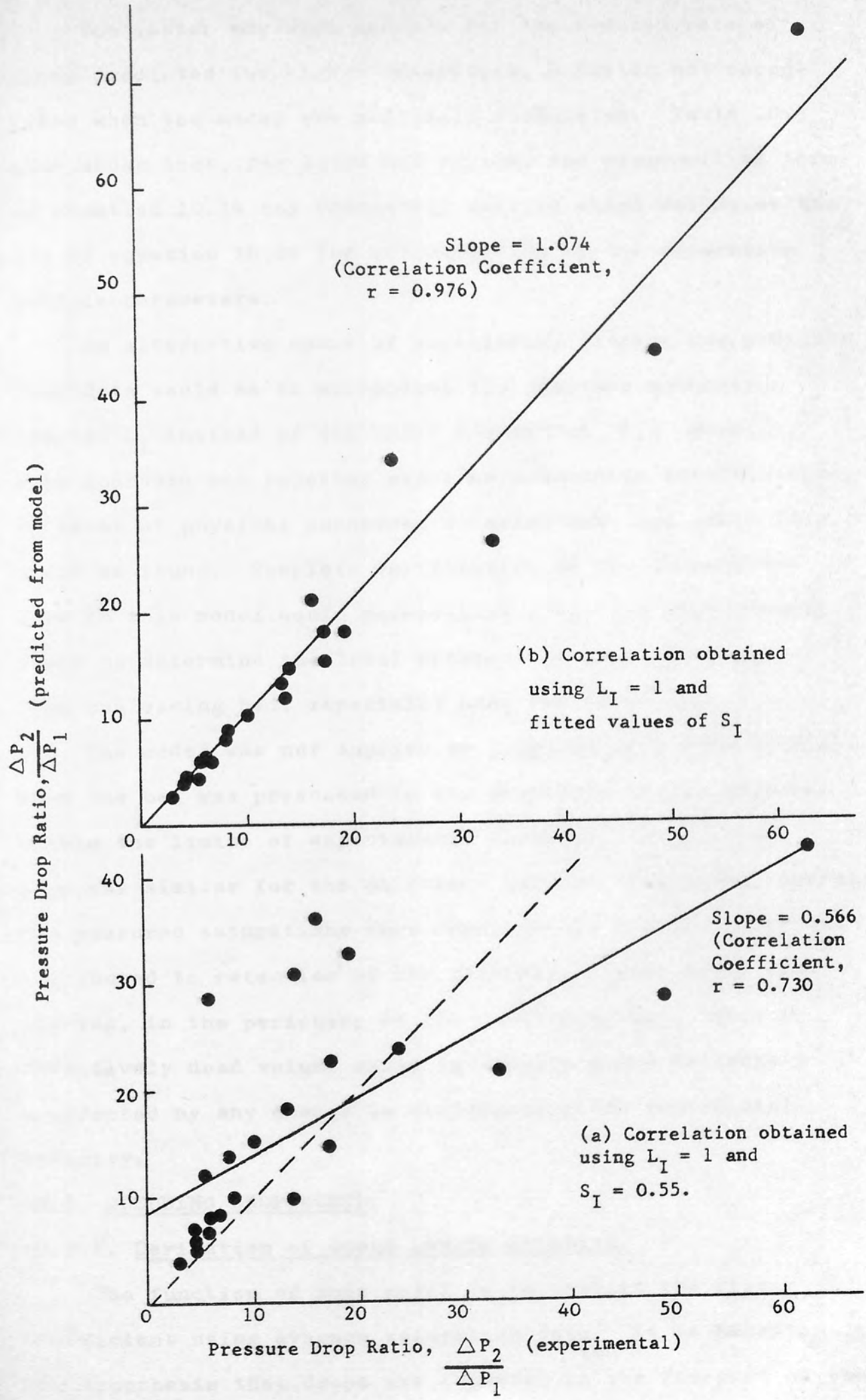

Fig.10.11. Comparison of Experimental and Predicted Pressure Drop.

The latter may also account for the reduced rate of decay predicted for higher velocities, a factor not recognised when the model was initially formulated. Table 10.5 also shows that, for large bed depths, the exponential term of equation 10.14 has completely decayed which validates the use of equation 10.29 for determination of the saturation profile parameters.

An alternative means of empirically fitting the pressure drop data would be to manipulate the constant saturation length, L_I instead of the inlet saturation, S_I. However, this approach was rejected since no reasonable justification, in terms of physical phenomena occuring near the inlet face, could be found. Complete verification of the assumptions made in this model would necessitate a further experimental study to determine the local saturations in a relatively deep coalescing bed, especially near the inlet face.

The model was not applied to pressure drop data obtained when the bed was presoaked in the dispersed phase, because, within the limits of experimental accuracy, the pressure drop was similar for the different initial conditions, whereas the measured saturations were considerably higher. This was attributed to retention of the dispersed phase, after presoaking, in the periphery of the coalescing bed. This is effectively dead volume whose saturation would be largely unaffected by any change in continuous phase superficial velocity.

10.7. QUEUEING DROP MODEL.

10.7.1. Derivation of Queue Length Equation.

The function of this model is to predict the filter coefficient using average saturation data. It is based on the hypothesis that drops are captured in the forepart of the bed where they accumulate until coalescence into a dispersed

phase continuum occurs. The dispersed phase is then conveyed in discrete channels to the release sites located on the exit face of the coalescer. As shown in Fig 10.12, the model recognises an analogy between drops waiting to coalesce into a dispersed phase continuum and 'customers' queueing at a service facility. A coalescer may therefore be considered to behave as a number of service channels in parallel, each of mean service rate, μ . The 'customer' arrival rate, due to capture by fibres and held drops, has a mean value, λ . Prediction of the mean queue length may then be employed to estimate the position of the service facility in the bed and hence determine the dispersed phase saturation.

This analogy may be pursued further by considering 'customer impatience' at a service facility which corresponds to redispersion of drops before coalescence into the continuum. The fraction of 'customers' which join the queue when there are n units in the system is given by,

$$f_n = e^{\frac{-\alpha n}{\mu}} \qquad 10.30$$

This expression indicates that redispersion becomes more important as the saturation increases (n increases) or as coalescence time increases (θ or $1/\mu$ increases). The 'impatience factor', α which must be determined experimentally is analogous to the ratio describing the rate of coalescence to the rate of drop capture [64].

If there are n units in the queueing system, the probability that there are n units in the system at time t+dt is $P_n(t+dt)$. If the processes which cause a transition from this state are independent of time which is true for steady state operation,

$$P_n(t+dt) = \sum_m T_{mn}(dt)\ P_m(t) \qquad [128] \qquad 10.31$$

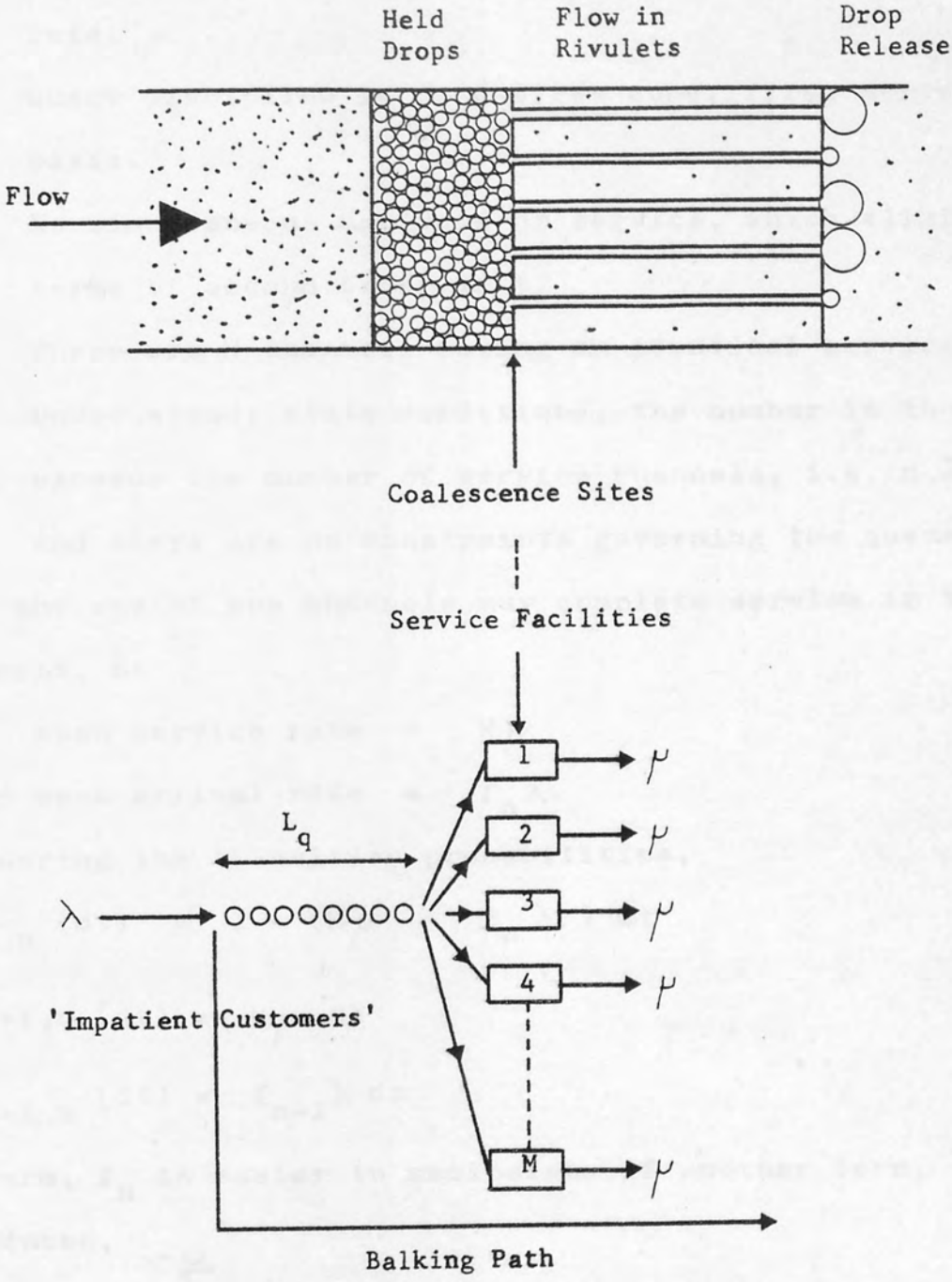

Fig 10.12 Diagrammative representation for analogy between Coalescence Process and Multiple Channel Queueing System.

The following assumptions are now introduced,

(i) Poisson arrival distribution of mean arrival rate, λ .

(ii) Exponential service distribution of mean service rate, μ .

(iii) Queue discipline is on a first come, first served basis.

(iv) No simultaneous arrivals or service, which eliminates terms of second order in t.

(v) There are M channels having an identical service rate.

(vi) Under steady state conditions, the number in the system exceeds the number of service channels, i.e. $n \geqslant M$ and there are no constraints governing the queue length.

Since any one of the channels may complete service in the time increment, dt

mean service rate = $M\mu$

and mean arrival rate = $f_n \lambda$

Considering the transition probabilities,

$$T_{n,n}(dt) = 1 - (M\mu + f_n \lambda)\, dt \qquad 10.32$$

$$T_{n+1,n}(dt) = M\mu\, dt \qquad 10.33$$

$$T_{n-1,n}(dt) = f_{n-1}\lambda\, dt \qquad 10.34$$

The term, f_n is easier to manipulate if another term, γ is introduced,

$$\gamma = e^{-\frac{\alpha}{2\mu}}$$

$$\text{then } f_n = \gamma^{2n} \quad ; \quad f_{n-1} = \gamma^{2n-2} \qquad 10.35$$

substituting for the transition probabilities from equations 10.32, 10.33 and 10.34 into equation 10.31 and noting that,

$$P_n(t+dt) = P_n(t)\, dt + dP_n$$

gives the following,

$$P_n(t)dt + dP_n = \left[M\mu\, P_{n+1}(t) + \left\{1-(M\mu + \gamma^{2n}\lambda)\right\} P_n(t) + \gamma^{2n-2}\lambda\, P_{n-1}(t)\right] dt \qquad 10.36$$

dividing by dt and setting $\frac{dP_n}{dt} = 0$ for steady state conditions,

$$M\mu P_{n+1} + \gamma^{2n-2}\lambda P_{n-1} - (M\mu + \gamma^{2n}\lambda)P_n = 0 \qquad 10.37$$

equation 10.37 takes a special form for n = 0 since P_{-1} does not exist and there is zero probability of moving from the state, n = 0 by completion of a service operation.

i.e. $P_{-1} = 0$; $n\mu P_n = 0$; $\gamma^{2n} = 1$

$$\therefore \quad \mu P_1 - \lambda P_o = 0 \qquad 10.38$$

dividing equation 10.37 by μM and defining the utilisation factor, $\rho = \frac{\lambda}{\mu M}$,

$$P_{n+1} + \rho\gamma^{2n-2} P_{n-1} - (1 + \rho\gamma^{2n})P_n = 0 \qquad 10.39$$

for $n \geqslant M$.

If $n \leqslant M$, equation 10.39 becomes,

$$\left.\begin{aligned} (n+1)P_{n+1} + \rho\gamma^{2n-2} P_{n-1} - (n + \rho\gamma^{2n})P_n = 0 \\ P_1 = \rho P_o \quad \text{where} \quad \rho = \frac{\lambda}{\mu} \end{aligned}\right\} \qquad 10.40$$

The general solution of these equations is obtained by successively increasing the value of n, hence,

$$P_n = \frac{\rho^n \gamma^{n(n-1)}}{n!} P_o \qquad 1 \leqslant n \leqslant M \qquad 10.41$$

$$P_n = \frac{\rho^n \gamma^{n(n-1)} M^M}{M!} P_o \qquad M \leqslant n \qquad 10.42$$

The sum of the probabilities for all possible states of the system must be unity,

$$\therefore \quad \sum_{n=1}^{\infty} P_n = 1$$

from equation 10.42,

$$\sum_{n=1}^{\infty} \frac{\rho^n \gamma^{n.(n-1)} M^M P_o}{M!} = 1$$

$$\text{hence, } P_o = \frac{M!}{M^M \sum_{n-1}^{\infty} \rho^n \gamma^{n(n-1)}} \qquad 10.43$$

The length of the queue, L_q is given by,

$$L_q = \sum_{n=1}^{\infty} n P_n$$

$$\therefore \quad L_q = \frac{\sum_{n=1}^{\infty} n \rho^n \gamma^{n(n-1)}}{\sum_{n=1}^{\infty} \rho^n \gamma^{n(n-1)}} \qquad 10.44$$

10.7.2. Filter Coefficient.

Experimental data, as discussed in Chapter 8, indicates that secondary drops in the effluent arise because they are not captured rather than being produced by redispersion effects. The filter coefficient may therefore be related to the fraction of customers, f_n which undergo 'balking'. Writing equation 10.35 for steady state conditions when $n = L_q$,

$$f_{L_q} = \gamma^{2L_q} \qquad 10.45$$

Now, from Section 10.1, the filter coefficient, λ_c is given by,

$$\lambda_c = \frac{-\log_e (1 - f_{L_q})}{L} \qquad 10.46$$

Substituting for f_{L_q} from equation 10.45 and the bed depth, L,

$$\lambda_c = \frac{-\log_e (1 - \gamma^{2L_q})}{2d_c N_L} \qquad 10.47$$

The length of the 'queue', L_q, given by equation 10.44 is independent of the number of channels but is a function of γ. Assuming a utilisation factor of 1.0, values of 'queue' length were generated for different 'impatience' factors using a computer program and the results presented in Fig 10.13.

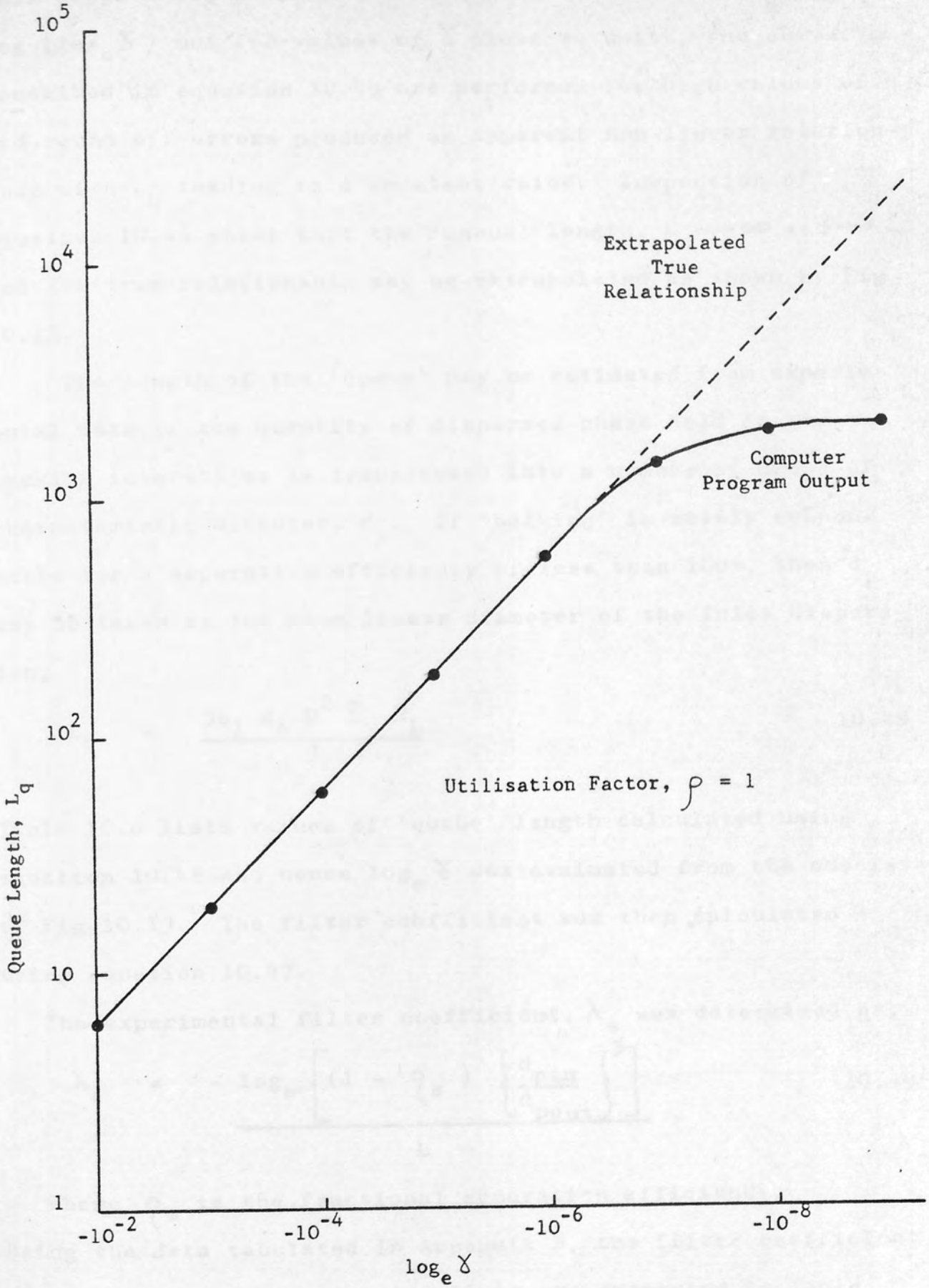

Fig 10.13. Variation of Steady State Queue length with degree of 'Balking'.

This graph shows a linear relationship between log (L_q) and log ($\log_e \gamma$) but for values of γ close to unity, the summations contained in equation 10.44 are performed for high values of n and round off errors produced an apparent non-linear relationship with L_q tending to a constant value. Inspection of equation 10.44 shows that the 'queue' length, $L_q \longrightarrow \infty$ as $\gamma \longrightarrow 1$ and the true relationship may be extrapolated as shown by Fig 10.13.

The length of the 'queue' may be estimated from experimental data if the quantity of dispersed phase held in the packing interstices is transformed into a number of drops of characteristic diameter, d_p. If 'balking' is solely responsible for a separation efficiency of less than 100%, then d_p may be taken as the mean linear diameter of the inlet dispersion,

$$L_q = \frac{3e_1 \, d_c \, D^2 \, \bar{S} \, N_L}{d_p^{\,3}} \qquad 10.48$$

Table 10.6 lists values of 'queue' length calculated using equation 10.48 and hence $\log_e \gamma$ was evaluated from the abscissa of Fig 10.13. The filter coefficient was then calculated using equation 10.47.

The experimental filter coefficient, λ_e was determined as,

$$\lambda_e = \frac{-\log_e \left[(1 - \eta_s) \left\{ \frac{d_{pin}}{d_{pout}} \right\}^3 \right]}{L} \qquad 10.49$$

where η_s is the fractional separation efficiency.

Using the data tabulated in Appendix H, the filter coefficient values obtained from equation 10.49 are presented in Table 10.6. Agreement between experimental and calculated filter coefficients within one order of magnitude was obtained for low velocities although experimental values were consistently lower. Above the critical velocity for this packing, the

Velocity $u(\times 10^{-2}$ m/s	Number Layers, N_L	Numberdrops in Queue, L_q $(\times 10^6)$	$\log_e \gamma$	Calculated Filter Coefficient, λ_c (m^{-1})	Experimental Filter Coefficient, λ_e (m^{-1})
0.5	10	22.43	-1×10^{-15}	27737	6118
"	20	38.10	-4×10^{-16}	14753	3418
"	30	53.76	-1.8×10^{-16}	10084	3003
"	40	65.84	-1.45×10^{-16}	7568	2470
"	60	98.37	-5.7×10^{-17}	5191	-
"	90	140.98	-3.2×10^{-17}	3500	702
1.5	10	9.29	-6.5×10^{-15}	27250	6139
"	20	15.20	-2.3×10^{-15}	14073	2623
"	30	19.56	-1.6×10^{-15}	9442	1836
"	60	37.59	-4×10^{-16}	4921	732
"	90	53.80	-1.8×10^{-16}	3361	512
"	120	70.59	-1.2×10^{-16}	2539	509
2.5	10	6.61	-1.3×10^{-14}	26671	972
"	30	14.07	-2.3×10^{-15}	9424	353
"	60	23.52	-1×10^{-15}	4799	458
"	90	35.28	-4.2×10^{-16}	3284	585

Table 10.6 (a) Comparison between Experimental and Predicted Filter Coefficients for S300 mesh.

Velocity $u(x10^{-2}$ m/s	Number Layers, N_L	Number drops in Queue, L_q $(x10^6)$	$\log_e \gamma$	Calculated Filter Coefficient, λ_c (m^{-1})	Experimental Filter Coefficient, λ_e (m^{-1})
3.5	10	6.61	$-1.3x10^{-14}$	26671	160
"	30	12.45	$-3.2x10^{-15}$	9310	167
"	60	21.83	$-1x10^{-15}$	4820	113
"	90	29.05	$-6x10^{-16}$	3254	380
7.0	10	7.17	$-1x10^{-14}$	26968	-
"	30	11.38	$-4x10^{-15}$	9237	263
"	60	19.98	$-1.6x10^{-15}$	4715	242
"	90	27.21	$-7x10^{-16}$	3238	241
"	120	31.36	$-5.5x10^{-16}$	2442	191

Table 10.6(b) Comparison between Experimental and Predicted Filter Coefficients for S300 mesh.

agreement rapidly deteriorates due to low separation efficiencies.

The only factor in the queueing model which depends on superficial velocity is the average saturation term of equation 10.48 but this alone does not adequately account for the effect of velocity. Inclusion of the phenomenon of 'reneging' into the model which corresponds to drops which join the 'queue' but leave due to redispersion may improve the prediction of filter coefficients. In Appendix B, it was demonstrated that the critical drop diameter for release is very sensitive to velocity so that the d_p term of equation 10.48 could be replaced by d_{pc} given by equation B.1.

Alternatively a velocity dependant term could be introduced into the expression postulated for 'customer impatience'. (equation 10.30).

Also, the model assumes a step change in saturation which is an oversimplification since the longitudinal variation of saturation would suggest that the analogy be better represented by a system of multiple channels in series. However, this statistical approach to determination of the filter coefficient yields results which are within the range of values predicted by previous models as shown in Section 10.1 and therefore refinement of the model by further work is justified.

CONCLUSIONS

1. Packings, consisting of varying numbers of fine woven meshes in a series arrangement, provided suitable media for investigation of the effects of operating conditions and bed properties on the coalescence of secondary dispersions. Stainless steel meshes are preferred to nylon since the latter was found to be susceptible to swelling in aqueous environments.

2. Measurements of separation efficiency and coalesced drop sizes indicated the existence of a critical velocity above which breakthrough of the dispersion occurred. For beds initially free from dispersed phase, this velocity was found to be approximately 1.5×10^{-2} m/s. Presoaking the packings in dispersed phase increased this value to 3.5×10^{-2} m/s without increasing the two phase pressure drop. The shorter periods required to attain steady state operation emphasize the desirability of the presoaking operation.

3. A theoretical comparison of drop capture mechanisms demonstrated that direct and indirect interception are most significant under operating conditions encountered in this study but diffusion and London-Van der Waals forces may predominate for drops of less than 1μm diameter. Gravity forces cannot be neglected because they increase as coalescence produces larger drops. The drop capture efficiency, for beds initially free from dispersed phase, may be estimated using

$$\eta_{GI} = \frac{1}{2A}\left[2(1+N_R)\log_e(1+N_R)+\left(\frac{1}{1+N_R}\right)-(1+N_R)\right]+N_G$$

Application of this equation to typical operating conditions show that the drop capture rate is likely to be highest in the forepart of the bed.

4. The single phase pressure drop results were satisfactorily correlated by the Blake-Kozeny equation,

$$\left[\frac{\Delta P_1}{\mu_c}\right]\left[\frac{e_1^3}{(1-e_1)^2}\cdot\frac{d_c^2}{16N_L BT}\right] = Ku$$

Comparison of experimental values of the Kozeny constant, K, with various models describing flow through porous media showed that Keller's equation provided the best description for $0.4 < e_1 < 0.7$

$$K = \frac{e_1^2}{T(1-e_1)A}$$

$$\text{where } A = 1.257\left[1-\left(\frac{d_c}{d_c+d_a}\right)\right]^{2.5}$$

5. Two phase pressure drop results expressed as $\frac{\Delta P_2}{\Delta P_1}\left[\frac{\mu_c}{\mu_d}\right]$ to compensate for temperature and variations in single phase permeability, caused by the packing technique, were correlated with superficial velocity and bed depth,

$$\frac{\Delta P_2}{\Delta P_1}\left[\frac{\mu_c}{\mu_d}\right] = Cu^a L^b$$

The values of the constant, C, and exponent, b, varied considerably with mesh type and saturation history but the data from all experiments indicated that ΔP_2 is proportional to $\sqrt{u}$.

6. An expression, based on the Blake-Kozeny equation, was derived to predict the two phase pressure drop from knowledge of the saturation profile,

$$\frac{\Delta P_2}{\Delta P_1} = \frac{d_c^2}{16(1-e_1)L} \int_0^L f(s)dl$$

A model was postulated from inspection of experimentally determined saturation profiles from other studies in which the local saturation decays exponentially from a constant value near the inlet face to a constant value in the downstream part of the bed,

$$S = S_I \qquad 0 < l \leq L_I$$

$$S = (S_I - S_E)e^{-k(l-L_I)} + S_E \qquad L_I \leq l \leq L$$

The parameters of this model were determined from average saturation data and used in the evaluation of $\int_0^L f(s)dl$. Specification of the inlet saturation, S_I, for a given superficial velocity produced good agreement between the predicted and experimental pressure drop. Saturation profiles inferred in this way were consistent with previous experimental results.

7. A preliminary study has been undertaken to investigate the feasibility of describing coalescence in a packed bed by analogy with a multiple channel queueing system. The saturation in the bed was interpreted as a queue of discrete drops waiting to coalesce into a continuum and uncaptured drops considered as 'impatient customers' at the service facility (coalescence site). An expression for the queue length was derived and through the use of average saturation data, the filter coefficient was predicted. Reasonable agreement for low superficial velocities was obtained but at higher velocities, predicted values were consistently higher than experimental values. Therefore, although refinement of the model is necessary to increase the

dependance on velocity, this novel approach is concluded to be valuable since the predicted values of filter coefficient lie within the range of values calculated from previous models.

8. A holographic technique has been successfully developed to measure drop sizes of dilute, secondary dispersions and hence to determine the filter coefficient. The method may be employed to characterise both O/W and W/O dispersions and in situ measurement eliminates sampling errors. The three-dimensional properties of images generated by reconstructed holograms permit storage of large quantities of data on a single photographic plate which may be examined at leisure. The technique also has considerable potential for automatic analysis of the reconstructed images by continuous scanning.

Measurements made using this technique showed that the diameter of secondary drops in the effluent remained fairly constant and similar to the mean diameter of the inlet dispersion. This suggests that some secondary drops pass through the bed without interception rather than being generated by redispersion phenomena. A quantitative analysis of the critical diameter for drop release supported this conclusion.

9. Based on this theoretical and experimental study, a mechanism of coalescence of secondary dispersions is proposed;

Drops are captured by direct and indirect interception, primarily in the forepart of the bed. The drops reside in the bed, either attached to fibres or intercepted by pores, where coalescence occurs until they attain such a size when

hydrodynamic forces exceed the restraining interfacial tension and adhesion forces. The drops are then squeezed through the packing interstices into a dispersed phase continuum. The dispersed phase is then conveyed in rivulets, within fixed channels, to the exit face where drops are formed and released by the mechanism of 'ballooning' (drip-point).

RECOMMENDATIONS FOR FURTHER WORK

1. This study has been restricted to investigation of the effects of superficial velocity and bed properties, viz., bed depth, fibre diameter and aperture diameter. It is recommended that the range of values employed for fibre and aperture diameters be extended to determine the optimum conditions where large drops are formed with a high separation efficiency. Since high drop capture efficiencies are realised using fine fibres and large drops are produced by meshes with wide apertures, it would be useful to perform experiments where the mesh size increases through the bed.

   The effects of system properties should also be investigated using other suitable dispersed phases.

2. An experimental study, combining variation of liquid system properties for different mesh materials, would be desirable to elucidate the relationships existing between wetting effects and the coalescence parameters, pressure drop and filter coefficients. A more fundamental study is necessary to determine how wettability may be characterised for two phase flow in packed beds when coalescence occurs simultaneously. More specifically, this may be investigated by considering the passage of a drop through a model interstice under the action of hydrodynamic forces, caused by flow of the surrounding continuous phase, for different wetting situations.

3. Mathematical models developed in this work have been based largely on assumed saturation profiles and consequently it would be desirable to confirm the

assumptions by experiment. This could be achieved by permeability measurements over relatively deep beds of glass ballotini. Granular media may be easily characterised and it would be feasible to study the effects of particulate matter, suspended in the continuous phase, since the bed may be regenerated by fluidisation. Irrigation of the packing may also be incorporated to alleviate blocking of the pores.

4. Holography has been used successfully to determine the diameters of secondary droplets but the technique ultimately depends on analysis of photographs by manual counting. It is therefore recommended that a method be sought whereby the reconstructed images may be recorded on videotape and then automatically scanned and analysed to yield quantitative results.

APPENDICES

APPENDIX A.

DETERMINATION OF THE HAMAKER CONSTANT.

An equation for calculating Hamaker's constant for a system of two immiscible liquids and a solid is presented by Sherony and Kinter[129] This equation is,

$$Q = 6 \pi r_{22}^2 \left(\sqrt{\sigma_d^d} - \sqrt{\sigma_c^d} \right) \left(\sqrt{\sigma_s^d} - \sqrt{\sigma_c^d} \right) \qquad A.1$$

where r_{22} is the intemolecular distance

σ_c^d, σ_d^d and σ_s^d are the London-Van der Waal's component to the surface tensions of the continuous, dispersed, and solid phases, respectively.

The terms of Equation A.1 were obtained directly from the data of Fowkes[130],

for water-hydrocarbon systems, $6 \pi r_{22}^2 = 1.44 \times 10^{-18}$ m^2

for steel , $\sigma_s^d = 0.1080$ N/m

for water , $\sigma_c^d = 0.0218$ N/m

for toluene , $\sigma_d^d = \sigma_d = 0.0285$ N/m

$\therefore Q = 1.44 \times 10^{-18} \left(\sqrt{0.0285} - \sqrt{0.0218} \right) \left(\sqrt{0.108} - \sqrt{0.0218} \right)$

Hamaker constant, $Q = 0.55 \times 10^{-20}$ J.

APPENDIX B.

CALCULATION OF CRITICAL DIAMETER FOR DROP RELEASE.

Rosenfeld[75] developed the following equation by equating the drag force to the sum of the adhesion and London Van der Waal's forces for an undeformed drop,

$$\frac{d_{pc}}{d_c} = \frac{Q^2}{144\pi^2 r_o^4}\left[\frac{3\,\mu_c u_I\, K(1 + 2\mu_c/3\,\mu_d)}{(1 + \mu_c/\mu_d)} - \sigma_{cd}(1+\cos\theta_e)\right]^{-2} - 1 \qquad \text{B.1.}$$

The critical drop diameter may be estimated by making the following assumptions for values of parameters in this equation. If complete non-wetting is assumed, corresponding to point contact between drop and collector, $\theta_e = 180^o$ and thus $\sigma_{cd}(1 + \cos\theta_e) = 0$. For a sphere-cylinder geometry, $r_o = 5 \times 10^{-10}$ m.[75] The factor, K which modifies the value of the drag force term, was introduced to account for fibre interaction.

Equation B.1 will now be applied to the data of Bitten[62] who studied the coalescence of water drops on glass fibres. His experiments were conducted under the following conditions,

$\mu_d = 1.0 \times 10^{-3}$ Ns/m^2 , $\mu_c = 2.5 \times 10^{-3}$ Ns/m^2

$d_c = 6\ \mu$m , $u_I = 1.52 \times 10^{-2}$ m/s

$Q = 0.2 \times 10^{-20}$ J (calculated using equation given in Appendix A).

Insertion of these values into equation B.1 predicts a critical diameter of 30 μm which differs considerably from the observed value of 400 μm. Application of this equation is therefore likely to produce an underestimation of actual critical diameters.

For packed beds, the velocity term, u_I must take account of the porosity of the packing and also the reduction of this porosity due to the dispersed phase saturation,

hence,

$$u_I = \frac{u}{e_1(1 - s)}$$

For a stainless steel mesh of the type used in this experimental study,

$$d_c = 30.5 \ \mu m.$$

$$e_1 = 0.6995$$

A typical maximum value of saturation, S is 0.5 for low porosity beds and the maximum superficial velocity for this study was 7.0×10^{-2} m/s. The physical properties used are given in Appendices A and D . Substitution of these values into equation B.1 yields,

$$d_{pc} = 30.5 \times 10^{-6} \frac{(0.55 \times 10^{-20})2}{144\pi^2(5\times10^{-10})^4} \left[\frac{1.0\times3\times10^{-3}\times7\times10^{-2}(1+1.12)}{0.6995 \times 0.5(1+1.68)}\right]^{-2} - 1$$

hence,

Minimum critical drop diameter, $d_{pc} = 15.5 \ \mu m.$

d_{pc} was calculated for superficial velocities of 0.5×10^{-2} and 5×10^{-2} m/s. to be 9.0 mm. and 59.7 μm. respectively. Since the aperture diameter of this mesh is 53.0 μm., these results indicate that redispersion of drops is likely for velocities greater than about 5×10^{-2} m/s. At lower velocities, drops which may become detached from a collector should be immediately recaptured by the pore catchment mechanism.

High porosity fibrous beds ($e > 0.9$) operate with a lower maximum saturation of approximately 0.2 [65] and the fibres used are typically between 1 μm and 13 μm diameter (see Chapter 4). The critical diameter, d_{pc} was estimated to be 80.8 μm using $d_c = 7 \ \mu m$ and $u = 5 \times 10^{-2}$ m/s. Pore size distribution data is not readily available for beds of this type and a rough estimate of the mean pore size was determined assuming an isotropic bed with the fibres

arranged in a cubic pattern. For a porosity of 0.9 and fibre diameter of 7 μm, a value of 22.7 μm was obtained. When the latter is compared to a critical drop diameter of 80.8 μm, it may be concluded that pore catchment is also significant in high porosity beds.

Maximum values of saturation were used for these calculculations but if the variation of saturation with bed depth and superficial velocity were considered, the critical diameter would increase. Further, as drops grow by coalescence, the contact angle decreases[95] and the $\sigma_{cd}(1+\cos\theta_e)$ term of equation B.1 becomes significant which also increases the value of d_{pc}. Additional adhesion forces are created due to 'bridging' effects which have been observed[131] when drops simultaneously contact two or more adjacent fibres.

The calculations completed in this section indicate that the hypothesis to justify the travelling drop model, where drops are redispersed into the flowing continuous phase, should be rejected for both low and high porosity beds.

APPENDIX C

EQUIPMENT DESIGN

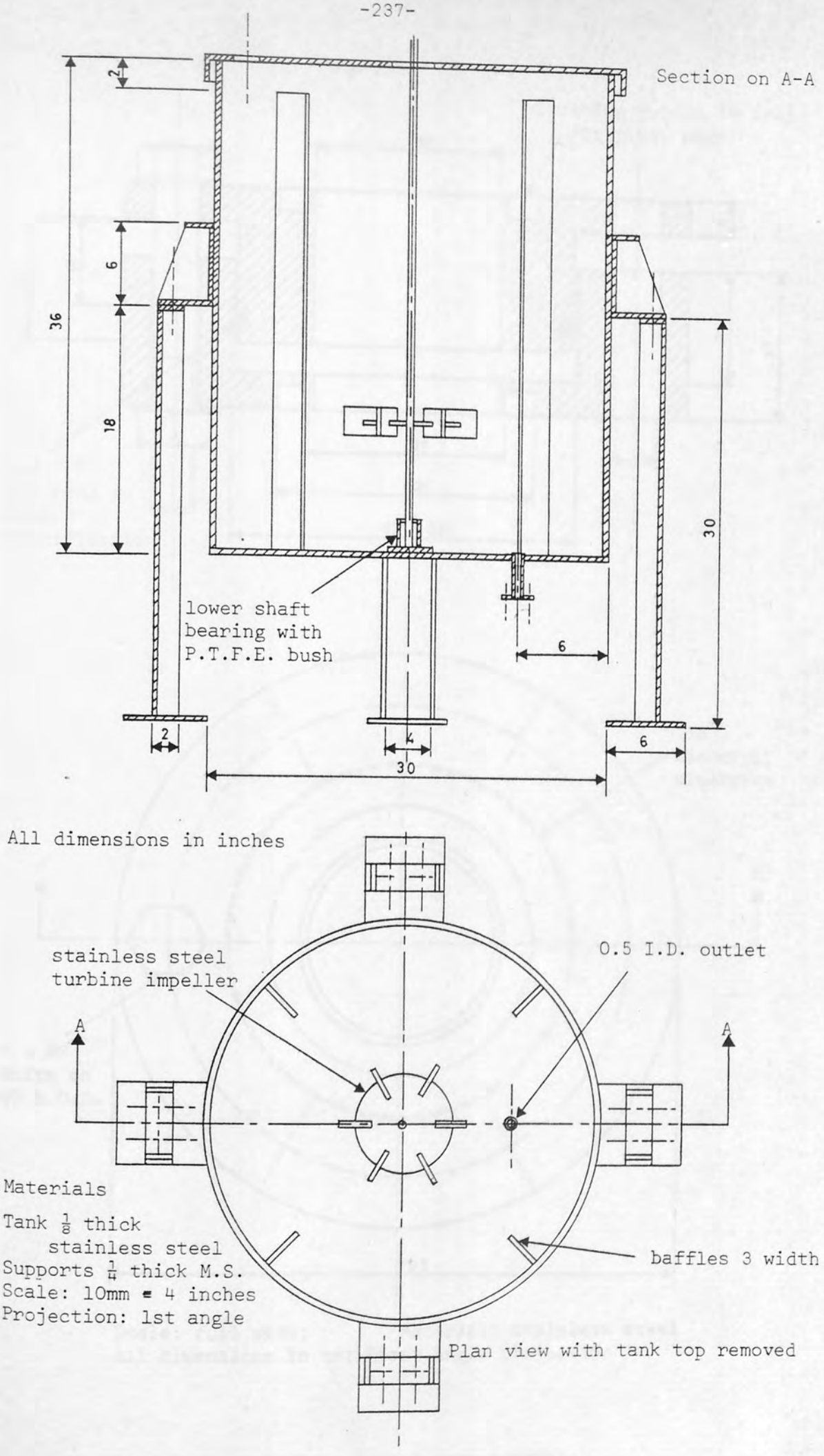

Fig. C.1 Design of continuous phase reservoir

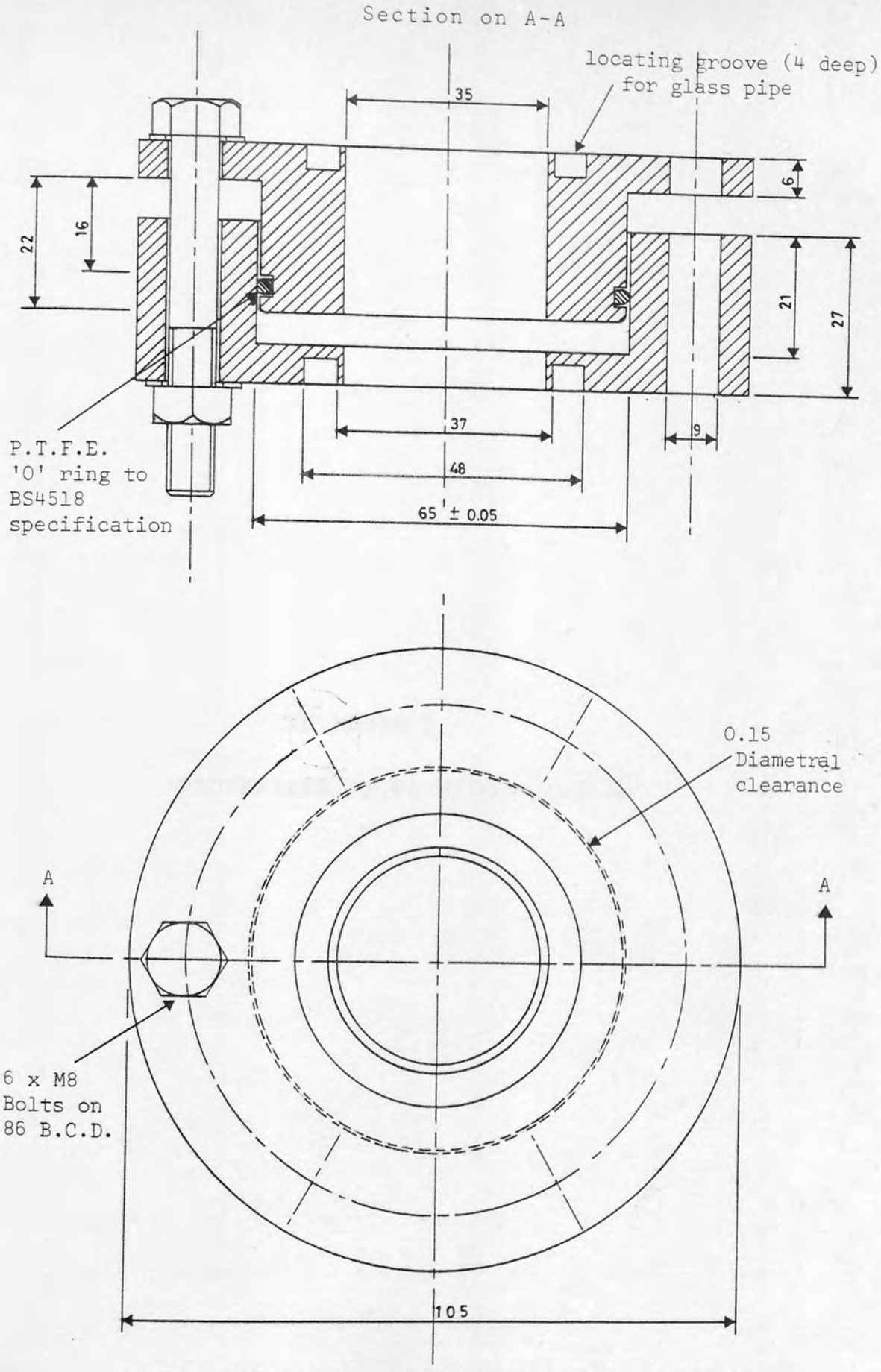

Scale: full size; Material: stainless steel
All dimensions in mm; First angle projection

Fig. C2 Design of coalescer assembly

APPENDIX D

PROPERTIES OF PACKING MATERIALS

The physical and chemical properties of the materials used are listed and compared in Table D.1.

Property	Nylon (Type 66)	Polyester	Stainless Steel
Specific Gravity	1.14	1.38	7.83
Tenacity (dry)(grams/ denier)	4.0-6.5	4.0-6.5	-
Tensile Strength (dry) (kg/mm^2)	41-67	50-81	77
Relative wet strength (%)	90-95	100	100
Elongation at Breaking Point (wet) %	24-40	15-30	12
Moisture absorption at 65% RH (20°C)	3.8	0.4	0
Melting Point (°C)	240-250	250-260	1300
Softening Point (°C)	235	220-240	1300
Normal working temp. range (°C)	-40to 115	-75to 150	0 to 300
Recommended Max. operating temp. (°C)	100	150	300
Abrasion resistance	v.good	v.good	v.good
Resistance to acids	fair	v.good	fair
Resistance to alkalis	v.good	fair	fair
Resistance to organic solvents	good	good	v.good

Table D.1. Properties of Packing Materials.[132]

This study was designed to investigate the effects of mesh geometry on coalescence efficiency and pressure drop so that it was necessary to discover the extent of swelling of the nylon mesh fibres caused by water absorption. It was found that the single phase permeability of a full twill nylon mesh decreased as the immersion time in water increased as shown by Fig D.1. The initial permeability was then used to calculate the Kozeny constant as described in Section 9.3.

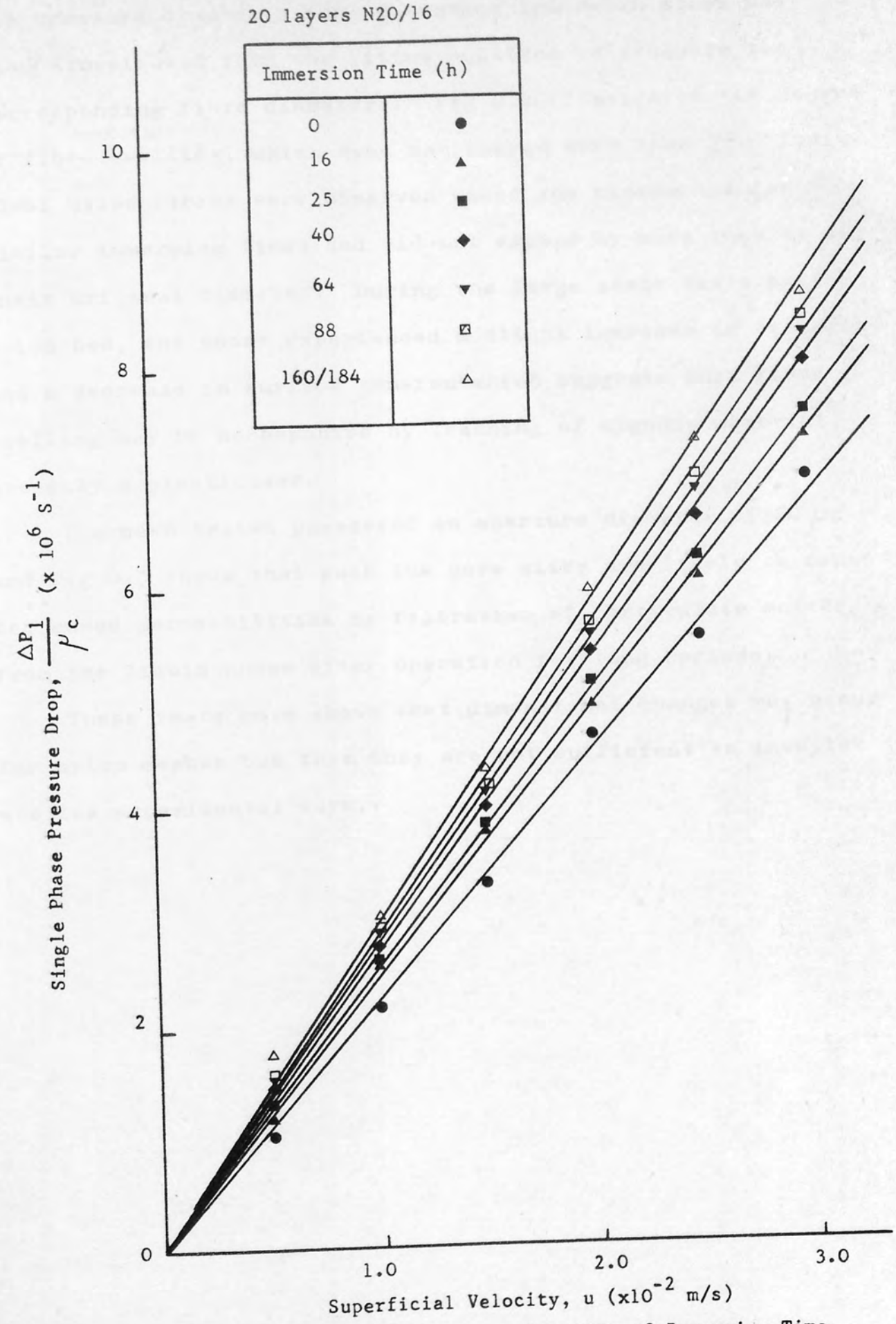

Fig D.1 Nylon mesh permeability as a function of Immersion Time.

The pressure drop data for subsequent immersion times was then substituted into the fitted equation to evaluate the corresponding fibre diameters. Fig D.2 illustrates the degree of fibre swelling, which does not exceed more than 7%. Individual nylon fibres were observed under the microscope for similar immersion times and did not expand by more than 4% of their original diameter. During the large scale tests on the nylon bed, the water experienced a slight increase in viscosity and a decrease in surface tension which suggests that fibre swelling may be accompanied by leaching of organic material, possibly a plasticiser.

The mesh tested possessed an aperture diameter of 20 μm and Fig D.3 shows that such low pore sizes are likely to cause decreased permeabilities by filtration of particulate matter from the liquid phase after operation for long periods.

These tests have shown that dimensional changes may occur for nylon meshes but that they are not sufficient to invalidate the experimental work.

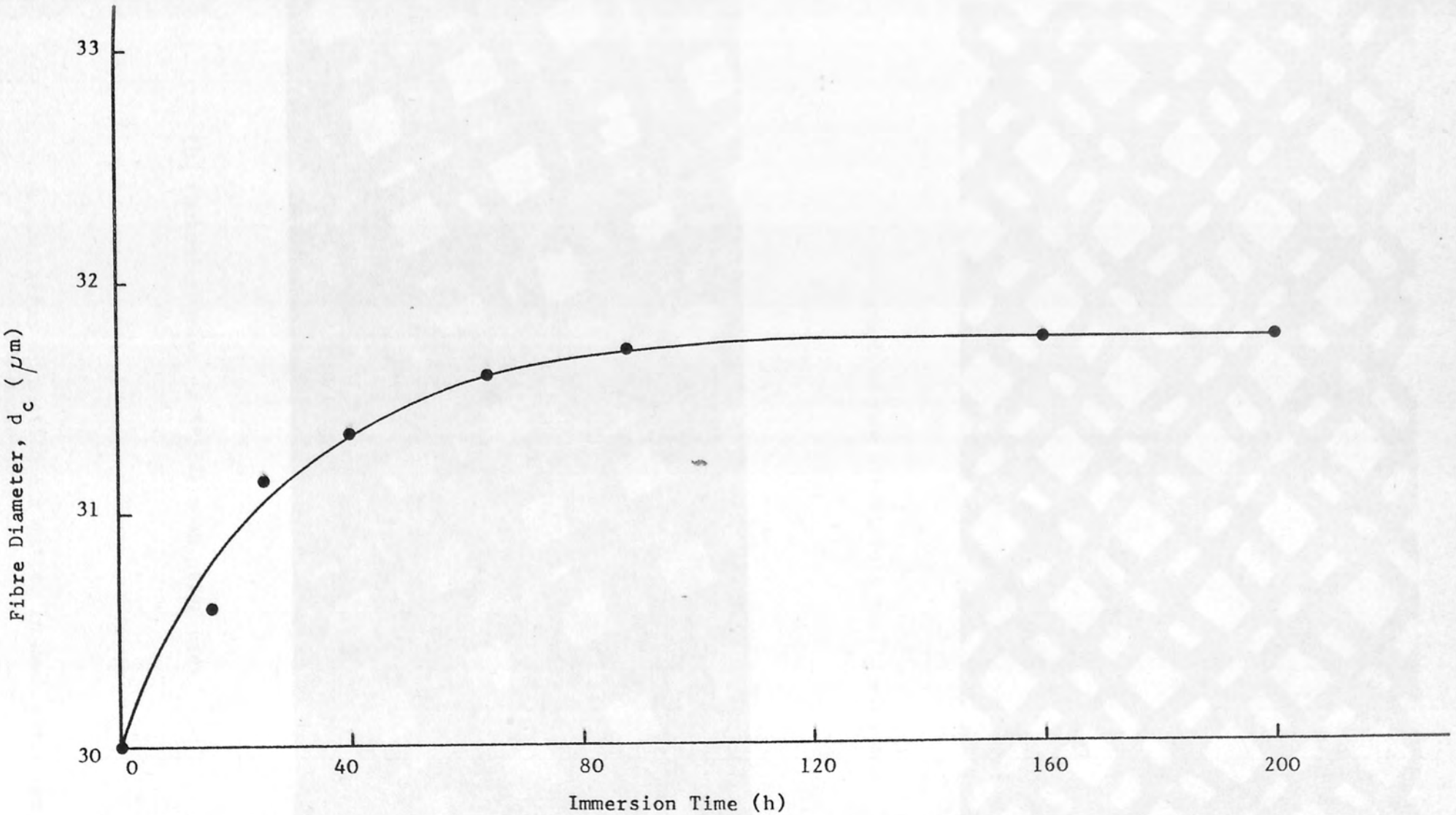

Fig D.2 Swelling of Nylon Fibres determined by Permeability Testing.

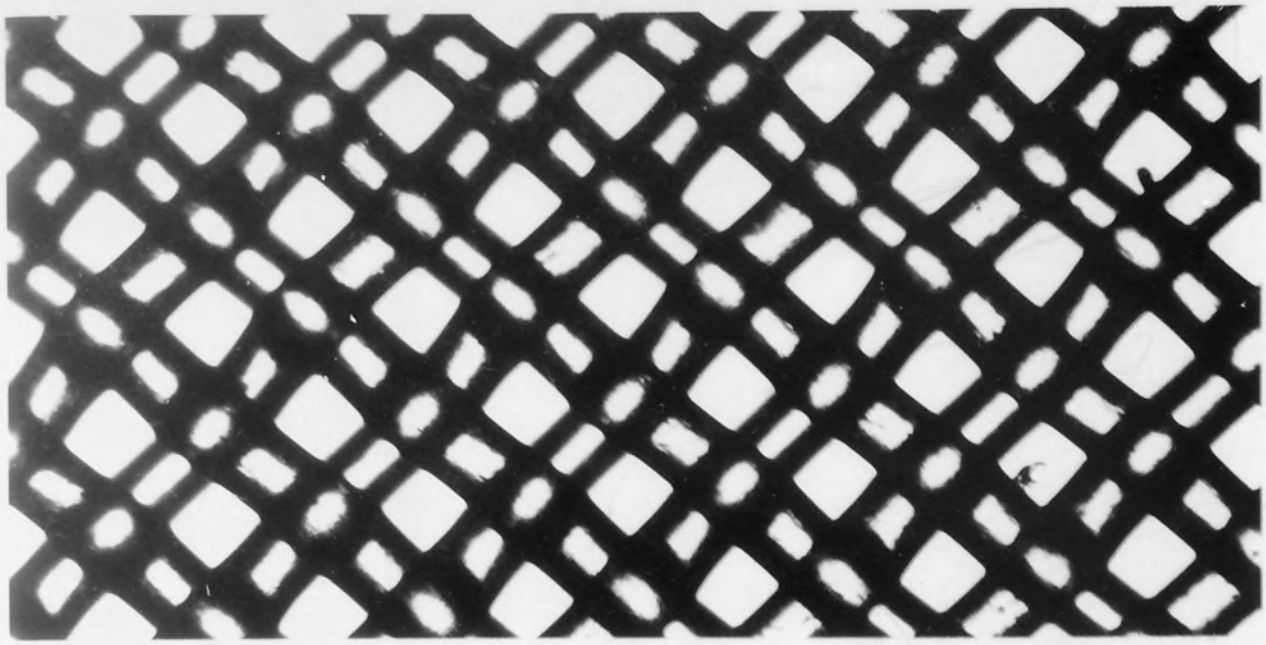

(a) Photomicrograph of new N25/21 full twill nylon mesh

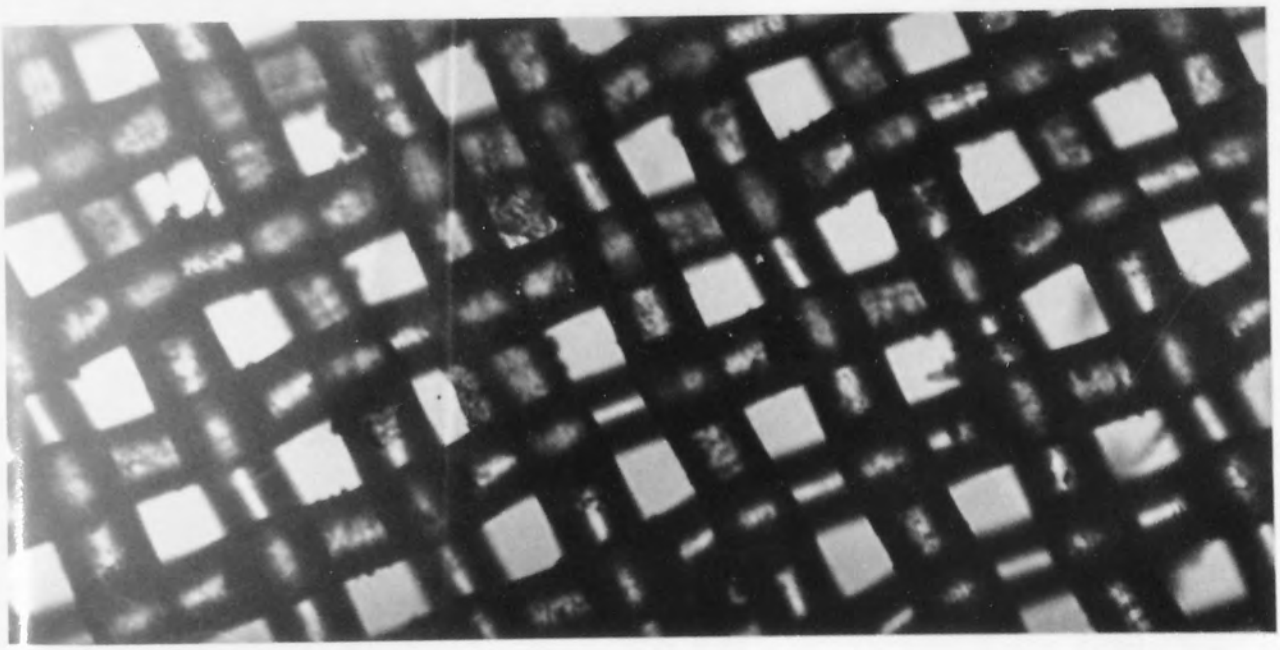

(b) Photomicrograph of N25/21 mesh after use.

Fig. D.3 Accumulation of particulate matter in mesh after use in a coalescing bed

APPENDIX E

PHYSICAL PROPERTIES OF LIQUID SYSTEM

As temperature changes were inevitable during operation of the coalescer, the physical properties of the liquid system were determined as a function of temperature. The temperature coefficient of density for both continuous and dispersed phases is low and in the temperature range between 10°C and 30°C, it is sufficient to take one value,

Density of Water, $\rho_c = 998 \pm 2$ kg/m^3 [133]

Density of Toluene, $\rho_d = 867 \pm 3$ kg/m^3 [133]

The remaining relevant properties are presented as a function of temperature in Figs E.1, E.2 and E.3. Viscosity and mutual solubility data were extracted from the literature [134] but since interfacial tension is sensitive to the purity of the two phases, this was measured with a Du Nouy Tensiometer. Interfacial tension was found to remain constant over the operational temperature range as shown by Fig E.2.

To ensure that the phases were mutually saturated, analysis of the effluent samples was completed using the method of extraction as described in Appendix F and the data presented on Fig E.3. Proximity of these data points to the equilibrium solubility curve shows that negligible mass transfer by dissolution or precipitation is likely, thus ensuring operation at the desired phase ratio.

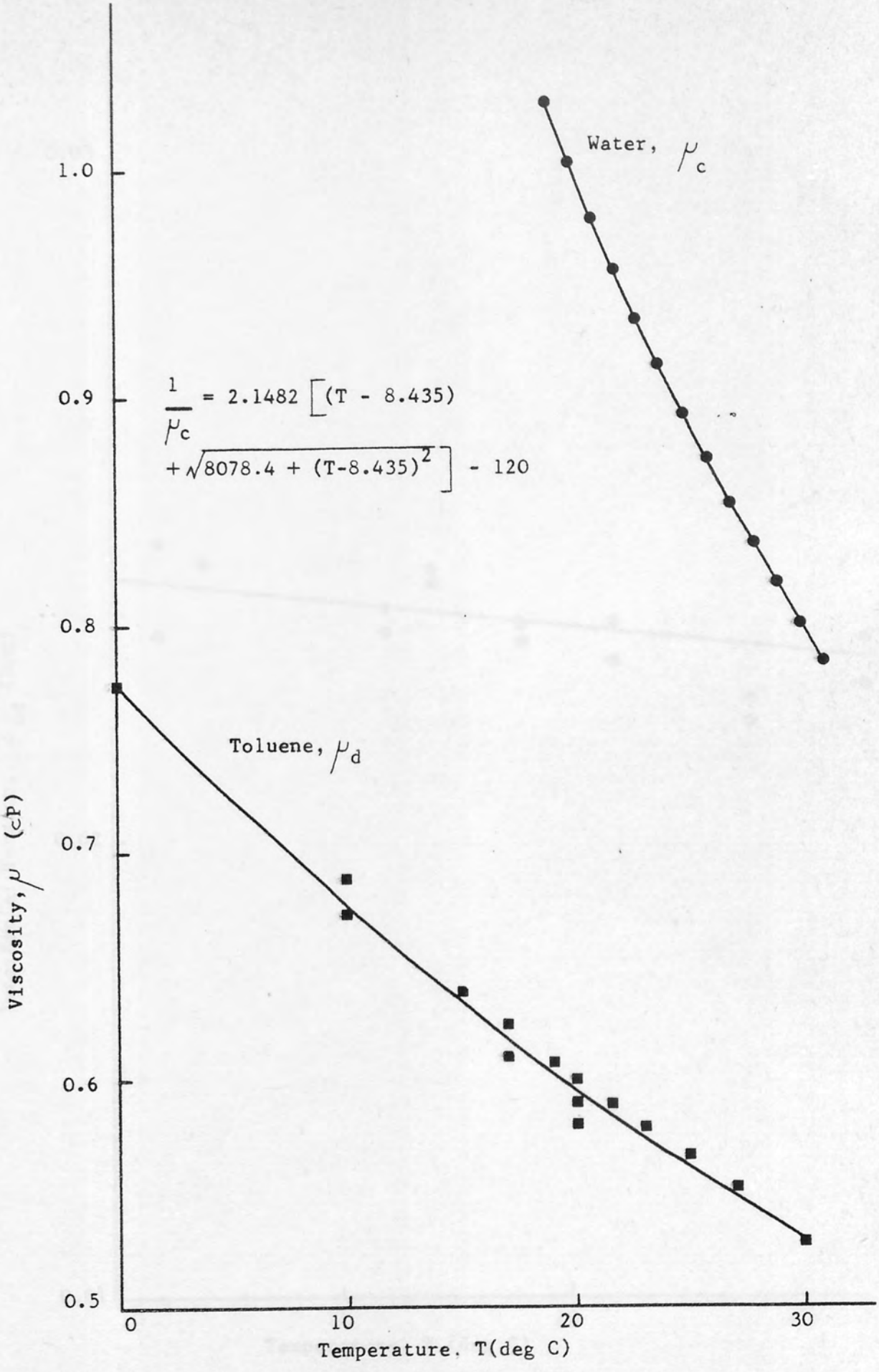

Fig E.1 Phase Viscosities as a function of Temperature.

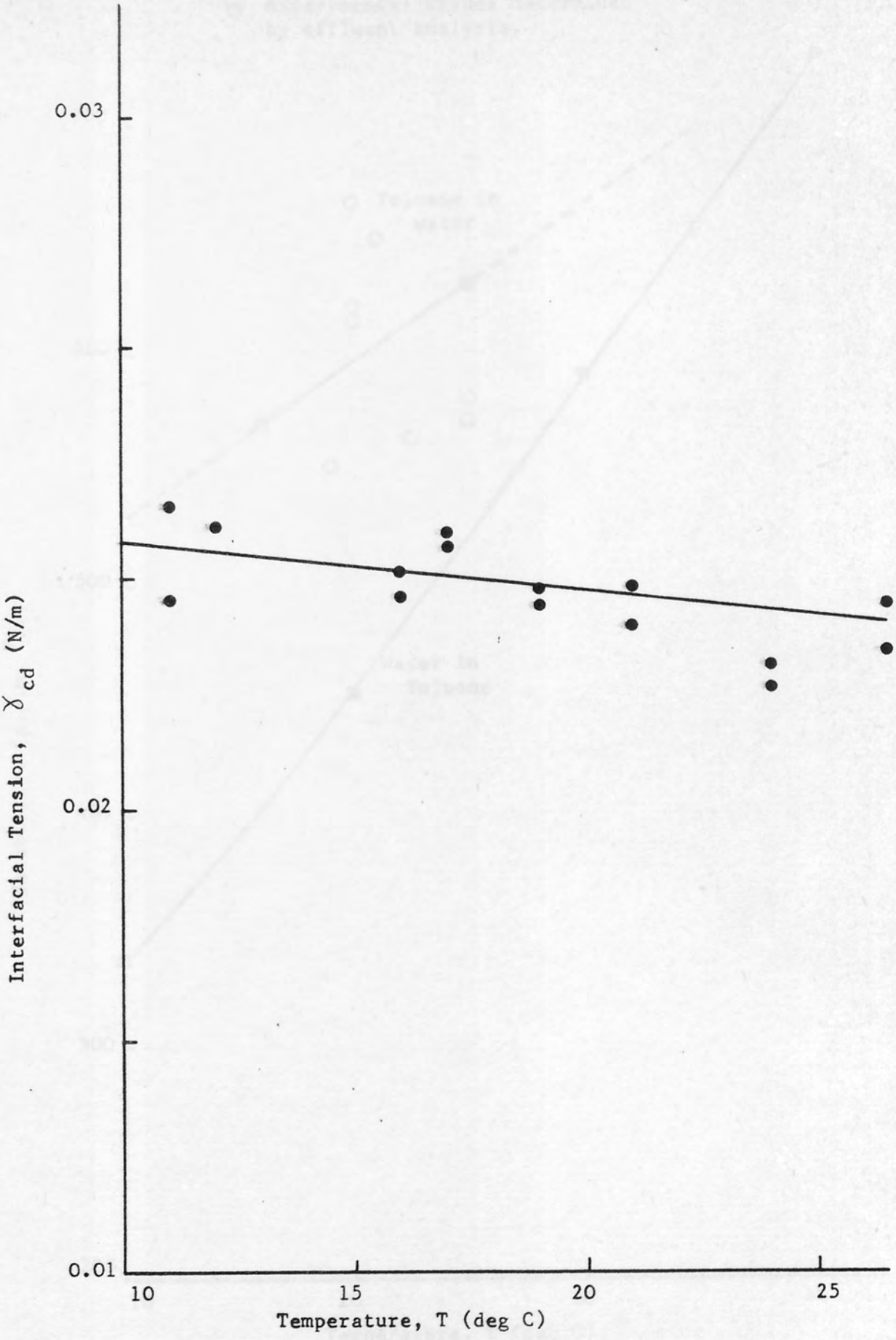

Fig E.2 Interfacial Tension for Toluene/Water system as a function of Temperature.

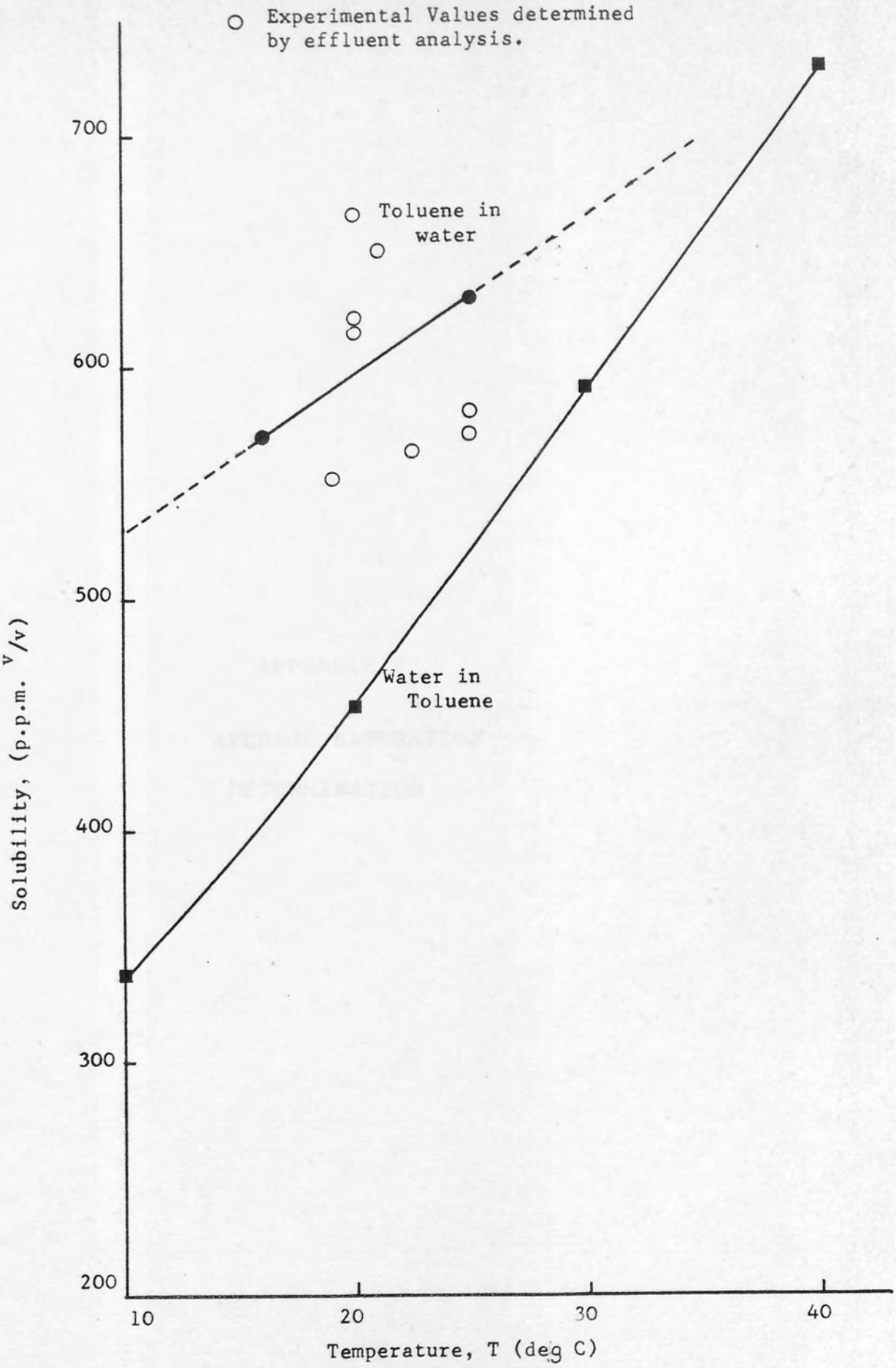

Fig E.3 Mutual Solubility of Toluene/Water System as function of Temperature.

APPENDIX F

AVERAGE SATURATION DETERMINATION

The average saturation in the bed was determined on completion of an experimental run by measuring the quantity of toluene retained in the interstices of the packing. The coalescer assembly was dismantled and the bed rapidly immersed in 50 cm^3 of ethyl acetate to extract the toluene. This procedure was repeated twice so that the dispersed phase was finally dissolved in 150 ml to produce a concentration of approximately 1% $^{v}/_{v}$. The latter was selected as a solvent since the quantity of toluene present could be determined using gas liquid chromatography under the following conditions:

Chromatograph : Pye Series 104

Column : PE G 400 on Chromosorb B

Oven temperature : 100°C

Detector : Flame Ionisation.

Carrier Gas : Nitrogen at flowrate of 40 cm^3/min.

Sample volume : 0.1 μl

Repeated analysis demonstrated that the accuracy of the technique was such that average saturation values could be determined to $\pm$ 0.05. The results are given in Appendix H.

APPENDIX G.

HOLOGRAM DEVELOPMENT PROCEDURE AND PROCESSING SOLUTIONS.

The following procedure, developed by Phillips [113] was employed to produce phase holograms of the effluent dispersion. The quality of the holograms developed by the process were of a high standard thus permitting quantitative analysis of the drops by photography of the real images formed on reconstruction.

Processing Steps All at 20°C.	Time (min)	Solution Composition.
1.Wash and Harden	10	'Drysonal'[a]
2.Wash	3	-
3.Develop	8	'Neofin Blue'[a](concentrated) +0.3mg/m^3 Benzotriazole +120mg/m^3 Sodium Metaborate.
4.Wash	5	-
5.Fix	3	Agfa Gaevert G334 solution
6.Wash	3	-
7.Bleach	10	15mg/m^3 Ferric Nitrate 3.3mg/m^3 Potassium Bromide. 0.3 mg/m^3 Phenosafranine 20 mg/m^3 Glycerol 50 mg/m^3 Propan-2-ol.
8.Wash	15	-
9.Rinse	1	'Drysonal'[a]

a - obtained from Tetrenal Photoproducts.

APPENDIX H

TABULATED EXPERIMENTAL DATA

Mesh Type : S300				Initial Condition : Dispersed phase free				
Run No.	Temperature (deg.C)	Bed Depth	Velocity ($\times 10^{-2}$ m/s)	Average Saturation, $\bar{S}$	Pressure Drop $\frac{\Delta P_2}{\Delta P_1} \cdot \frac{\mu_c}{\mu_d}$	Separation Efficiency (%)	Effluent Drop Size (μm)	Coalesced Drop Size (mm)
79	20.5	10	0.5	0.338	62.744	96.0	28.6	3.10
80	19.0	20	"	0.287	49.010	96.9	30.4	2.88
38	18.5	30	"	0.270	24.844	98.3	38.7	2.95
19	20.0	40	"	0.248	38.338	99.0	-	3.02
29	20.0	60	"	0.247	17.403	-	-	3.00
46	18.0	90	"	0.236	13.561	95.5	31.0	1.06
73	22.5	10	1.5	0.292	16.156	94.3	41.3	0.42
75	24.0	20	"	0.239	17.408	95.6	31.6	0.52
39	19.5	30	"	0.205	13.451	96.2	29.9	0.82
32	15.0	60	"	0.197	8.219	93.0	30.6	0.45
74	19.5	90	"	0.188	5.639	96.2	35.9	0.57
72	22.5	120	"	0.185	4.640	98.7	37.8	0.49

Mesh Type : S 300			Initial Condition : Dispersed phase free					
Run No.	Temperature (deg.C)	Bed Depth	Velocity ($\times 10^{-2}$ m/s)	Average Saturation, $\bar{S}$	Pressure Drop $\frac{\Delta P_2}{\Delta P_1} \cdot \frac{\mu_c}{\mu_d}$	Separation Efficiency (%)	Effluent Drop Size (μm)	Coalesced Drop Size (mm)
81	21.0	10	2.5	0.258	19.166	68.3	27.5	0.69
40	23.5	30	"	0.183	10.133	70.9	27.2	0.75
33	15.0	60	"	0.153	6.453	79.4	34.2	0.51
48	21.0	90	"	0.153	4.397	81.1	55.4	0.52
82	19.5	10	3.5	0.258	13.990	44.5	28.1	0.58
41	26.0	30	"	0.162	7.860	48.9	29.3	0.60
34	26.0	60	"	0.142	6.022	47.3	30.7	0.60
49	22.0	90	"	0.126	4.082	50.6	52.5	0.63
77	28.5	10	7.0	0.280	6.065	28.0	-	0.62
83	20.0	30	"	0.148	5.318	19.2	36.2	0.50
71	24.5	60	"	0.130	4.061	22.2	40.9	0.36
84	21.5	90	"	0.118	3.962	20.5	47.7	0.36
76	27.0	120	"	0.102	2.850	23.2	48.3	0.48

Mesh Type : S 300 — Initial Condition : Presoaked in dispersed phase.

Run No.	Temperature (deg.C)	Bed Depth	Velocity ($\times 10^{-2}$ m/s)	Average Saturation, $\bar{S}$	Pressure Drop $\frac{\Delta P_2}{\Delta P_1} \cdot \frac{\mu_c}{\mu_d}$	Separation Efficiency (%)	Effluent Drop Size (μm)	Coalesced Drop Size (mm)
42	19.5	30	0.5	0.405	22.312	99.8	27.7	4.00
31	17.0	60	"	0.274	12.750	101.6[a]	42.9	3.72
50	18.0	90	0.5	0.326	27.253	99.0	78.1	3.07
43	21.5	30	1.5	0.345	12.487	96.8	31.0	3.61
35	20.0	60	"	0.243	11.136	97.1	34.1	3.50
51	18.0	90	"	0.282	5.319	97.6	-	2.87
44	26.0	30	2.5	0.331	10.367	94.4	33.5	2.18
36	16.0	60	"	0.200	7.627	93.9	36.2	2.44
52	21.0	90	"	0.230	3.800	95.8	-	2.27
45	27.0	30	3.5	0.330	8.479	49.4	31.0	0.82
37	15.5	60	"	0.198	7.794	53.6	33.3	1.73
53	27.0	90	"	0.195	3.873	82.4	33.3	1.32

a - value 100% attributable to measurement error

Mesh Type : S300								
Run No.	Temperature (deg.C)	Bed Depth	Velocity ($\times 10^{-2}$ m/s)	Average Saturation, $\bar{S}$	Pressure Drop $\frac{\Delta P_2}{\Delta P_1} \frac{\mu_c}{\mu_d}$	Separation Efficiency(%)	History[a] (Previous Velocity)	Coalesced Drop Size (mm)
19	20.0	40	0.5	0.248	38.338	99.0	0(free)	3.02
	19.5	"	2.5	-	10.432	96.3	0.5	1.60
	27.0	"	3.5	-	9.029	96.5	2.5	0.87
	28.5	"	1.5	-	11.013	98.1	3.5	3.18
	25.5	"	3.5	-	8.167	95.2	1.5	0.67
	20.0	"	0.5	-	18.126	99.6	3.5	3.52
	20.0	"	0.5	-	16.762	97.9	0.5	3.23
	24.0	"	1.5	-	9.596	97.0	0.5	1.27
	23.0	"	3.5	-	8.160	94.3	1.5	0.83
	22.5	"	2.5	-	8.468	95.5	3.5	1.24

a - Velocity changed during one run.

Mesh Type : Polyester/Nylon.								
Run No	Temperature (deg.C)	Bed Depth.	Velocity ($\times 10^{-2}$ m/s)	Average Saturation, $\bar{S}$	Pressure Drop $\frac{\Delta P_2}{\Delta P_1} \frac{\mu_c}{\mu_d}$	Separation Efficiency(%)	Initial Condition	Coalesced Drop Size (mm)
PE 53/33								
17	19.0	40	0.5	-	25.209	97.2	free [a]	7.44
	17.0	"	1.5	-	14.133	99.0	-	3.95
	25.0	"	2.5	-	7.531	96.1	-	3.24
	28.5	"	3.5	-	8.243	97.6	-	2.65
N53/36								
18	18.5	40	0.5	-	23.268	99.4	free [a]	2.72
	23.0	"	1.5	-	13.695	92.9	-	3.25
	21.5	"	2.5	-	8.639	97.0	-	1.39
	24.0	"	3.5	-	7.836	96.6	-	1.36

a - velocity changed during one run.

Mesh Type : N53/36

Run No.	Temperature (deg.C)	Bed Depth	Velocity ($\times 10^{-2}$ m/s)	Average Saturation, $\bar{S}$	Pressure Drop $\frac{\Delta P_2}{\Delta P_1} \cdot \frac{\mu_c}{\mu_d}$	Separation Efficiency (%)	Initial Condition	Coalesced Drop Size (mm)
18	21.0	40	0.5	-	23.268	100.9	free	2.72
	"	"	1.5	-	13.695	97.4	-	3.25
	"	"	2.5	-	8.639	98.8	-	1.39
	"	"	3.5	-	7.837	95.0	-	1.36
64	20.0	60	0.5	0.101	10.077	98.9	free	3.93
54	19.5	"	1.5	0.076	7.189	99.1	free	2.73
66	20.0	"	2.5	0.060	4.463	97.5	free	1.18
68	25.0	"	3.5	0.054	4.580	93.6	free	0.75
65	20.0	"	0.5	0.125	10.587	96.3	presoaked	3.35
55	21.0	"	1.5	0.105	6.258	97.2	presoaked	2.13
67	22.0	"	2.5	0.078	4.903	98.7	presoaked	1.08
69	20.5	"	3.5	0.071	4.345	96.1	presoaked	0.77

Mesh Type : Nylon

Run No.	Temperature (deg.C)	Bed Depth	Velocity ($x10^{-2}$ m/s)	Average Saturation, $\bar{S}$	Pressure Drop $\frac{\Delta P_2}{\Delta P_1} \cdot \frac{\mu_c}{\mu_d}$	Separation Efficiency (%)	Initial Condition	Coalesced Drop Size (mm)
N70/45								
60	20.0	60	1.5	0.074	7.764	89.6	free	2.08
61	18.0	60	1.5	0.085	8.927	97.8	presoaked	3.10
N69/38								
58	20.5	60	1.5	0.085	6.415	90.0	free	1.25
59	21.5	60	1.5	0.119	6.025	98.1	presoaked	1.89
N70/29								
62	23.0	60	1.5	0.057	7.481	95.3	free	3.54
63	21.0	60	1.5	0.066	11.223	97.4	presoaked	3.34
N25/18								
56	22.0	60	1.5	0.130	4.056	99.2	free	2.90
57	21.0	60	1.5	0.218	4.220	100.6	presoaked	2.52

APPENDIX I.

DERIVATION OF ALGORITHM FOR TORTUOSITY FACTOR.

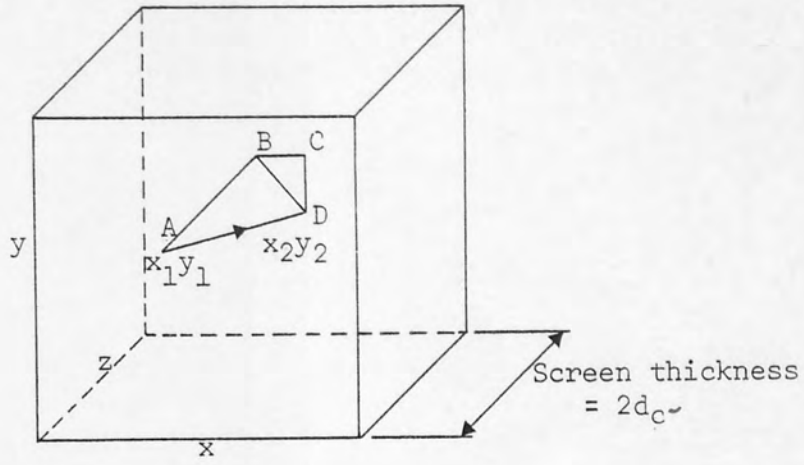

Consider $\triangle$ BCD in xy plane

$$BD^2 = \left[(x_2 - x_1)^2 + (y_2 - y_1)^2\right] d_a^{\,2}$$

Consider $\triangle$ ABD

$$AD^2 = AB^2 + BD^2$$

$$= (2d_c)^2 + \left[(x_2 - x_1)^2 + (y_2 - y_1)^2\right] d_a^{\,2}$$

$$\therefore AD = d_a \left[4F^2 + (x_2 - x_1)^2 + (y_2 - y_1)^2\right]^{0.5}$$

where $F = \dfrac{d_c}{d_a}$

Then, defining a Tortuosity factor, T as,

$$T = \frac{\left(\dfrac{AD}{2d_c} + 1\right)}{2}$$

$$T = 0.5 \left\{ \frac{\left[4F^2 + (x_2 - x_1)^2 + (y_2 - y_1)^2\right]^{0.5}}{2F} + 1 \right\}$$

The Tortuosity factor, T was calculated by insertion of the co-ordinates (x_1, y_1) and (x_2, y_2) from a random number generator (see Appendix J). This procedure was repeated a number of times, corresponding to the number of layers of mesh used in the coalescer. This was an attempt

to simulate the geometry of the bed which was prepared by laying single meshes, one upon another, so that their relative orientations and positions were fairly random.

APPENDIX J

COMPUTER PROGRAM FOR ANALYSIS OF SINGLE PHASE PRESSURE DROP DATA

```
20  REM   CORRELATION OF PRESSURE DROP DATA BY LINEAR REGRESSION
30  DIM A(16),D(250),N(20),V(50),X(600),Y(600),Z(250)
40  READ K
45  REM   READ FLUID VELOCITIES
50  FOR I=1,K: READ V(I): NEXT I
60  INPUT K1
70  M=1:K3=0
100  REM   INPUT MESH PARAMETERS
110  INPUT W,D1,D6,N3,K2
120  REM   EVALUATION OF PACKING PROPERTIES
130  IF W=2 THEN 150
140  A3=12*3.14159*N3*SQR((N3*D6)↑2+1): GOTO 160
150  A3=6*3.14159*N3*(SQR((N3*D6)↑2+1)+1)
160  E=1-A3*D6/48:D2=(1/N3-D6)/12:B=D6/6
170  C1=100/(12*2.54)
180  A3=A3*C1:D2=D2/C1:B=B/C1
190  REM   LOOP FOR DIFFERENT BED DEPTHS
200  FOR J=1,K2
210  REM   INPUT NUMBER OF MESH LAYERS
220  INPUT N1
224  PRINT "              SINGLE PHASE PRESSURE DROP DATA": PRINT
225  PRINT TAB(15);"MESH:          NO. OF LAYERS:";N1: PRINT
230  REM   CALCULATION OF TORTUOSITY FACTOR BY RANDOM NO. GENERATION
240  Q=0:F=D6/D1
250  A1=8*J+3:A2=8*J-3
260  X(0)=RND(A1)
270  FOR I=1,N1:X(I)=RND(0): NEXT I
280  Y(0)=RND(A2)
290  FOR I=1,N1:Y(I)=RND(0): NEXT I
300  FOR N2=2,N1
310  Q1=D1*SQR(4*F↑2+(X(N2)-X(N2-1))↑2+(Y(N2)-Y(N2-1))↑2)
320  Q=Q+Q1: NEXT N2
330  Q=Q/(2*D6*(N1-1))
340  Q=(Q+1)/2
341  PRINT Q
345  PRINT TAB(15);" VELOCITY    TEMPERATURE  PRESSURE DROP"
346  PRINT TAB(15);"   M/SEC.      DEG.C        N/M↑2"
350  REM   LOOP FOR CORRESPONDING PRESSURE DROPS & TEMPERATURES
```

```
360  FOR I=1,K
370  INPUT P,T
375  PRINT TAB(15);V(I),T,P
380  REM   CALCULATION OF FLUID VISCOSITY
390  M1=.1/(2.1482*((T-8.435)+SQR(8078.4+(T-8.435)↑2))-120)
400  Z(M)=(P/M1)*(E↑3/(A3↑2*N1*B*G))
410  M=M+1
420  NEXT I
425  FOR I=1,14: PRINT : NEXT I
430  REM   COUNTER FOR NO. OF "Y" VALUES FOR EACH "X" VALUE
440  K3=K3+1
450  NEXT J
470  REM   SEQUENCE FOR REARRANGEMENT OF DATA FOR REGRESION
480  M=1:D(M)=V(1):J2=2
490  FOR I=1,K
500  N(I)=K3:J1=I*(1+N(I))+1
520  M=M+1
530  IF M=J1 THEN D(M)=V(I+1): GOTO 550
540  J=(M-J2)*K+I:D(M)=Z(J): GOTO 520
550  J2=J2+(1+N(I)): NEXT I
555  REM   ENTER LINEAR REGRESSION ANALYSIS SUBROUTINE
556  FOR I=1,16:A(I)=0: NEXT I
560  CALL (1,K,N(1),D(1),A(1))
570  FOR I=1,16: PRINT A(I): NEXT I
571  R=SQR(1-A(9)/(A(6)-A(7))): PRINT "R=",R
575  GOTO 70
580  STOP
590  END
700  DATA 15
710  DATA .5E-02,.15E-01,.25E-01,.35E-01,.45E-01,.55E-01,.65E-01,.75E-01
720  DATA .7E-01,.6E-01,.5E-01,.4E-01,.3E-01,.2E-01,.1E-01
```

SINGLE PHASE PRESSURE DROP DATA

MESH: S300 NO. OF LAYERS: 10

VELOCITY M/SEC.	TEMPERATURE DEG. C	PRESSURE DROP N/M↑2
.5E-02	18.5	78
.15E-01	18.5	195
.25E-01	18.5	313
.35E-01	18.5	438
.45E-01	18	595
.55E-01	18	736
.65E-01	18	869
.75E-01	18	1026
.7E-01	18	948
.6E-01	18	807
.5E-01	18	673
.4E-01	18	532
.3E-01	18	399
.2E-01	18	266
.1E-01	18	133

SINGLE PHASE PRESSURE DROP DATA

MESH: S300 NO. OF LAYERS: 20

VELOCITY M/SEC.	TEMPERATURE DEG. C	PRESSURE DROP N/M↑2
.5E-02	19.5	141
.15E-01	19.5	368
.25E-01	20	587
.35E-01	20	814
.45E-01	20	1081
.55E-01	20	1316
.65E-01	20	1574
.75E-01	20	1833
.7E-01	20	1692
.6E-01	20	1449
.5E-01	20	1198
.4E-01	20	963
.3E-01	20	712
.2E-01	20	485
.1E-01	20	258

SINGLE PHASE PRESSURE DROP DATA

MESH: S300 NO. OF LAYERS: 60

VELOCITY M/SEC.	TEMPERATURE DEG. C	PRESSURE DROP N/M↑2
.5E-02	23.5	313
.15E-01	23.5	791
.25E-01	21	1574
.35E-01	20	2225
.45E-01	19	3032
.55E-01	20	3666
.65E-01	20	4364
.75E-01	19.5	5124
.7E-01	19.5	4724
.6E-01	19.5	4050
.5E-01	19	3369
.4E-01	19	2695
.3E-01	19	1997
.2E-01	19	1331
.1E-01	19	665

SINGLE PHASE PRESSURE DROP DATA

MESH: S300 NO. OF LAYERS: 60

VELOCITY M/SEC.	TEMPERATURE DEG. C	PRESSURE DROP N/M↑2
.5E-02	19.5	352
.15E-01	19.5	1042
.25E-01	19.5	1708
.35E-01	19	2421
.45E-01	19	3196
.55E-01	19	3925
.65E-01	19	4677
.75E-01	19	5508
.7E-01	19	5092
.6E-01	19	4356
.5E-01	19	3619
.4E-01	18.5	2875
.3E-01	18.5	2146
.2E-01	18.5	1449
.1E-01	18.5	705

SINGLE PHASE PRESSURE DROP DATA

MESH: S300 NO. OF LAYERS: 90

VELOCITY M/SEC.	TEMPERATURE DEG.C	PRESSURE DROP N/M↑2
.5E-02	18	485
.15E-01	18.5	1457
.25E-01	18.5	2397
.35E-01	18	3361
.45E-01	17.5	4552
.55E-01	17.5	5515
.65E-01	17.5	6573
.75E-01	17.5	7623
.7E-01	18	7012
.6E-01	18	6001
.5E-01	18	4967
.4E-01	18	3925
.3E-01	18	2922
.2E-01	18	1958
.1E-01	18	987

SINGLE PHASE PRESSURE DROP DATA

MESH: S300 NO. OF LAYERS: 120

VELOCITY M/SEC.	TEMPERATURE DEG.C	PRESSURE DROP N/M↑2
.5E-02	22	658
.15E-01	22	1935
.25E-01	21.5	3165
.35E-01	20.5	4458
.45E-01	20.5	5868
.55E-01	20.5	7169
.65E-01	20.5	8524
.75E-01	20.5	9903
.7E-01	20	9135
.6E-01	20	7819
.5E-01	20	6550
.4E-01	20	5194
.3E-01	19.5	3854
.2E-01	19.5	2601
.1E-01	19.5	1292

APPENDIX K.

COMPUTER PROGRAM FOR ANALYSIS OF TRANSIENT PRESSURE DROP DATA

```
10  REM                    PROGRAM DELP 8
20  REM          PROCESSING AND PLOTTING OF TRANSIENT PRESSURE DROP DATA
30  DIM S(45,10),H(45,10),P(45,10),R(45,10),N(10)
35  DEF FNA(T)=.1/(2.1482*((T-8.435)+SQR(8078.4+(T-8.435)↑2))-120)
36  DEF FNB(T)=.1E-02*(.771691-.963663E-02*T+.563896E-04*T↑2)
37  INPUT J1
38  FOR J=1,J1
40  INPUT N(J)
50  FOR I=1,N(J)
60  INPUT S(I,J),H(I,J),P(I,J)
70  S(I,J)=S(I,J)*.1E-02
80  NEXT I
85  NEXT J
90  CALL (1)
100  CALL (2,-1,10,-1,16)
110  CALL (3,2,0,0,E)
120  CALL (3,1,9,0,E)
140  CALL (3,2,0,15,E)
150  CALL (3,1,0,0,E)
265  FOR J=1,J1
270  FOR I=1,N(J)
280  M2=FNB(H(I,J))
290  R(I,J)=(P(I,J)/M2)*.1E-05
295  IF S(I,J)>9 THEN 310
300  CALL (3,1,S(I,J),R(I,J),E)
310  NEXT I
311  CALL (3,2,0,0,E)
312  NEXT J
320  CALL (3,2,-.125,-.25,E): CALL (4,7): PRINT "0";
321  FOR I=2,14,2:I1=-.75
322  CALL (3,2,I1,I,E): CALL (4,7): PRINT I;
323  NEXT I
324  FOR I=1,9
325  I1=-.5
326  I2=I-.75
328  CALL (3,2,I2,I1,E): CALL (4,7): PRINT I
329  NEXT I
370  CALL (4,7)
380  CALL (5)
```

```
385  FOR J=1,J1
386  S7=P(1,J)/FNA(H(1,J))*.1E-05
390  PRINT TAB(20),"       MESH:                    NØ. OF LAYERS:"
395  PRINT
400  PRINT TAB(20),"     SYSTEM:                SATURATION HISTORY:"
405  PRINT
406  PRINT TAB(20),"   VELOCITY:"
410  PRINT
411  PRINT TAB(29),"  TIME        TEMPERATURE      PRESSURE DROP"
420  PRINT TAB(29),"  SEC.           DEG.C.           1/SEC."
425  FOR I=1,N(J):S(I,J)=S(I,J)*1000
430  PRINT TAB(29),S(I,J),H(I,J),R(I,J): NEXT I
431  S4=Ø:S3=Ø
432  FOR I=N(J),1,-1
433  N1=N(J)+1-I
434  S4=S4+R(I,J)
435  S3=S3+R(I,J)↑2
436  S5=S4/N1: IF (S3-S4↑2/N1)<Ø THEN 442
437  S2=.252E-01*S5
438  S1=SQR((S3-S4↑2/N1)/N1)
439  IF I=1 THEN 442
440  IF S1<S2 THEN 446
442  PRINT : PRINT TAB(20);"TIME TO STEADY STATE=";S(I,J);"SEC.": PRINT
443  PRINT TAB(15),"STEADY STATE PRESSURE DROP=",S5,"1/SEC."
444  IF S(1,J)>Ø THEN  PRINT : PRINT : GOTO 447
445  S8=S5/S7: PRINT : PRINT TAB(20),"PRESSURE DROP RATIO=",S8: GOTO 447
446  NEXT I
447  N2=21-N(J): IF N(J)>21 THEN N2=35-(N(J)-21)
448  FOR I=1,N2: PRINT : NEXT I
449  NEXT J
450  STOP
460  END
```

MESH: S300 NØ. OF LAYERS: 10

SYSTEM: TOLUENE SATURATION HISTORY: FREE

VELOCITY: 0.1 x 10^{-2}m/s

TIME SEC.	TEMPERATURE DEG. C.	PRESSURE DROP 1/SEC.
Ø	18.5	.244813E-01
100	20.5	.518535E-01
250	21.5	.914372E-01
500	22	.119255
1000	23.5	.202994
1500	24	.340378
2000	25	.344512
2500	25	.358645
3000	26	.432716
5000	26	.55967
5500	21.5	.54185
7500	24.5	.561954
8500	25	.565352

TIME TO STEADY STATE= 3000 SEC.

STEADY STATE PRESSURE DROP= .532309 1/SEC.

PRESSURE DROP RATIO= 37.0011

MESH: S300 NØ. OF LAYERS: 60

SYSTEM: TOLUENE SATURATION HISTORY: FREE

VELOCITY: 1.0 x 10^{-2}m/s

TIME SEC.	TEMPERATURE DEG. C.	PRESSURE DROP 1/SEC.
Ø	19.5	1.07399
250	20	4.8062
500	20	7.26334
1100	20.5	7.74458
1500	20.5	7.38996
2500	20.5	8.07242
3000	20.5	8.33504
3500	20.5	8.72812
4000	20.5	8.92383
4500	20.5	8.91044
5000	20.5	9.1212
5500	20.5	9.85384
6000	20.5	9.52767
6500	21	10.1651
7000	21	10.2307
7500	21	10.4159
8000	21	10.6666

TIME TO STEADY STATE= 6000 SEC.

STEADY STATE PRESSURE DROP= 10.2012 1/SEC.

PRESSURE DROP RATIO= 15.9644

MESH: S300 NØ. OF LAYERS: 10

SYSTEM: TOLUENE SATURATION HISTORY: FREE

VELOCITY: 1.5×10^{-2} m/s

TIME SEC.	TEMPERATURE DEG. C.	PRESSURE DROP 1/SEC.
Ø	20	.272645
100	21	1.81928
250	21.5	2.5196
500	21.5	2.75835
1000	22	2.77523
1500	22	2.53502
2000	22	2.53502
2500	22.5	2.65849
3000	22.5	2.65849
3500	22.5	2.65849

TIME TO STEADY STATE= 1000 SEC.

STEADY STATE PRESSURE DROP= 2.63679 1/SEC.

PRESSURE DROP RATIO= 16.1562

MESH: S300 NØ. OF LAYERS: 20

SYSTEM: TOLUENE SATURATION HISTORY: FREE

VELOCITY: 1.5×10^{-2} m/s

TIME SEC.	TEMPERATURE DEG. C.	PRESSURE DROP 1/SEC.
Ø	20	.59849
100	20	2.70817
250	20	4.5585
500	20.5	6.00163
1000	20.5	5.72563
2000	21.5	5.91632
2500	22.5	6.15001
3000	23	6.33581
3500	24	6.41307
4000	25	6.36728

TIME TO STEADY STATE= 2000 SEC.

STEADY STATE PRESSURE DROP= 6.2365 1/SEC.

PRESSURE DROP RATIO= 17.4079

MESH: S300 NO. OF LAYERS: 90

SYSTEM: TOLUENE SATURATION HISTORY: FREE

VELOCITY: 1.5×10^{-2} m/s

TIME SEC.	TEMPERATURE DEG. C.	PRESSURE DROP 1/SEC.
0	19	2.34009
100	19	5.35182
250	19	7.77073
750	19	7.95137
1000	19	8.05319
1500	19	7.95137
2000	19.5	8.00041
2500	19.5	7.55925
3000	19.5	8.00041
3500	19.5	8.00041
4000	20	7.60581

TIME TO STEADY STATE= 3500 SEC.

STEADY STATE PRESSURE DROP= 7.80311 1/SEC.

PRESSURE DROP RATIO= 5.63911

MESH: S300 NO. OF LAYERS: 120

SYSTEM: TOLUENE SATURATION HISTORY: FREE

VELOCITY: 1.5×10^{-2} m/s

TIME SEC.	TEMPERATURE DEG. C.	PRESSURE DROP 1/SEC.
0	19.5	3.19719
100	21	5.93245
250	21.5	7.85344
500	21.5	8.38343
1000	22	8.62213
1500	22	8.71583
2600	22	8.95605
3000	22.5	9.17187
3500	22.5	9.10503

TIME TO STEADY STATE= 500 SEC.

STEADY STATE PRESSURE DROP= 8.82572 1/SEC.

PRESSURE DROP RATIO= 4.63962

MESH: S300 NØ. OF LAYERS: 10

SYSTEM: TOLUENE SATURATION HISTORY: FREE

VELOCITY: 7.0×10^{-2} m/s

TIME SEC.	TEMPERATURE DEG. C.	PRESSURE DROP 1/SEC.
Ø	23	1.49859
1ØØ	24	6.15299
35Ø	25	6.22771
5ØØ	25	6.22771
1ØØØ	27	6.37882
15ØØ	28	6.45516
175Ø	28.5	6.49351

TIME TO STEADY STATE= Ø SEC.

STEADY STATE PRESSURE DROP= 5.6335 1/SEC.

PRESSURE DROP RATIO= 6.Ø65Ø2

MESH: S300 NØ. OF LAYERS: 60

SYSTEM: TOLUENE SATURATION HISTORY: FREE

VELOCITY: 7.0×10^{-2} m/s

TIME SEC.	TEMPERATURE DEG. C.	PRESSURE DROP 1/SEC.
Ø	21	7.8443
1ØØ	24.5	18.6ØØ7
25Ø	24.5	18.6ØØ7
5ØØ	25.5	18.8261
1ØØØ	27	19.3373
15ØØ	28.5	19.6279
2ØØØ	3Ø	2Ø.Ø959

TIME TO STEADY STATE= 25Ø SEC.

STEADY STATE PRESSURE DROP= 19.2976 1/SEC.

PRESSURE DROP RATIO= 4.Ø61Ø4

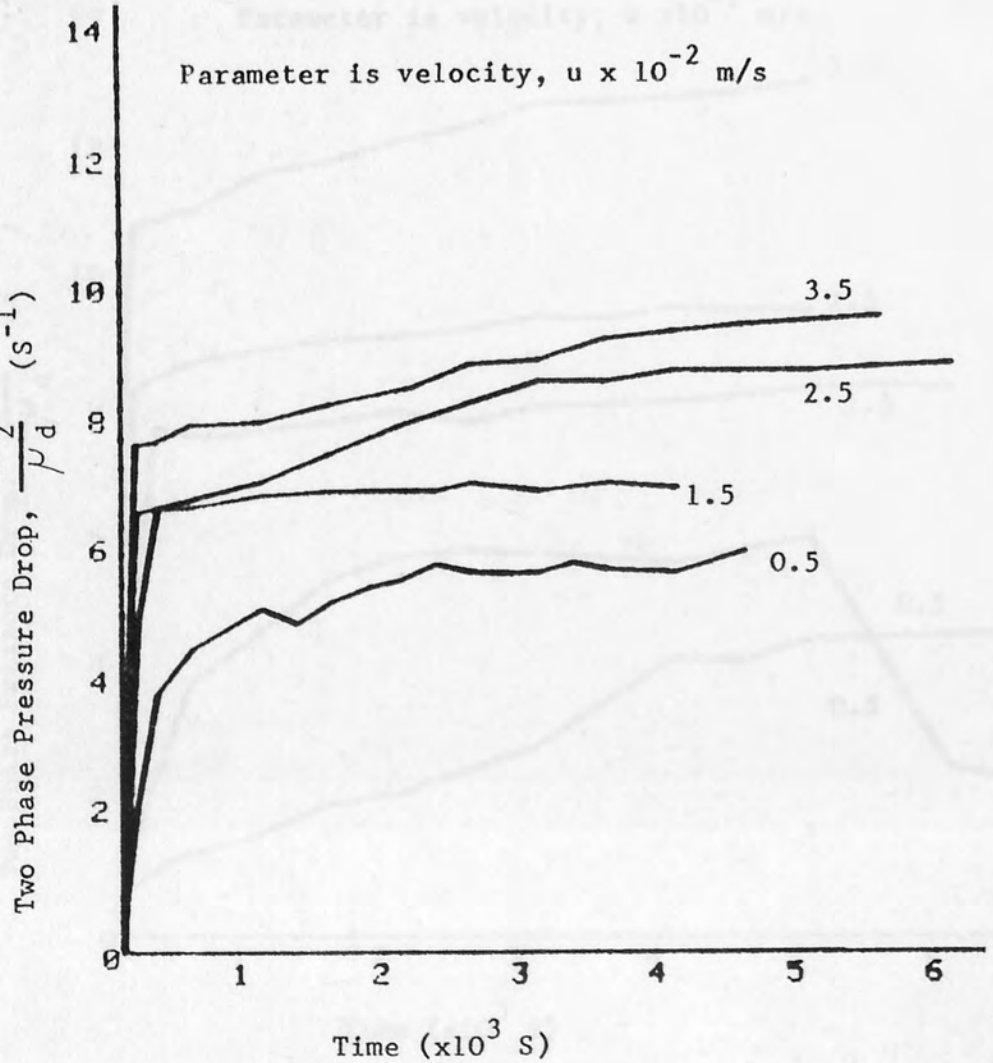

(a) Presoaked in Continuous Phase.

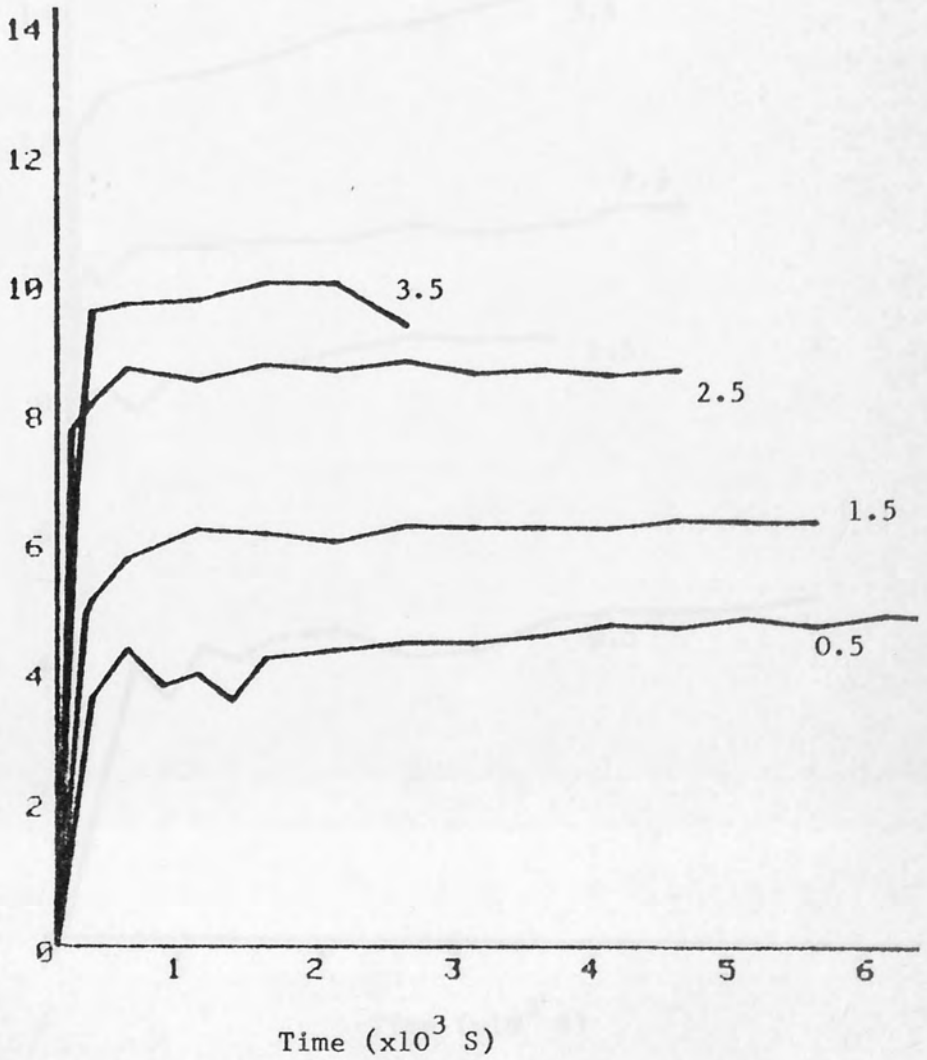

(b) Presoaked in Dispersed Phase.

Fig K.1. Transient Two Phase Pressure Drop for 30 layers of S300 Mesh.

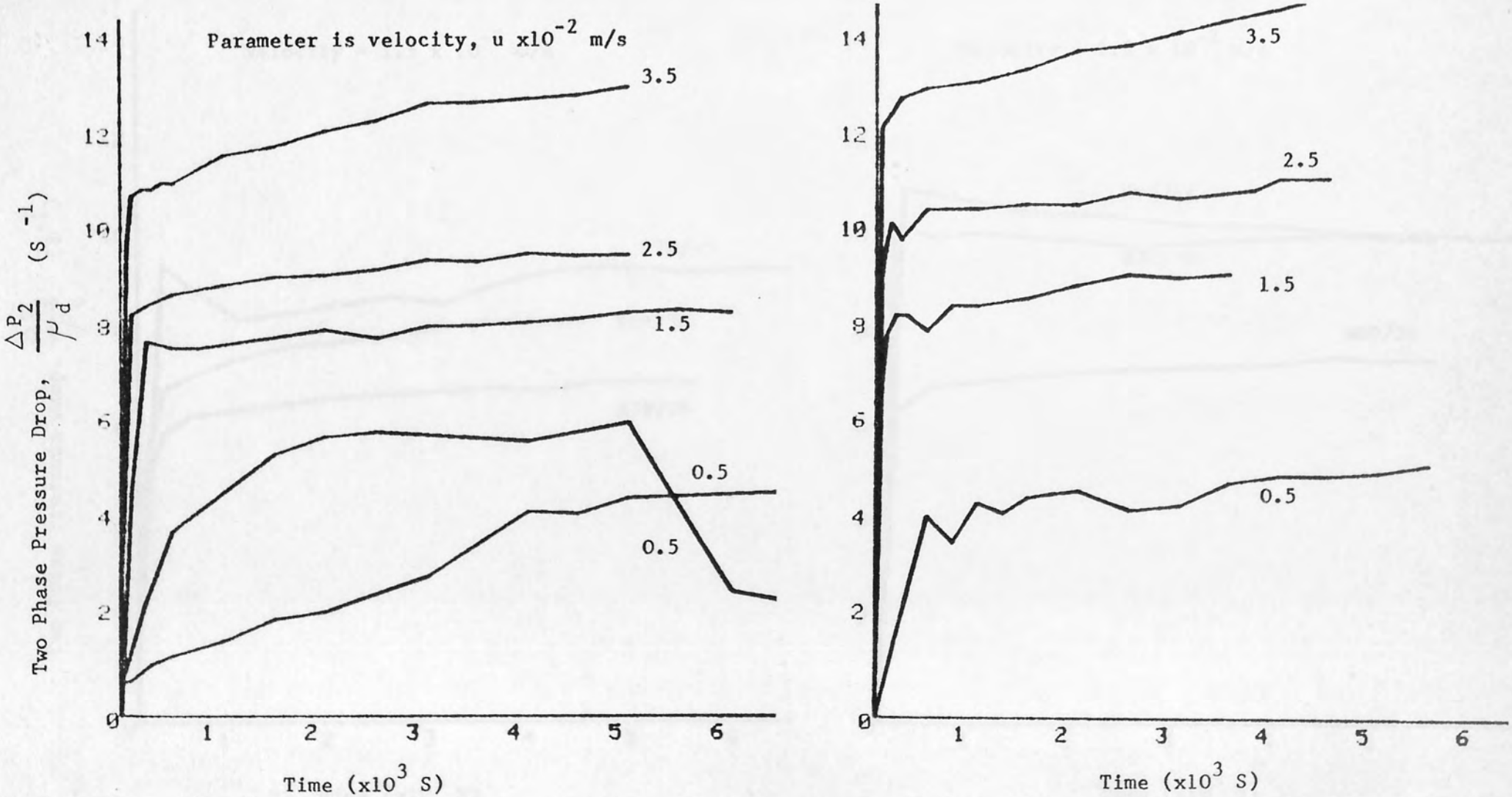

(a) Presoaked in Continuous Phase.

(b) Presoaked in Dispersed Phase.

Fig K.2. Transient Two Phase Pressure Drop for 60 layers of S300 Mesh.

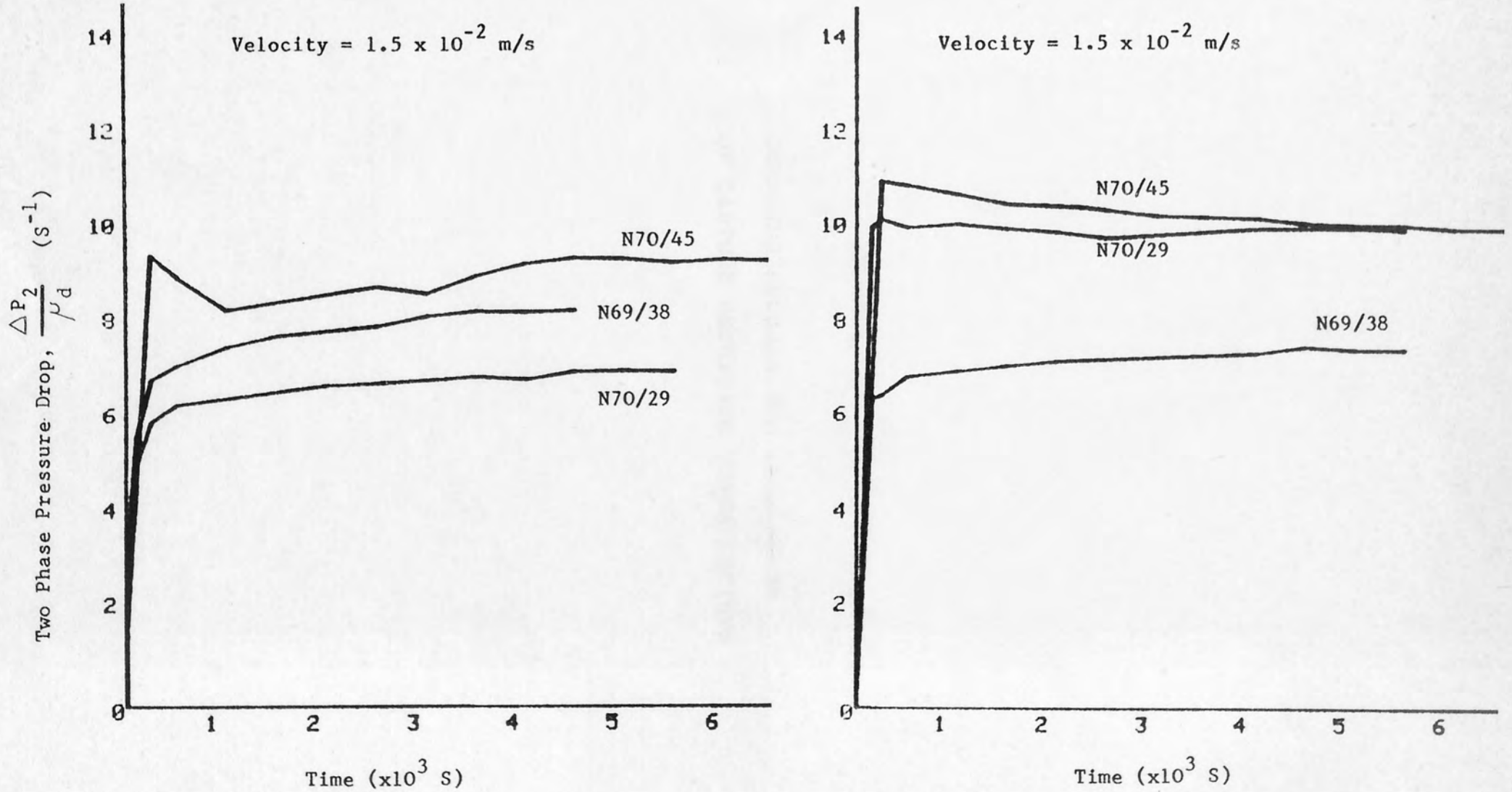

(a) Presoaked in Continuous Phase.

(b) Presoaked in Dispersed Phase.

Fig. K.3 Transient Two Phase Pressure Drop for 60 layers of Nylon Mesh.

APPENDIX L

COMPUTER PROGRAM FOR EVALUATION OF CAPTURE MECHANISM CONTRIBUTIONS

```
10  REM        EVALUATION OF CAPTURE MECHANISM CONTRIBUTIONS
11  REM          FOR S300 MESH ; TOLUENE-WATER SYSTEM
20  DIM F(7),N(7),P(7)
30  READ D1,D3,E
40  READ R3,M3,R4
50  READ K,T,0,G1
60  FOR L=1,7
70  READ F(L)
80  NEXT L
81  FOR M=1,7: READ P(M): NEXT M
90  FOR M=1,7
100  READ V
101  PRINT "VELOCITY=",V,"M/S": PRINT :V=V/E
102  PRINT "DROP SIZE          TOTAL       SIGNIFICANT       %REL"
103  PRINT "(MICRON)        EFFICIENCY     MECHANISM       CONTR"
110  FOR L=1,6
120  D2=F(L)*.1E-05
125  REM        CALCULATION OF DIMENSIONLESS GROUPS
130  R=D2/D3
140  R5=D3*V*R3/M3
150  H=2-LOG(R5)
160  S=(D2↑2*R3*V)/(9*M3*D3)
170  G=(D2↑2*(R4-R3)*G1)/(18*M3*V)
180  P5=(3*3.14159*D3*D2*V*M3)/(K*T)
190  N1=8*H*G/(9*3.14159*R↑2*M3*V*D2↑2)
195  REM        CALCULATION OF CAPTURE EFFICIENCIES
200  N(1)=(2*(1+R)*LOG(1+R)+1/(1+R)-(1+R))/(2*H)
210  N(2)=2.16/((2*H)↑.33333*P5↑.66667)
220  N(3)=-G
230  N(4)=R↑2/H*(3*3.14159*N1/4)↑.33333
240  N6=N(1)+N(2)+N(3)+N(4)
250  PRINT F(L),N6
260  FOR I=1,4
270  C=INT(N(I)*100/N6)
280  IF C<1 THEN 300
290  IF I=1 THEN  PRINT TAB(30);"INTERCEPTION",TAB(46);C
291  IF I=2 THEN  PRINT TAB(30);"DIFFUSION",TAB(46);C
292  IF I=3 THEN  PRINT TAB(29);"SEDIMENTATION",TAB(46);C
293  IF I=4 THEN  PRINT TAB(29);"LONDON FORCES",TAB(46);C
300  NEXT I
305  PRINT
310  NEXT L
315  FOR I=1,P(M): PRINT : NEXT I
320  NEXT M
330  STOP : END :FINISH
500  DATA .53E-04,.305E-04,.6995
510  DATA 1000,.1E-02,866.9
520  DATA .138048E-22,293,.55E-20,9.81
530  DATA .1,1,5,10,25,50,100
535  DATA 1,1,1,1,7,6,20
540  DATA .1E-03,.1E-02,.5E-02,.1E-01,.25E-01,.5E-01,.1
```

VELOCITY= .1E-02 M/S

DROP SIZE (MICRON)	TOTAL EFFICIENCY	SIGNIFICANT MECHANISM	%RELATIVE CONTRIBUTION
.1	.222527E-02		
		DIFFUSION	95
		LONDON FORCES	4
1	.119493E-02		
		INTERCEPTION	17
		DIFFUSION	38
		SEDIMENTATION	4
		LONDON FORCES	40
5	.757116E-02		
		INTERCEPTION	62
		DIFFUSION	2
		SEDIMENTATION	16
		LONDON FORCES	18
10	.247844E-01		
		INTERCEPTION	70
		SEDIMENTATION	20
		LONDON FORCES	9
25	.124406		
		INTERCEPTION	71
		SEDIMENTATION	25
		LONDON FORCES	3
50	.412309		
		INTERCEPTION	67
		SEDIMENTATION	30
		LONDON FORCES	1

VELOCITY= .1E-03 M/S

DROP SIZE (MICRON)	TOTAL EFFICIENCY	SIGNIFICANT MECHANISM	%RELATIVE CONTRIBUTION
.1	.88728E-02		
		DIFFUSION	97
		LONDON FORCES	1
1	.333375E-02		
		INTERCEPTION	4
		DIFFUSION	56
		SEDIMENTATION	15
		LONDON FORCES	24
5	.189697E-01		
		INTERCEPTION	17
		DIFFUSION	3
		SEDIMENTATION	66
		LONDON FORCES	12
10	.669071E-01		
		INTERCEPTION	17
		SEDIMENTATION	75
		LONDON FORCES	5
25	.3854		
		INTERCEPTION	15
		SEDIMENTATION	82
		LONDON FORCES	1
50	1.47221		
		INTERCEPTION	13

VELOCITY= .5E-02 M/S

DROP SIZE (MICRON)	TOTAL EFFICIENCY	SIGNIFICANT MECHANISM	%RELATIVE CONTRIBUTION
.1	.902696E-03		
		DIFFUSION	90
		LONDON FORCES	8
1	.848545E-03		
		INTERCEPTION	35
		DIFFUSION	20
		SEDIMENTATION	1
		LONDON FORCES	42
5	.827297E-02		
		INTERCEPTION	83
		SEDIMENTATION	3
		LONDON FORCES	12
10	.280434E-01		
		INTERCEPTION	90
		SEDIMENTATION	3
		LONDON FORCES	6
25	.13841		
		INTERCEPTION	93
		SEDIMENTATION	4
		LONDON FORCES	2
50	.436568		
		INTERCEPTION	93
		SEDIMENTATION	5
		LONDON FORCES	1

VELOCITY= .1E-01 M/S

DROP SIZE (MICRON)	TOTAL EFFICIENCY	SIGNIFICANT MECHANISM	%RELATIVE CONTRIBUTION
.1	.632274E-03		
		DIFFUSION	88
		LONDON FORCES	11
1	.830012E-03		
		INTERCEPTION	44
		DIFFUSION	14
		LONDON FORCES	40
5	.972962E-02		
		INTERCEPTION	88
		SEDIMENTATION	1
		LONDON FORCES	10
10	.335846E-01		
		INTERCEPTION	93
		SEDIMENTATION	1
		LONDON FORCES	4
25	.166561		
		INTERCEPTION	96
		SEDIMENTATION	1
		LONDON FORCES	1
50	.522979		
		INTERCEPTION	96
		SEDIMENTATION	2

VELOCITY= .25E-01 M/S

DROP SIZE (MICRON)	TOTAL EFFICIENCY	SIGNIFICANT MECHANISM	%RELATIVE CONTRIBUTION
.1	.418569E-03		
		INTERCEPTION	1
		DIFFUSION	82
		LONDON FORCES	16
1	.94468E-03		
		INTERCEPTION	58
		DIFFUSION	7
		LONDON FORCES	33
5	.137069E-01		
		INTERCEPTION	92
		LONDON FORCES	6
10	.482869E-01		
		INTERCEPTION	96
		LONDON FORCES	3
25	.241387		
		INTERCEPTION	98
		LONDON FORCES	1
50	.757321		
		INTERCEPTION	98

VELOCITY= .1 M/S

DROP SIZE (MICRON)	TOTAL EFFICIENCY	SIGNIFICANT MECHANISM	%RELATIVE CONTRIBUTION
.1	.332417E-03		
		INTERCEPTION	6
		DIFFUSION	63
		LONDON FORCES	30
1	.251449E-02		
		INTERCEPTION	79
		DIFFUSION	1
		LONDON FORCES	18
5	.474883E-01		
		INTERCEPTION	97
		LONDON FORCES	2
10	.171294		
		INTERCEPTION	98
		LONDON FORCES	1
25	.865654		
		INTERCEPTION	99
50	2.7213		
		INTERCEPTION	99

VELOCITY= .5E-01 M/S

DROP SIZE (MICRON)	TOTAL EFFICIENCY	SIGNIFICANT MECHANISM	%RELATIVE CONTRIBUTION
.1	.334307E-03		
		INTERCEPTION	2
		DIFFUSION	75
		LONDON FORCES	22
1	.125866E-02		
		INTERCEPTION	68
		DIFFUSION	4
		LONDON FORCES	27
5	.209523E-01		
		INTERCEPTION	95
		LONDON FORCES	4
10	.747426E-01		
		INTERCEPTION	97
		LONDON FORCES	2
25	.375747		
		INTERCEPTION	99
50	1.17981		
		INTERCEPTION	99

VELOCITY= .5E-02 (M/S)

BED DEPTH	FRACTION NOT CAPTURED
1	.513025
2	.397916
3	.331231
4	.286467
5	.253794
10	.165959
20	.995533E-01
30	.698821E-01
40	.525194E-01
50	.410098E-01
60	.328109E-01
70	.266909E-01
80	.219732E-01
90	.182496E-01
100	.152585E-01
110	.12823E-01
120	.108193E-01

APPENDIX M.

FORMULATION OF EQUATION TO DESCRIBE CRITICAL TRAJECTORY OF A DROP APPROACHING A CYLINDRICAL COLLECTOR.

In Section 10.2 it was shown that London-Van der Waal's forces may aid capture of drops having a diameter less than about 10 μm. Spielman and Goren[68] derived an equation to describe the critical trajectory of a drop approaching a cylindrical fibre and their equation was used as a basis for a more detailed investigation into the role of London forces. Their result, which is based on a force balance for a drop in the vicinity of the collector, is,

$$-\sin\Theta_p \frac{dH}{d\Theta_p} = \frac{f_1(H)}{f_3(H)}\left[f_2(H)\cos\Theta_p + \frac{N_{Adc} f_{ret}}{(H+2)^2 H^2}\right] \qquad M.1$$

M.1. London Attractive Force.

The term of equation M.1 containing the Adhesion number is based on the original expression of Hamaker (see equation 5.6) for the London force acting between a sphere and a plane surface. Consideration of the interactions for a sphere/plane system is acceptable when the Interception number is very small. However, when the drop diameters are dimensionally close to the collector diameter, it follows that equations describing the London attraction between a sphere and cylinder will provide a better description that is also consistent with the flow model based on flow over an array of parallel cylinders. Rosenfeld[75] derived an expression for the London force between a sphere and cylinder, thus,

$$F_{Ad} = \frac{-2Qa_p^3}{3(2a_p+h)^2 h^2}\left[\frac{a_c}{a_c+a_p+h}\right]^{0.5}\left[1 - \frac{0.2h(2a_p+h)}{a_c(a_c+a_p+h)}\right] \qquad M.2$$

where a_p and a_c are the drop and collector radius

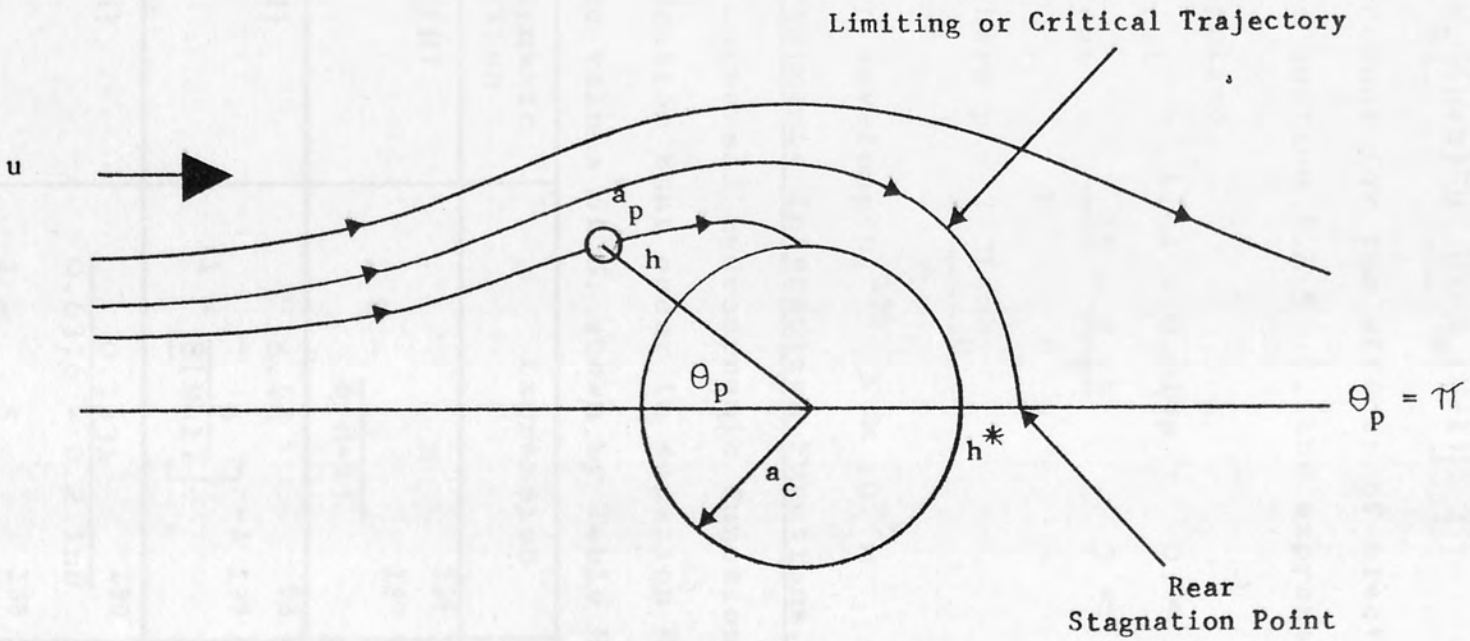

Fig M.1 Qualitatively Depicted Trajectories for Cylindrical Collector.

respectively and h is the separation between drop and collector as shown by Fig M.1 which also presents the co-ordinate system. Defining the dimensionless separation, $H = \frac{h}{a_p}$, equation M.2 may be rearranged to,

$$F_{Ad} = \frac{2Q}{3a_c N_R}\left[\frac{1}{(H+2)^2 H^2}\right]\left[\frac{1}{1+N_R(H+1)}\right]^{0.5}\left[1 - \frac{0.2\ N_R^2 H(H+2)}{1+N_R(H+1)}\right] \qquad M.3$$

To account for the effects of electromagnetic retardation (see Section 5.2.5), the expression given by Kruyt [135] was applied,

$$\left.\begin{aligned} f_{ret} &= 1.01 - 0.014p \qquad 0 < p < 3 \\ f_{ret} &= \frac{2.45}{p} - \frac{2.04}{p^2} \qquad 3 < p < \infty \end{aligned}\right\} \qquad M.4$$

$$\text{where } p = \frac{2\pi Ha_p}{\lambda}$$

The London wavelength, [135] $\lambda \simeq 10^{-7}$m .

M.2. Hydrodynamic Interaction Functions.

The universal hydrodynamic functions of the dimensionless separation that occur in equation M.1 are known for asynptotic values of H; shown by Table M.1.

Hydrodynamic function	Expression	Constraint
$f_1(H)$	H [136]	$H \rightarrow 0$
	$1 - \frac{9}{8(H+1)}$ [137]	$H \rightarrow \infty$
$f_2(H)$	6.46 [68]	$H \rightarrow 0$
	$1 - \left[\frac{9}{8(H+1)}\right]^{-1}$ [137]	$H \rightarrow \infty$
$f_3(H)$	$\frac{0.7431}{0.6376 - 0.2\ \ln H}$ [138]	$H < 0.003$
	$1 - \frac{5}{16(H+1)^3}$ [138]	$H > 0.003$

Table M.1. Asymptotic Behaviour of Universal Hydrodynamic Functions.

The variation of these functions is shown graphically in

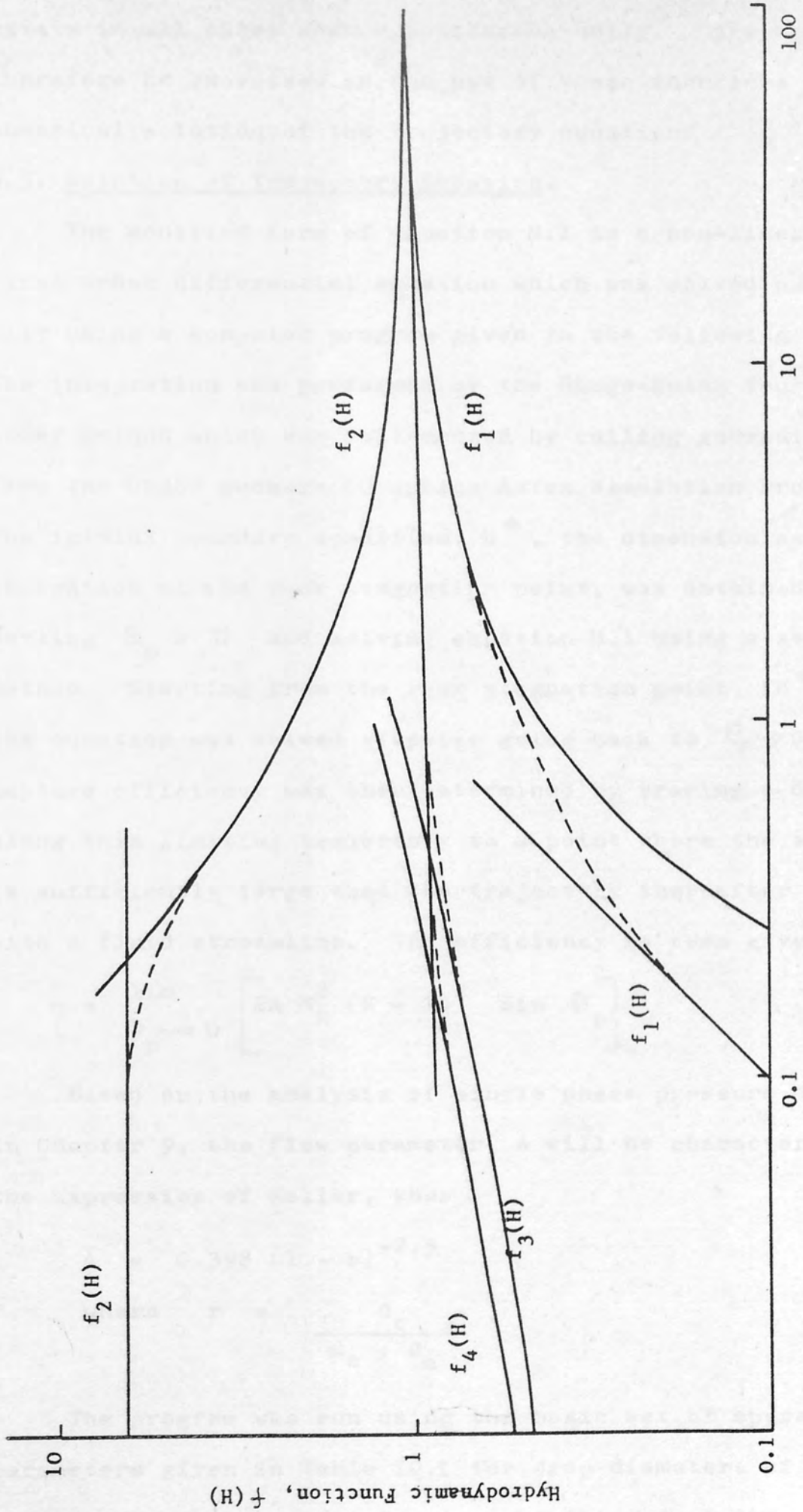

Fig. M.2 Behaviour of Hydrodynamic Functions with Separation illustrating discontinuities.

Fig M.2 from which it may be observed that a discontinuity exists in all cases when H approaches unity. Care must therefore be exercised in the use of these functions during numerical solution of the trajectory equation.

M.3. Solution of Trajectory Equation.

The modified form of equation M.1 is a non-linear, first order differential equation which was solved numerically using a computer program given in the following section. The integration was performed by the Runge-Kutta fourth order method which was implemented by calling subroutines from the GRASP package (Graphics Aston Simulation Program). The initial boundary condition, H^*, the dimensionless separation at the rear stagnation point, was obtained by setting $\Theta_p = \pi$ and solving equation M.1 using a search method. Starting from the rear stagnation point, (H^*, π), the equation was solved stepwise going back to $\Theta_p \rightarrow 0$. The capture efficiency was then determined by tracing a drop along this limiting trajectory to a point where the separation is sufficiently large that the trajectory thereafter coincides with a fluid streamline. The efficiency is then given by[68],

$$\eta = \lim_{\Theta_p \rightarrow 0} \left[2A \, N_R^2 \, (H + 1)^2 \, \text{Sin} \, \Theta_p \right] \qquad \text{M.5}$$

Based on the analysis of single phase pressure drop data in Chapter 9, the flow parameter, A will be characterised by the expression of Keller, thus

$$A = 0.398 \, (1 - r)^{-2.5} \qquad \text{M.6}$$

where $r = \dfrac{d_c}{d_c + d_a}$

The program was run using the basic set of operating parameters given in Table 10.1 for drop diameters of 1, 5 and 10 μm and the output is given at the end of this appendix.

Using the graph plotting subroutines of the package, the associated critical trajectories are plotted below the numerical output. The discontinuity observed when H approaches unity is due to use of the asymptotic forms of the universal hydrodynamic functions.

```
9  REM   COMPUTATION OF CAPTURE EFFICIENCY FROM EQUATION
10  REM   DESCRIBING CRITICAL DROP TRAJECTORY
11  DIM S(300),A(1000),B(1000)
20  REM  INPUT GENERAL SYSTEM PROPERTIES
25  READ B1,G,L1,M3,F3,R2
30  REM  INPUT MESH PROPERTIES
35  READ A3,D4,N3,V5
50  REM  INPUT SUPERFICIAL VELOCITY
55  READ U2
60  REM  INPUT HAMAKER CONSTANT
65  READ Q
70  REM  INPUT A.S.P. PARAMETERS
80  READ P,E,M,I
270  REM  EVALUATION OF INTERSTITIAL VELOCITY
280  U1=U2/V5
281  PRINT "SUPERFICIAL VELOCITY=",U2,"M/S."
290  REM      CALCULATION OF FLOW PARAMETER AFTER KELLER
303  A4=1/(2*(2-LOG(2*R3*A3*U1/M3)))
302  REM  INPUT DROP RADIUS
303  READ A1
304  A8=2*A1: PRINT "DROP DIAMETER=",A8,"M.": PRINT
305  IF A8>D4 THEN  PRINT "DROP DIAMETER> APERTURE": GOTO 905
306  D3=2*A3
307  R5=D3/(D3+D4)
308  H1=1.257*(1-R5)↑2.5
309  A4=1/(2*H1)
310  REM  EVALUATION OF INTERCEPTION,ADHESION & GRAVITY GROUPS
320  R=A1/A3
330  N1=G*A3↑2/(9*3.14159*M3*A4*U1*A1↑4)
340  N2=(2*(R2-R3)*G*A3↑2)/(9*M3*A4*U1)
350  PRINT "INTERCEPTION NUMBER=",R
355  PRINT "ADHESION NUMBER=",N1
360  PRINT "GRAVITY NUMBER=",N2: PRINT
364  REM  DETERMINATION OF SEPARATION AT REAR STAGNATION POINT
365  I=1:C=1:H2=1:J=1
366  H=.1E-05
367  GOSUB 2000
368  IF ABS((W2-F2)/W2)<C THEN 372
369  IF W2>F2 THEN 374
370  J=2:H=(1-H2)*H
371  GOTO 377
372  IF C<.1E-01 THEN 410
373  H2=.5*H2:C=.1*C:I=1: GOTO 369
374  IF J>1 THEN 376
375  H=H*10: GOTO 367
376  H=(1+H2)*H
377  I=I+1
378  IF I<20 THEN 367
379  H2=H2*.5: GOTO 367
410  PRINT "SEPARATION AT REAR STAGNATION POINT=",H: PRINT
490  REM                                    INITIALISATION SECTION
495  PRINT "     THETA          DH/DT              H"
496  PRINT
499  D7=1
500  CALL (1,P1)
505  T=22*(1-P1)/7
510  D5=0:K=1:S(K)=1:J=1
520  REM                                    DERIVATIVE SECTION
530  CALL (2,P,E,Z1,Z2)
535  A(J)=T:B(J)=H:J=J+1
540  IF T>.1 THEN 586
560  REM      COMPARISON OF DROP TRAJECTORY WITH FLUID STREAMLINE
570  K=K+1:S(K)=(H+1)↑2*SIN(T):C=ABS((S(K)-S(K-1))/S(K-1))
575  IF C>.1E-01 THEN 586
576  IF D7>1 THEN 586
577  PRINT : PRINT "TRAJECTORY/STREAMLINE COINCIDENCE"
```

```
 578  REM     CALCULATION OF CAPTURE EFFICIENCY
 579  E1=2*A4*R↑2*S(K)
 580  PRINT : PRINT "CYLINDER CAPTURE EFFICIENCY=",E1: PRINT
 581  D7=2
 586  REM              TESTING THE VALUES OF PRINT & TERMINAL FLAGS
 587  IF Z2=1 THEN 600
 590  PRINT T,D5,H
 600  IF Z1=2 THEN  PRINT "TERMINAL VALUE OF THETA ATTAINED": GOTO 85
 610  REM                                  INTEGRATION SECTION
 615  IF T<.3 THEN M=.5E-02
 620  CALL (3,P1,M,I)
 630  CALL (4,H,-D5)
 640  T=22*(1-P1)/7
 650  GOSUB 2000
 660  Y4=F2*COS(T)
 670  D5=-(P1/F3*(Y4+W2))/SIN(T)
 675  IF P1>.5 THEN D5=-D5
 676  IF H>1000 THEN 850
 680  GOTO 530
 850  GOTO 880
 870  REM  PLOTTING OF DROP CRITICAL TRAJECTORIES
 880  CALL (5)
 890  CALL (6,-45,80,-25,60)
 900  CALL (7,2,-45,0,F)
 910  CALL (7,1,35,0,F)
 920  A3=INT(A3*.1E07):A1=A1*.1E07
 930  CALL (7,2,-A3,0,F)
 940  X=-A3:S1=1:S2=.25
 950  Y=S1*SQR(A3↑2-X↑2)
 960  CALL (7,1,X,Y,F)
 970  IF X=A3 THEN S1=-S1:S2=-S2
 980  X=X+S2
 990  IF X<-A3 THEN 1005
1000   GOTO 950
1005   CALL (8,7)
1010   FOR I=1,J
1020   Z=A3+A1*(1+B(I))
1030   Y=Z*SIN(A(I)):X=Z*COS(A(I))
1035   X=-X
1040   CALL (7,1,X,Y,F)
1050   NEXT I
1060   CALL (8,7)
1070   CALL (9)
1130   STOP : END
1500   DATA 1,9.81,.1E-06,.1E-02,1000,866.9
1510   DATA .1525E-04,.53E-04,.3E05,.6995
1530   DATA .5E-02
1540   DATA .55E-20
1550   DATA .1,1,.1E-01,4
1560   DATA .25E-05
1999   REM        COMPUTATION OF UNIVERSAL HYDRODYNAMIC FUNCTIONS
2000   IF H>.5 THEN F1=1-(9/(8*(H+1))):F2=1/F1:  GOTO 2020
2010   F1=H:F2=6.46
2020   IF H>.1 GOTO 2030
2025   F6=.6376-.2*LOG(H):F3=.7431/F6:F4=.8436/F6
2026   GOTO 2040
2030   F3=1-(5/(16*(H+1)↑3)):F4=F3
2040   P2=44/7*A3*R*H/L1
2050   IF P2>3 THEN F5=2.45/P2-2.04/P2↑2:  GOTO 2070
2060   F5=1.01-.14*P2
2070   X1=1/((H+2)↑2*H↑2)
2080   X2=SQR(1/(1+R*(H+1)))
2090   X3=1-(.2*R↑2*H*(H+2))/(1+R*(H+1))
2100   W2=N1*X1*X2*X3*F5
2110   RETURN
```

SUPERFICIAL VELOCITY= .5E-02 M/S.
DROP DIAMETER= .1E-05 M.

INTERCEPTION NUMBER= .327869E-01
ADHESION NUMBER= .817123E-01
GRAVITY NUMBER= -.761783E-02

SEPARATION AT REAR STAGNATION POINT= .4852EE-01

THETA	DH/DT	H
3.14286	0	.4852EE-01
2.82857	.126118E-01	.497941E-01
2.51429	-.373687E-01	.521105E-01
2.2	-.674708E-01	.572677E-01
1.88572	-.118488	.663315E-01
1.57143	-.220764	.82EEE2E-01
1.25714	-.420732	.113627
.942859	-1.11063	.183376
.628574	-4.04336	.40223
.314288	-3.28551	.706423

TRAJECTORY/STREAMLINE COINCIDENCE

CYLINDER CAPTURE EFFICIENCY= .111041E-02

.299726E-05 -.333638E 00 845.422

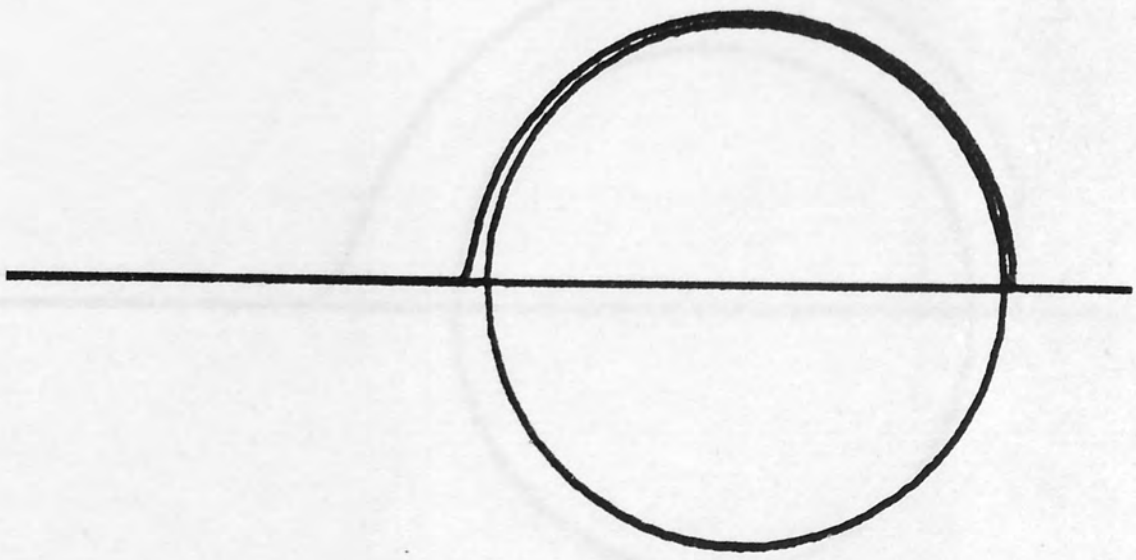

SUPERFICIAL VELOCITY= .5E-02 M/S.
DROP DIAMETER= .5E-05 M.

INTERCEPTION NUMBER= .163934
ADHESION NUMBER= .13074E-03
GRAVITY NUMBER= -.761783E-02

SEPARATION AT REAR STAGNATION POINT= .212868E-02

THETA	DH/DT	H
3.14286	0	.212868E-02
2.82857	8.98418	.398726
2.51429	1.47026	.715918
2.2	.767422	.823938
1.88572	.341885	.878217
1.57143	.664824E-03	.895047
1.25714	.339545	.911725
.942859	.757121	.965473
.628574	1.42579	1.07115
.314288	3.15937	1.28234

TRAJECTORY/STREAMLINE COINCIDENCE

CYLINDER CAPTURE EFFICIENCY= .263106E-01

.299726E-05 .333638E 06 842.191

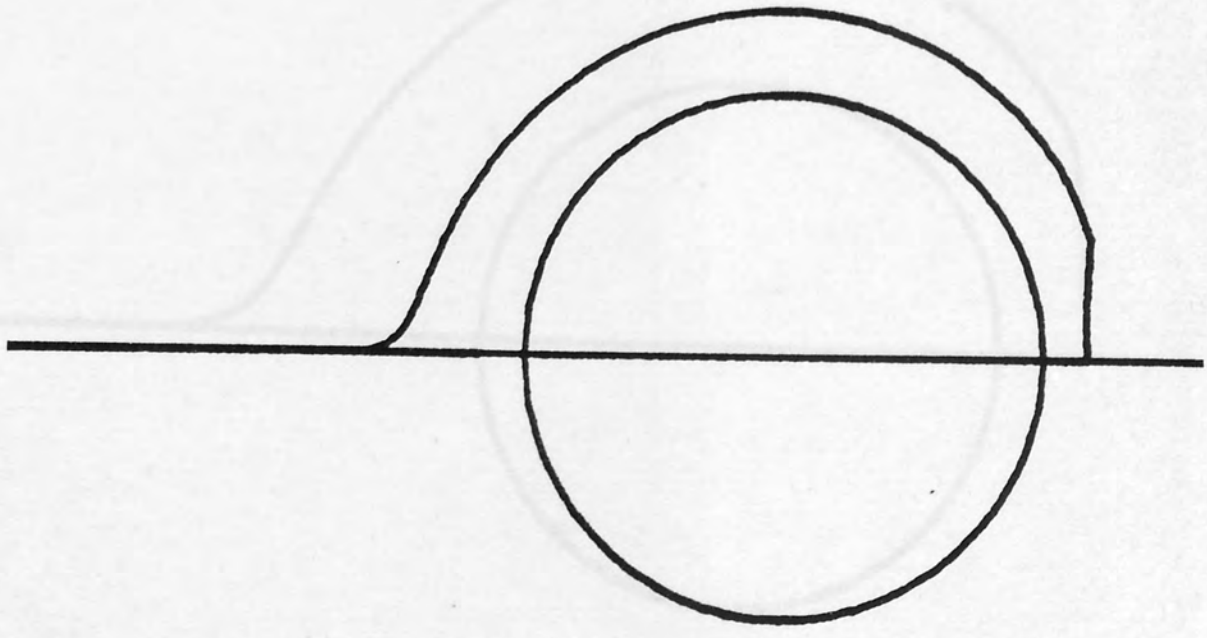

SUPERFICIAL VELOCITY= .5E-02 M/S.
DROP DIAMETER= .1E-04 M.

INTERCEPTION NUMBER= .327869
ADHESION NUMBER= .817121E-05
GRAVITY NUMBER= -.761783E-02

SEPARATION AT REAR STAGNATION POINT= .5200000E-03

THETA	LH/L1	H
3.14286	0	.5200000E-03
2.82857	3.36507	.132386
2.51429	1.50926	.536792
2.2	.782611	.64729
1.88572	.347781	.702572
1.57143	.675944E-03	.719686
1.25714	.344939	.736635
.942859	.767706	.791184
.628574	1.44151	.898176
.314288	3.18199	1.11125

TRAJECTORY/STREAMLINE COINCIDENCE

CYLINDER CAPTURE EFFICIENCY= .933547E-01

.299726E-05 .333638E 06 842.902

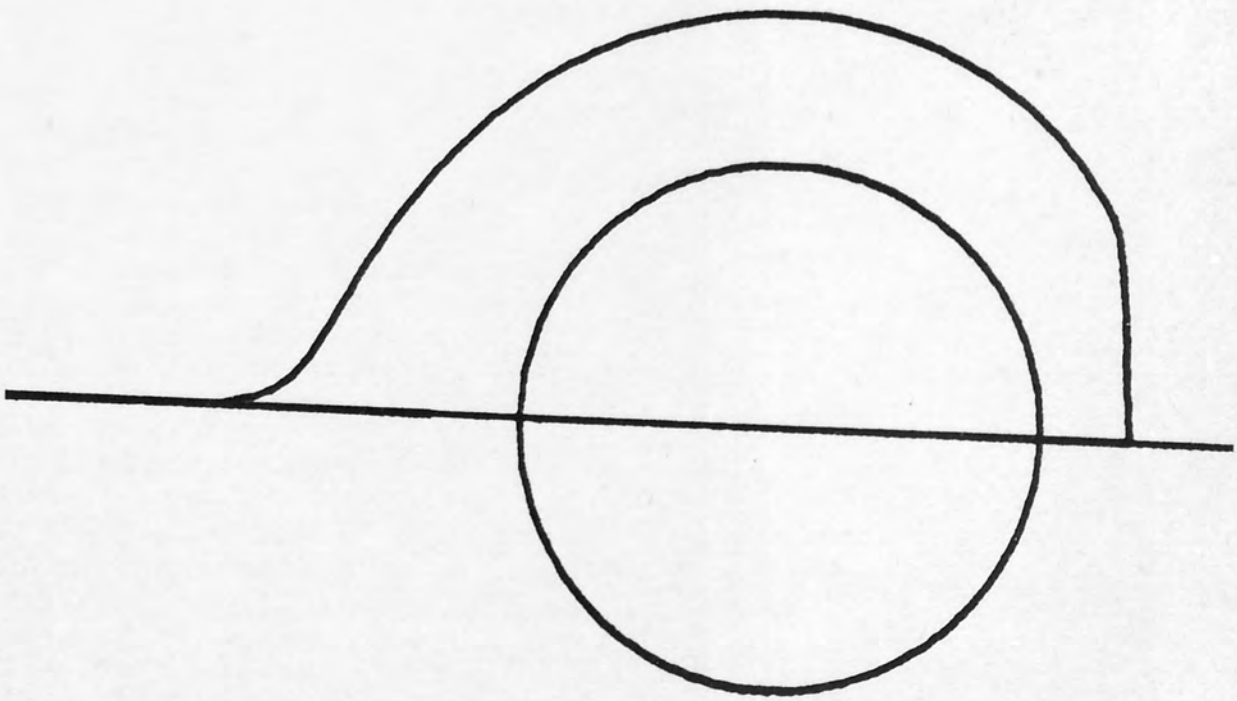

APPENDIX N

COMPUTER PROGRAM TO CALCULATE INITIAL DROP CAPTURE RATE IN COALESCER

```
10  REM       CALCULATION OF DROP CAPTURE RATE BY DIRECT INTERCEPTION
20  REM       AND LONDON FORCES FOR A BED WITH ZERO INITIAL SATURATION
40  DIM D(50),N(50),F(120)
50  READ D1,D3,A2,C1,E5,R4,R3
55  READ G1,M3,0
56  FOR K=1,5
60  READ U1
70  DEF FNW(D)=113.525-3.44166*D+.221507E-01*D↑2
80  A1=1-(D1/(D1+D3))↑2
90  R2=.5*D3/(D1+D3)
100   REM       HYDRODYNAMIC FUNCTION AFTER KELLER
110   H=1.257*(1-2*R2)↑2.5
114   PRINT TAB(15);"VELOCITY=",U1,"(M/S)": PRINT
120   I=1
130   D2=2
140   F1=U1*A2*C1
150   W1=FNW(D2)
160   D2=D2+2
170   W2=FNW(D2)
180   F2=.1E-01*(W1-W2)*F1
190   D(I)=(D2-1)*.1E-05
200   N(I)=6*F2/(3.14159*D(I)↑3)
210   I=I+1:W1=W2
220   IF D2=54 THEN 235
230   GOTO 160
235   C=10
236   PRINT : PRINT TAB(15);"BED DEPTH  FRACTION NOT CAPTURED"
240   FOR L=1,120
250   F3=0
260   FOR J=1,I-1
270   R=D(J)/D3
280   E3=2*(1+R)*LOG(1+R)-(1+R)+1/(1+R)
285   V=U1/E5
290   G=(D(J)↑2*(R4-R3)*G1)/(18*M3*V)
300   N1=8*H*Q/(9*3.14159*R↑2*M3*V*D(J)↑2)
310   E1=E3/(2*H)-G
320   E1=E1+R↑2/H*(3*3.14159*N1/4)↑.33333
330   N(J)=N(J)*(1-E1*A1)
335   IF N(J)<1 THEN N(J)=0
340   F3=F3+N(J)*3.14159*D(J)↑3/6
350   NEXT J
360   F4=F3/F1
365   IF L<6 THEN   PRINT TAB(15);L,F4
375   IF L=C THEN   PRINT TAB(15);L,F4: C=C+10
370   NEXT L
380   PRINT : PRINT
385   NEXT K
390   STOP
500   DATA .53E-04,.305E-04,.962112E-03,.5E-03,.6995,866.9,1000
510   DATA 9.81,.1E-02,.55E-20
520   DATA .5E-02
530   DATA .15E-01
540   DATA .25E-01
550   DATA .35E-01
560   DATA .7E-01
600   END
```

APPENDIX O.

EVALUATION OF SPECIFIC SURFACE FOR COALESCER CONTAINING DROPS OF DISPERSED PHASE.

Specific surface,

$$a = \frac{\text{(surface area of drops + surface area of fibres)}}{\text{(volume of drops + volume of fibres)}}.$$

let number of drops per unit volume of bed = N_p

then surface area = $N_p \pi d_p^2$

$$\text{volume} = N_p \pi \frac{d_p^3}{6}$$

let number of fibres per unit volume of bed = N_c

then surface area = $N_c \pi d_c 1$

$$\text{volume} = N_c \pi \frac{d_c^2}{4} 1$$

if void fraction of fibres = e_1

$$\text{then } N_c = \frac{4(1-e_1)}{\pi d_c^2 1}$$

if void fraction of drops = e_p

$$N_p = \frac{6(1-e_p)}{\pi d_p^3}$$

also two phase effective voidage, $e_2=(e_p+e_1)-1$

then $e_p = (e_2-e_1) +1$

but saturation, $S = 1 - \frac{e_2}{e_1}$

$$\text{or } e_2 = e_1 (1-S)$$

$$\therefore a = \frac{\left\{\frac{6}{d_p}(e_1 - e_2) + \frac{4}{d_c}(1 - e_2)\right\}}{(1-e_2)}$$

$$a = \frac{\left\{\frac{6}{d_p} e_1 S + \frac{4}{d_c}\left[1 - e_1(1-S)\right]\right\}}{\left[1-e_1(1-S)\right]}$$

APPENDIX P.

INTEGRATION OF PRESSURE DROP EQUATION.

In Section 10.5 solution of the equation describing the two phase pressure drop ratio was reduced to the problem of integration of the following polynomial expression,

$$\int_{L_I}^{L} f(S)dl = \frac{1}{k}\int_{ge^{-k(L-L_I)}+h}^{g+h} \frac{(av^4+bv^3+cv^2+dv+f)}{(v-h)\ (1-v)^3}\ dv \qquad P.1$$

Since the first term of the numerator is the same degree in v as the denominator, this must be considered separately. Substituting $z = (1-v)$, the first term becomes,

$$\frac{av^4}{(v-h)(1-v)^3} = \frac{a(1-z)^4}{z^3(1-h-z)}$$

$$= \frac{a}{(1-h-z)}\left[z - 4 + \frac{6}{z} - \frac{4}{z^2} + \frac{1}{z^3}\right]$$

then re-substituting $v = (1 - z)$

$$\frac{av^4}{(v-h)(1-v)^3} = a\left[\frac{-3}{(v-h)} - \frac{v}{(v-h)} + \frac{6}{(v-h)(1-v)} - \frac{4}{(v-h)(1-v)^2} + \frac{1}{(v-h)(1-v)^3}\right]$$

It is now possible to integrate the individual items on the right hand side,

$$\int_{ge^{-k(L-L_I)}+h}^{g+h} \frac{av^4}{(v-h)(1-v)^3}\ dv = a\left\{-\left[3\ \mathrm{Log}_e(v-h)\right] - \left[-h + v + h\ \log_e(v-h)\right] + \left[\frac{6}{(1-h)}\ \log_e\frac{(v-h)}{(1-v)}\right] - \frac{4}{(1-h)}\left[\frac{1}{(1-v)} - \frac{1}{(1-h)}\ \log_e\frac{(v-h)}{(1-v)}\right] + \right.$$

$$\frac{1}{2(1-h)}\left[\frac{-1}{(1-v)^2} - \frac{2}{(1-h)}\left\{\frac{1}{(1-v)} - \frac{1}{(1-h)}\log_e\frac{(v-h)}{(1-v)}\right\}\right]\Bigg\}$$

Further algebraic manipulation of the constituent terms reduces the above equation to a relatively simplified form,

$$\int_{ge}^{g+h} \frac{av^4}{(v-h)(1-v)^3}\,dv = a\left[\frac{(6h^2-8h+3)}{(1-h)^3}\log_e\frac{(v-h)}{(1-v)}\right]_{-k(L-L_I)}^{+h}$$

$$+\frac{h(9-8v)-(11-10v)}{2(1-h)^2(1-v)^2} - (h+3)\log_e(v-h) - (v-h)\Bigg] \qquad \text{P.2.}$$

Having evaluated the first term of the numerator, the remainder may now be resolved into partial fractions,

$$\text{i.e. } \frac{bv^3+cv^2+dv+f}{(v-h)(1-v)^3} = \frac{A}{(1-v)} + \frac{B}{(1-v)^2} + \frac{C}{(1-v)^3} + \frac{D}{(v-h)} \qquad \text{P.3.}$$

$$\text{or } bv^3+cv^2+dv+f = A(1-v)^2(v-h)+B(1-v)(v-h)+C(v-h)+D(1-v)^3$$

$$= A\left[v^3-(h+2)v^2+(2h+1)v-h\right]$$
$$+B\left[-v^2+(h+1)v-h\right] + C\left[v-h\right]$$
$$+D\left[-v^3+3v^2-3v+1\right]$$

equating coefficients,

v^3 : $b = A - D$

v^2 : $c = (h+2)A - B + 3D$

v : $d = (2h+1)A + (h+1)B + C - 3D$

v^o : $f = -hA - hB - hC + D$

Solution of these four simultaneous equations gives,

$$A = \frac{(3b+c)h^2 + (d-3b)h + (b+f)}{(1-h)^3} \qquad \text{P.4.}$$

$$B = \frac{h(3b+2c+d) - 2b - c + f}{(1-h)^2} \qquad \text{P.5.}$$

$$C = \frac{b+c+d+f}{(1-h)} \qquad \text{P.6.}$$

$$D = \frac{(3b+c)h^2 + (d-3b)h + (b+f)}{(1-h)^3} - b \qquad \text{P.7.}$$

Since the above expressions are independant of v, it is possible to integrate equation P.3 in its simple form,

$$\int_{ge}^{-k(L-L_I)} \frac{bv^3 + cv^2 + dv + f}{(v-h)(1-v)^3}\, dv \qquad \begin{matrix} g+h \\ +h \end{matrix}$$

$$= \left[-A \log_e(1-v) + \frac{B}{(1-v)} + \frac{C}{2(1-v)^2} + D \log_e(v-h) \right]_{ge}^{-k(L-L_I)} \qquad \begin{matrix} g+h \\ +h \end{matrix} \qquad \text{P.8.}$$

where the constants A,B,C and D are given by equations, P.4, P.5, P.6 and P.7 respectively.

Equation P.1 may now be equated to the sum of the components of the integral from equations P.2 and P.8, thus,

$$\int_{L_I}^{L} f(S)dl = \frac{1}{k} \left\{ \frac{a(6h^2-8h+3)}{(1-h)^3} \log_e \frac{(v-h)}{(1-v)} + a \left[\frac{h(9-8v)-(11-10v)}{2(1-h)^2(1-v)^2} \right] \right.$$
$$+ \left[D-a(h+3) \right] \log_e(v-h) - (v-h) - A \log_e(1-v)$$
$$\left. + \frac{B}{(1-v)} + \frac{C}{2(1-v)^2} \right\}_{ge}^{g+h} \qquad \begin{matrix} -k(L-L_I) \\ +h \end{matrix} \qquad \text{P.9.}$$

APPENDIX Q

COMPUTER PROGRAM FOR PREDICTION OF PRESSURE DROP USING MATHEMATICAL MODEL

```
420  REM          PREDICTION OF TWO PHASE PRESSURE DROP RATIO
440  PRINT "SLOPE OF SATURATION PLOT, B"
450  INPUT B
460  PRINT "CONSTANT SATURATION LENGTH, L1"
465  INPUT L1
466  PRINT "INLET SATURATION, SI"
470  INPUT S9
480  PRINT "OUTLET SATURATION, SE"
490  INPUT S5
491  PRINT "SUPERFICIAL VELOCITY, U"
492  INPUT U
500  READ D1, D3, E1
503  L1=L1*2*D3
504  B=B*2*D3
505  K=1/(B/(S9-S5)-L1)
507  PRINT : PRINT "DECAY FACTOR=", K
508  PRINT : PRINT "NUMBER OF        PRESSURE"
509  PRINT "  LAYERS          DROP RATIO"
510  X1=4/D3
520  X2=6/D1
530  X3=1-E1
540  X4=X2*E1↑2
550  X5=E1*(X1+X2*X3)
560  X6=X1*X3
570  Y1=X4↑2
580  Y2=2*X4*X5
590  Y3=2*X4*X6+X5↑2
600  Y4=2*X5*X6
610  Y5=X6↑2
620  Y6=S9-S5
630  Y7=S5
640  Z1=((3*Y2+Y3)*Y7↑2+(Y4-3*Y2)*Y7+Y2+Y5)/(1-Y7)↑3
650  Z2=((3*Y2+2*Y3+Y4)*Y7-2*Y2-Y3+Y5)/(1-Y7)↑2
660  Z3=(Y2+Y3+Y4+Y5)/(1-Y7)
670  Z4=Z1-Y2
680  W1=Y1*(6*Y7↑2-8*Y7+3)/(1-Y7)↑3
690  W2=Z4-Y1*(Y7+3)
695  M=1
699  C=10
700  FOR J=1, 120
710  I=1
720  L=J*2*D3
730  V=Y6+Y7
740  W3=Y1*(Y7*(9-8*V)-(11-10*V))/(2*(1-Y7)↑2*(1-V)↑2)
745  I1=W1*LOG((V-Y7)/(1-V))+W2*LOG(V-Y7)+W3-(V-Y7)
747  I1=I1-Z1*LOG(1-V)+Z2/(1-V)+Z3/(2*(1-V)↑2)
760  IF I=2 THEN 800
770  I2=I1
775  W4=EXP(-K*(L-L1))
776  IF W4>.1E-06 THEN 789
777  W4=.1E-06
778  IF M>1 THEN 789
779  PRINT : PRINT "EXPONENTIAL DECAYED AFTER"
780  PRINT J, "LAYERS": PRINT :M=2
789  V=Y6*W4+Y7
790  I=I+1: GOTO 740
800  P2=(I2-I1)/K
810  P1=L1*(Y1*S9↑4+Y2*S9↑3+Y3*S9↑2+Y4*S9+Y5)/(1-S9)↑3
820  P=D3↑2*(P1+P2)/(16*X3↑2*L)
825  P=P*1.724
830  IF J=C THEN  PRINT J, P: C=C+10
840  NEXT J
900  STOP : END
1000  DATA .25E-04, .305E-04, .6995
```

Q.2 PROGRAM OUTPUT FOR

CONSTANT INLET SATURATION

VALUE (S_I = 0.55)

```
SLOPE OF SATURATION PLOT,B
!1.1412
CONSTANT SATURATION LENGTH,L1
!1
INLET SATURATION,SI
!.55
OUTLET SATURATION,SE
!.226
SUPERFICIAL VELOCITY,U
!.005

DECAY FACTOR=   6499.6

NUMBER OF        PRESSURE
  LAYERS       DROP RATIO
    10           42.943
    20           28.6378
    30           23.8936
    40           21.5573

EXPONENTIAL DECAYED AFTER
    42          LAYERS

    50           17.7491
    60           14.791
    70           12.678
    80           11.0932
    90            9.86063
   100            8.87457
   110            8.06779
   120            7.39547
```

```
SLOPE OF SATURATION PLOT,B
!1.1789
CONSTANT SATURATION LENGTH,
!1
INLET SATURATION,SI
!.55
OUTLET SATURATION,SE
!.175
SUPERFICIAL VELOCITY,U
!.015

DECAY FACTOR=   7647.15

NUMBER OF        PRESSURE
  LAYERS       DROP RATIO
    10           36.1991
    20           22.6341
    30           18.1178

EXPONENTIAL DECAYED AFTER
    36          LAYERS

    40           14.9717
    50           11.9774
    60            9.98115
    70            8.55527
    80            7.48586
    90            6.6541
   100            5.98869
   110            5.44426
   120            4.99058
```

```
SLOPE OF SATURATION PLOT,B
!1.2071
CONSTANT SATURATION LENGTH,L1
!1
INLET SATURATION,SI
!.55
OUTLET SATURATION,SE
!.138
SUPERFICIAL VELOCITY,U
!.025

DECAY FACTOR=   8494.65

NUMBER OF        PRESSURE
  LAYERS       DROP RATIO
    10           32.9566
    20           19.7172
    30           15.3254

EXPONENTIAL DECAYED AFTER
    33          LAYERS

    40           11.9292
    50            9.54334
    60            7.95278
    70            6.81667
    80            5.96459
    90            5.30185
   100            4.77167
   110            4.33788
   120            3.97639
```

```
SLOPE OF SATURATION PLOT,B
!1.4445
CONSTANT SATURATION LENGTH,L1
!1
INLET SATURATION,SI
!.55
OUTLET SATURATION,SE
!.114
SUPERFICIAL VELOCITY,U
!.035

DECAY FACTOR=   7087.3

NUMBER OF        PRESSURE
  LAYERS       DROP RATIO
    10           30.9148
    20           18.0268
    30           13.7549

EXPONENTIAL DECAYED AFTER
   39          LAYERS

    40           11.3877
    50            9.11015
    60            7.59179
    70            6.50725
    80            5.69384
    90            5.0612
   100            4.55508
   110            4.14098
   120            3.7959
```

```
SLOPE OF SATURATION PLOT,B
!1.8660
CONSTANT SATURATION LENGTH,L1
!1
INLET SATURATION,SI
!.55
OUTLET SATURATION,SE
!.092
SUPERFICIAL VELOCITY,U
!.07

DECAY FACTOR=   5332.52

NUMBER OF        PRESSURE
  LAYERS       DROP RATIO
    10           28.7656
    20           16.3743
    30           12.3269
    40           10.3058
    50            9.07069

EXPONENTIAL DECAYED AFTER
   51          LAYERS

    60            7.62142
    70            6.53264
    80            5.71607
    90            5.08095
   100            4.57285
   110            4.15714
   120            3.81071
```

Q.3. PROGRAM OUTPUT FOR FITTED VALUES OF INLET SATURATION

```
SLOPE OF SATURATION PLOT,B
!1.1412
CONSTANT SATURATION LENGTH,L1
!1
INLET SATURATION,SI
!.615
OUTLET SATURATION,SE
!.226
SUPERFICIAL VELOCITY,U
!.005

DECAY FACTOR=  8477.87

NUMBER OF        PRESSURE
  LAYERS       DROP RATIO
    10           74.471
    20           44.4235
    30           34.4139

EXPONENTIAL DECAYED AFTER
   33          LAYERS

    40           26.7751
    50           21.4201
    60           17.85
    70           15.3
    80           13.3875
    90           11.9
   100           10.71
   110            9.73639
   120            8.92502
```

```
SLOPE OF SATURATION PLOT,B
!1.1789
CONSTANT SATURATION LENGTH,L1
!1
INLET SATURATION,SI
!.485
OUTLET SATURATION,SE
!.175
SUPERFICIAL VELOCITY,U
!.015

DECAY FACTOR=  5848.74

NUMBER OF        PRESSURE
  LAYERS       DROP RATIO
    10           21.2777
    20           15.135
    30           13.1258
    40           12.1515

EXPONENTIAL DECAYED AFTER
   47          LAYERS

    50           10.8434
    60            9.0362
    70            7.74531
    80            6.77715
    90            6.02413
   100            5.42172
   110            4.92883
   120            4.5181
```

```
SLOPE OF SATURATION PLOT,B
!1.2071
CONSTANT SATURATION LENGTH,L1
!1
INLET SATURATION,SI
!.485
OUTLET SATURATION,SE
!.138
SUPERFICIAL VELOCITY,U
!.025

DECAY FACTOR=  6613.79

NUMBER OF        PRESSURE
  LAYERS       DROP RATIO
    10           18.2279
    20           12.3262
    30           10.3832
    40            9.35209

EXPONENTIAL DECAYED AFTER
   41          LAYERS

    50            7.70521
    60            6.42101
    70            5.50372
    80            4.81575
    90            4.28067
   100            3.8526
   110            3.50237
   120            3.2105
```

SLOPE OF SATURATION PLOT, B
!1.8660
CONSTANT SATURATION LENGTH, L1
!1
INLET SATURATION, SI
!.415
OUTLET SATURATION, SE
!.092
SUPERFICIAL VELOCITY, U
!.07

DECAY FACTOR= 3431.68

NUMBER OF LAYERS	PRESSURE DROP RATIO
10	6.06266
20	4.7741
30	4.56703
40	4.48294
50	4.43434
60	4.40152
70	4.36857

EXPONENTIAL DECAYED AFTER 78 LAYERS

80	4.27632
90	3.80117
100	3.42106
110	3.11005
120	2.85088

SLOPE OF SATURATION PLOT, B
!1.4445
CONSTANT SATURATION LENGTH, L1
!1
INLET SATURATION, SI
!.475
OUTLET SATURATION, SE
!.114
SUPERFICIAL VELOCITY, U
!.035

DECAY FACTOR= 5461.96

NUMBER OF LAYERS	PRESSURE DROP RATIO
10	14.6054
20	9.81421
30	8.27781
40	7.51191

EXPONENTIAL DECAYED AFTER 50 LAYERS

50	7.04636
60	5.87197
70	5.03311
80	4.40397
90	3.91464
100	3.52318
110	3.20289
120	2.93598

NOMENCLATURE

Symbols have the following meanings except where specifically indicated in the text:

a - specific surface area (m^2/m^3)

a' - surface area per unit volume of screen (m^2/m^3)

a_c - collector radius (m)

a_p - drop radius (m)

A - flow parameter (-)

B - mesh thickness (m)

C - fractional concentration of dispersion (-)

d_a - aperture diameter (m)

d_c - collector diameter (m)

d_{ce} - effective collector diameter (m)

d_p - drop diameter (m)

d_{pc} - critical drop diameter for release (m)

d_{pe} - exit drop diameter (m)

$\mathscr{D}$ - molecular diffusion coefficient (m^2/s)

D - diameter of coalescing bed (m)

e - voidage fraction (-)

f - friction factor (-)

$f(H)$ - universal hydrodynamic function (-)

f_{ret} - electromagnetic retardation correction factor (-)

F_{Ad} - adhesion force (N)

F_{DL} - double layer force (N)

F^* - dimensionless drag force (-)

g - acceleration due to gravity =9.81 (m/s^2)

h - drop/collector separation (m)

H - dimensionless separation between drop and collector = $\frac{h}{a_p}$ (-)

H^* - dimensionless separation at rear stagnation point

I - mass capture rate (m^3/s)

k - saturation profile parameter characterising rate of decay (-)

k' - Boltzman's constant = 1.38048×10^{-23} (J/K)

K - Kozeny constant (-)

ℓ - distance into coalescing bed from inlet face (m)

ℓ_{max} - film resolution (lines/mm)

L - bed depth (m)

L_I - length of bed near inlet face having constant saturation value (m)

L_q - length of queue (-)

m_o - hologram recording magnification (-)

m_1 - hologram reconstruction magnification (-)

M - number of service channels in queueing system (-)

n - number of units in queueing system (-)

N_{Ad} - adhesion number = $\frac{4Q}{9\pi N_R^2} \frac{1}{\mu_c u d_p^2}$ (-)

N_c - mesh count (m^{-1})

N_{DL} - double layer group = $\frac{Kd_p}{2}$ (-)

N_{E2} - electrokinetic group = $\left(\frac{2\zeta_p\zeta_c}{\zeta_p^2+\zeta_c^2}\right)$ (-)

N_G - gravity number = $\frac{d_p^2(\rho_d-\rho_c)g}{18\mu_c u}$ (-)

N_L - number of mesh layers (-)

N_{Pe} - Pe clet number $\frac{d_c u}{\mathcal{D}}$ (-)

N_R - interception number = $\frac{d_p}{d_c}$ (-)

N_{Rd} - direct interception number = $\frac{d_p}{d_a}$ (-)

N_{Re} - Reynolds number = $\frac{d_c u \rho_c}{\mu_c}$ (-)

N_{Re}'' - modified Reynolds number = $\frac{d_c u \rho_c}{\mu_c(1-e_1)}$ (-)

N_{Sh} - Sherwood number = $\frac{I}{\pi d_c \mathcal{D} C}$ (-)

N_{Stk} - Stokes number = $\frac{d_p^2 \rho_c u}{9\mu_c d_c}$ (-)

P_n - probability that n units present in queueing system (-)

ΔP - pressure drop (N/m^2)

Q - Hamaker constant (J)

r - mesh geometric parameter = $\frac{d_c}{d_c+d_a}$ (-)

r_{22} - intermolecular distance (m)

S - local saturation of dispersed phase (-)

$\overline{S}$ - average saturation in bed (-)

S_I - saturation near inlet face of bed (-)

S_E - saturation near exit face of bed (-)

t - time (s)

T - tortuosity factor (-)

u - superficial velocity (m/s)

u_I - interstitial velocity (m/s)

u_o - object distance from sample to photographic plate (m)

v_o - distance from spatial filter to photographic plate (m)

Greek Letters

α - 'customer impatience' factor (-)

β - ratio of number of collisions to number of coalescence events (-)

γ - interfacial tension (N/m)

ϵ - dielectric constant of continuous phase

σ - surface tension (N/m)

η - drop capture efficiency (-)

η_c - coalescence efficiency (-)

μ - viscosity (Ns/m^2)

μ - service rate in queueing system (s^{-1})

ρ - density (kg/m^3)

ρ - utilisation factor in queueing system = $\frac{\lambda}{M\mu}$ (-)

λ - arrival rate in queueing system (s^{-1})

λ_c - theoretical filter coefficient (m^{-1})

λ_e - experimental filter coefficient (m^{-1})

λ_o - wavelength of hologram recording illumination (m)

λ_l - wavelength of hologram reconstruction illumination (m)

θ_e - equilibrium contact angle (rad.)

θ - coalescence time (s)

θ_p - polar co-ordinate for drop/collector system (rad.)

Subscripts

1 - single phase flow

2 - two phase flow

c - continuous phase

d - dispersed phase

D - diffusion

DI - direct interception

G - gravity (sedimentation)

I - interception

II - inertial impaction

L - London forces

T - total

REFERENCES

1. Institute of Petroleum (Proc. Seminar) 4th-8th May (1970) "Water Pollution by Oil".

2. Science Research Council (U.K.), Science Board, Chemistry Committee, "Report on the Science of Colloidal Dispersions", Jan., (1972).

3. Bikerman, J.J., Ind. Eng. Chem., 57,(1), pp 59-62 (1965).

4. Sherman, P., "Emulsion Science", Academic Press, London (1968).

5. Meissner, H.P., Chertow, B., Ind. Eng. Chem., 38 (8), 856, (1946).

6. Saito, H., Shinoda, K., Jl. Coll. Interfac. Sci., 24, pp 10-15 (1967).

7. Shinoda, K., Jl. Coll. Interfac. Sci., 24, pp 4-9 (1967).

8. Prince, L.M., Jl. Coll. Interfac. Sci., 23, pp 165-173 (1967).

9. Hermanie, P.H.J., van der Waarden, M., Jl. Coll. Interfac. Sci., 21, pp 513-521 (1966).

10. Wilkinson, M.J., B.Sc. Project Report, January (1974) University of Aston.

11. Carroll, B.J., Lucassen, J., "Theory and Practice of Emulsion Technology" Symp., Soc. Chem. Ind., Brunel Univ., pp 29-41 (1974).

12. Ford, R.E., Fumidge, G.G.L., Jl. Coll. Interfac. Sci., 22, pp 331-341 (1966).

13. Selker, A.H., Sleicher, C.A., Can. Jl. Chem. Eng., 43 pp 298-301 (1965).

14. Rowe, E.L., Jl. Pharm. Sci., 54, (2), pp 260-264 (1965).

15. Becher, P., Jl. Coll. Interfac. Sci., 24, pp 91-96 (1967).

16. Narasinga, E.V.L., Kumar, R., Kuloor, N.R., Chem. Eng. Sci., 21, pp 867-880 (1966).

17. Polichronakis, C., M.Sc. Thesis, University of Aston, October (1972).

18. Ullman, J.M., B.Sc. Project Report, University of Aston, January (1974).

19. Farley, R., Valentin, F.H.H., A.I.Ch.E.-I.Chem.E. Symposum Series No. 1. pp 1:39-1:48 (1965).

20. Bossy, G., Adv. in Water Pollution Research 2(3) pp 14/1-14/6 San Fransisco and Hawaii (1970).

21. Walters, J.K., Fennell, B.V., "Theory and Practice of Emulsion Technology", Symp., Soc. Chem. Ind., Brunel Univ., (1974).

22. Hayes, J.G., et al. Chem. Eng. Prog., 45, 235 (1949).

23. Chilingar, G.V., Beeson, C.M. "Surface Operations in Petroleum Production", Elsevier, New York (1969).

24. Franklin, J.S., Effl. Water Treat. Jl., October, pp 655-657 (1973).

25. Becher, P., "Emulsions, Theory and Practice", Rheinhold, New York (1968).

26. Osterman, J.W., Filtration and Separation, March, 127 (1966).

27. Lissant, K.J., Jl. Coll. Interfac. Sci., 22, pp 462-468 (1966).

28. Allak, A.M.A., Ph.D. Thesis, University of Aston, (1973).

29. Hill, J.B., Ind. Eng. Chem., 31, 1361 (1939).

30. Wang, L.K., Yang, J.Y., Dahm, D.B., Chemistry and Industry, 13 (5), 562 (1975).

31. Waterman, L.C., Chem. Eng. Prog., 61, (10), 51 (1965).

32. Walton, A.E., 'Design and Application of Electrostatic Coalescers' I.Ch.E. Symposium: Separation of Liquid Dispersions, Manchester, 3rd November (1977).

33. Lock, J., Processing, 41, October (1976).

34. Iggleden, G.J., 'Design and Application of Tilted Plate Separators', I.Ch.E. Symposium: Separation of Liquid Dispersions, Manchester, 3rd November (1977).

35. Outlook - 'Waste Water Treatment with air flotation', Process Engineering, 7, (11), 996 (1973).

36. Sallabanks, L.G.A., 'Treating Ballast Water Oily Waste', I.Ch.E. Meeting, University of Surrey, Guildford, 28th May (1975).

37. Clayton, R., Hiebenthal, D., Illmer, M. 'The Application of the Dissolved Air Flotation Process for Waste Water Treatment', I.Ch.E. Symposium: Separation of Liquid Dispersions, Manchester, 3rd November, (1977).

38. Chieu, J., Gloyna, E.F., Schechter, R.S., 'Coalescence of emulsified oil wastewater by fibrous beds', 30th Purdue Industrial Waste Conference, 611, May (1975).

39. Sareen, S.S., et al., A.I.Ch.E.Jl., 12(6), 1045 (1966).

40. Douglas, E., Elliott, I.G., Trans. Inst. Marine Eng., 74, (5), 164 (1962).

41. Davies, G.A., Jeffreys, G.V., Filtration and Separation; July/August 349 (1969).

42. Langdon, W.M., Naik, P.P., Wasan, D.T., Environ. Sci. & Tech., 6, (10), 905 (1972).

43. Hazlett, R.N., Carhart, H.W., Filtration and Separation, 456, July/August (1972).

44. Curtis, B.G., Filtration, 35, January/February (1964).

45. Bartle, J.W., Filtration and Separation, 1, September/October (1966).

46. Chambers, D.B., 'Oil Water Separation using Fibrous Materials', I.Ch.E. Symposium: Separation of Liquid Dispersions, Manchester, 3rd November, 1977.

47. Gammon, H. Filtration and Separation, 409, July/August (1973).

48. Gabriel, J.C., Parry, G., Filtration and Separation, 253, May/June (1977).

49. Jordan, G.V., Trans. A.S.M.E., 393, April (1955).

50. Burtis, T.A., Kirkbride, C.G., Trans. A.I.Ch.E., 42 (3), 413 (1946).

51. Voyutskii, S.S. et al., Dokl. Akad. Nauk., S.S.S.R., 91, 1155 (1953) [C.A. 49, 12053d (1955)].

52. Gudsen, R.C., M.Sc. Thesis, I.I.T. Chicago (1964).

53. Hazlett, R.N., Ind. Eng. Chem. Fundam., 8(4), 625(1969).

54. Vinson, C.G., Churchill, S.W., The Chem. Eng. Jl., 1, 110 (1970).

55. Voyutskii, S.S. et al., Izv. Vyssk. Ucked. Zaved. Khim. Technol. 2, 1970(1958) [C.A., 52, 19266a (1958)].

56. Langdon, W.M. et al., Petro/Chem. Engng. Nov., 34 (1963).

57. Rose, P.R., M.Sc. Thesis, I.I.T., Chicago (1969).

58. Lindenhofen, H.E., Filtration and Separation, July/August, 317 (1968).

59. Lindenhofen, H.E., Filtration and Separation, Sept./Oct. 567 (1969).

60. Harkins, W.D., 'The Physical Chemistry of Surface Films', Reinhold, New York (1952).

61. Huang, W.S., Ph.D. Thesis, I.I.T., Chicago (1968).

62. Bitten, J.F., Jl. Coll. and Interfac. Sci., 33(2), 265 (1970).

63. Ghosh, M.M., Brown, W.P., Jl. Water Pollution Control Fed., 47(8), 2101(1975).

64. Sherony, D.F., Kintner, R.C., Can. Jl. Ch.E., 49, 314 (1971).

65. Rosenfeld, J.I., Wasan, D.T., Proc. I.S.E.C. 74, Lyons, 319 (1974).

66. Spielman, L.A., Goren, S.L., Ind. Eng. Chem., 11(1), 66, (1972).

67. Spielman, L.A., Su, Y.P. Ind. Eng. Chem., 16(2), 272 (1977).

68. Spielman, L.A., Goren, S.L., Environ. Sci. & Tech., 4(2), 135 (1970).

69. Rajagopalan, R., Tien, C., Can. Jl. Ch.E., 55, 246 (1977).

70. Shalhoub, N.G., Ph.D. Thesis, University of Aston, Birmingham (1975).

71. Wilkinson, D., Mumford, C.J., Jeffreys, G.V., A.I.Ch.E.Jl. 21(5), 910 (1975).

72. Bradie, J.K. Ph.D. Thesis, Heriot Watt, Edinburgh (1969).

73. Pich, J. 'Aerosol Science' ed. Davies, C.N. Chapter 9 (Academic Press, London 1966).

74. Hamaker, H.C., Physica, 4, 1058 (1937).

75. Rosenfeld, J.I., Ph.D. Thesis, I.I.T., Chicago (1973).

76. Spielman, L.A., Fitzpatrick, J.A., Jl. Coll. and Interfac. Sci., 42(3), 607 (1973).

77. Aveyard, R., Haydon, D.A. 'Introduction to the principles of surface chemistry' (University Press, Cambridge, 1973).

78. Prieve, D.C., Ruckenstein, E., A.I.Ch.E.Jl. 20(6), 1178(1974).

79. Friedlander, S.K., Jl. Coll. and Interfac. Sci., 23, 157 (1967).

80. Emi, H., Okuyama, K., Yoshioka, N., Jl. Ch. Eng. Japan, 6(4), 349 (1973).

81. Wilkinson, D., Ph.D. Thesis, University of Aston in Birmingham (1974).

82. Lawson, G.B., Chemical and Process Engineering, 45, May (1967).

83. Brown, R. 'A microphotographic study of water coalescence', U.S. Army film RF 1916, Mobility Eng. R & D Command, Fort Belvoir, Virginia (1966).

84. Spielman, L.A., Goren, S.L., Ind. Eng. Chem. Fundam, 62, 10 (1970).

85. Bitten, J.F., Fochtman, E.G., Jl. Coll. and Interfac. Sci., 37(2), 312 (1971).

86. Hazlett, R.N., Ind. Eng. Chem. Fundam, 9 (3), 520 (1970).

87. Attarzadeh, G.R., Ph.D. Thesis, University of Aston, Birmingham (1979).

88. Yoshida, T., Kousaka, Y., Inake, S., Nakai, S., Ind. Eng. Chem. (Process Des. Dev.) 14(2), 101 (1975).

89. Singhal, A.K., Dranchuk, P.M., Can. Jl. Ch. Eng. 53, 3 (1975).

90. Forward, M.V., Smith, S.T. Trans. Textile Institute, TI58, Sept., (1954).

91. Hittit, H.A., Ph.D. Thesis, University of Aston, Birmingham (1972).

92. Calibration Data 'Metric Series Rotameters' G.E.C. Elliott Automation Group (1975).

93. Fattah, Ph.D. Thesis, University of Aston, Birmingham (1975).

94. McCaffery, F.G., Bennian, D.W., Jl. Can. Petrol. Tech., 13(4), 42 (1974).

95. Hossein, K.T., M.Sc. Thesis, University of Aston, Birmingham (1972).

96. Irani, R.R., Callis, C.F. 'Particle Size: Measurement Interpretation and Application' - John Wiley (1963).

97. Zinky, W.R., Annals. N. York Acad. Sci., 158,741 (1969).

98. Thompson, B.J. et al, App. Optics 6(3), 519 (1967).

99. Trolinger, J.D. Optical Engineering 14(5), 383 (1975).

100. Gabor, D. Proc. Roy. Soc. (A), 197, 483, (1947).

101. Thompson, B.J., Jl. Phys. E. (Scientific Instruments) 7, 781, (1974).

102. Code of Practice for protection of persons exposed to laser radiation in Universities (1972).

103. Webster, J.M., Jl. Photographic Soc. 19, 38 (1971).

104. Thompson, B.J., Parrent, G.B., Ward, J.H., Justh, B., Jl. App. Meteorology 5, 343, June (1966).

105. Silverman, B.A., Thompson, B.J., Parrent, G.B., U.S. Patent No. 3451 755, June (1969).

106. Kunkel, B.A., Jl. App. Meteorology, 10, 482, June (1971).

107. Bartlett, J.T., Adams, R.J., Microscope, 19(4), 424, (1971).

108. Bexon, R., Jl. Phys. E. (Scientific Instruments) 6, 245 (1973).

109. Pavitt, K.W., Jackson, M.C., Adams, R.J., Bartlett, J.T., Jl. Phys. E. (Scientific Instruments) 3, 973 (1970).

110. Agfa Gevaert Technical information - Photographic Materials for Holography, Afga Gevaert, London (1975).

111. Schultze, D., Laser Focus, June, 23 (1968).

112. Zinky, W.R. Annals. N.Y. Acad. Sci., 158, 741 (1969).

113. Phillips, N.J., Private Communication, Dept. Phys. Loughborough (1976).

114. Graube, A., App. Optics. 13, (12), 2942 (1974).

115 Tonna, J.A., B.Sc. Project Report, University of Aston, Birmingham (1977).

116. Spielman, L.A., Ph.D. Thesis, University of California, Berkeley, California (1968).

117. Sherony, D.F., Ph.D. Thesis, I.I.T., Chicago (1969).

118. Bird, R.B., Stewart, W.E., Lightfoot, E.N. 'Transport Phenomena' Chapter 6 (Wiley, New York, 1960).

119. Armour, J.C., Cannon, J.N., A.I.Ch.E.Jl. 14(3) 415 (1968).

120. Ingmanson, W.L., Han, S.T., Wilder, H.D., Myers, W.T. Tappi, 44(1), 47 (1961).

121. Rushton, A., Griffiths, P. Trans. Inst. Chem. Eng. 49 49 (1971).

122. Kirsch, A.A., Fuchs, N.A., Ann. Occup. Hyg., 10 23 (1967).

123. Spielman, L.A., Goren, S.L., Environ. Sci. & Tech. 2,(4), 279 (1968).

124. Euzen, J.P. et al., Proc. I.S.E.C. 1974, 5, 130, Lyons, Sept. (1974).

125. Pich, J., Aerosol Science, 4, 217, (1973).

126. Bear, J., 'Dynamics of fluids in porous media', American Elsevier, New York (1972).

127. Brown, G.G. 'Unit Operations', John Wiley, New York, (1950).

128. Morse, P.M., 'Queues, inventories and maintenance', Wiley, New York (1958).

129. Sheron y, D.F., Kintner, R.C., A.I.Ch.E.Jl., 17, (2), 291 (1971).

130. Fowkes, F.M., Ind. Eng. Chem., 56, (12), 40 (1964).

131. Davies, M., B.Sc. project report, University of Aston (1975).

132. Technical Data, 'Becosyn' meshes, Begg Cousland, Glasgow, (1974).

133. Perry, R.H., Chilton, C.H., 'Chemical Engineers Handbook', 5th ed., McGraw Hill, Tokyo, (1973).

134. Chemical Rubber Co., 'Handbook of Chemistry and Physics', 58th ed., Editor Weast, R.C., C.R.C. Press, Cleveland (1977).

135. Kruyt, H.R. 'Colloid Science', Vol. K, Elsevier, New York (1965).

136. Charles, G.E., Mason, S.G. Jl. Coll. Sci., 15, 236, (1960).

137. Spielman, L.A., Fitzpatrick, J.A., Jl. Coll. Interfac. Sci., 42,(3), 607 (1973).

138. Goldman, A.J., Cox, R.G., Brenner, H., Chem. Eng. Sci., 22, 637 (1967).